

WAVE PROPAGATION IN AN ELASTIC PLATE
RESTING ON AN ELASTIC FOUNDATION

Thesis by
James Reily Lloyd

In Partial Fulfillment of the Requirements
For the Degree of
Doctor of Philosophy

California Institute of Technology
Pasadena, California

1962

ACKNOWLEDGEMENTS

The author wishes to express his appreciation to Dr. Julius Miklowitz for his many helpful suggestions and encouragement during the course of this work.

Thanks are due the National Science Foundation and the Union Carbide Corporation for granting fellowships under which part of this work was completed, and the Western Data Processing Center, University of California at Los Angeles, for the use of their computing facility.

The author is also grateful for the assistance given by Barbara Rickert in typing the manuscript and Beverly McAllister for the preparation of the figures.

ABSTRACT

Presented is an analysis of wave propagation in an infinite elastic plate or beam on an elastic foundation. The results are presented in two parts:

1. The frequency spectra (frequency as a function of wave number) for the problem based on existing approximate bending theories are compared with the spectra based on the exact equations of motion from linear elasticity theory. The existence of complex wave numbers is established in each case. A distinct similarity is found between the spectrum representing the more exact theory of bending (Timoshenko bending mechanism) and the exact Rayleigh-Lamb spectrum for symmetric waves in a free elastic plate. Good agreement between approximate theories and the exact equations is found for soft foundations under the usual restrictions of low frequency-long waves.

2. The transient response is considered for the exact theory and the more exact theory of bending. In both cases suddenly applied line loads are considered. In the latter case the related point load problem is also studied. Two distinct integral transform methods of solution are presented and used in these problems. For one of these methods the contributions from the various modes, including the complex arms, are identified with certain integrals that are components of the solution. Results from numerical computation of these integrals are presented and analyzed for the more exact theory of bending using two different foundation stiffnesses.

TABLE OF CONTENTS

	<u>Page</u>
ACKNOWLEDGEMENTS	
ABSTRACT	
NOTATION	
INTRODUCTION	1
I. GOVERNING EQUATIONS AND STEADY WAVE PROPAGATION CHARACTERISTICS OF AN ELASTIC PLATE ON AN ELASTIC FOUNDATION	9
A. Exact Theory	9
Frequency Spectrum	13
B. Approximate Theories	31
1. Elementary Theory	31
Frequency Spectrum	32
2. More Exact Theory of Bending	34
Frequency Spectrum	39
II. TRANSIENT RESPONSE OF AN ELASTIC PLATE ON AN ELASTIC FOUNDATION	50
A. Approximate Theory	50
1. Statement of Problems and Formal Solutions	50
a. Line Load	50
b. Point Load	54
2. Evaluation of Formal Solutions	57
a. Line Load	58
b. Point Load	64
3. Correspondence Between Line Load and Point Load Solutions	68

	<u>Page</u>
B. Exact Theory	70
1. Statement of Problem and Formal Solution	71
2. Evaluation of Formal Solution	74
C. Discussion of Methods and Their Relation to Certain Wave Features	80
1. Comparisons of Methods 1 and 2	80
2. Extensions of Methods 1 and Approximations	84
a. Wave Front Expansions	84
b. Stationary Phase Approximations	87
c. Alternate Path of Integration	88
D. Discussion of Results from Numerical Computation	92
CONCLUSIONS	139
REFERENCES	141
APPENDIX A - The Geometric Behavior of Complex Frequency Spectra	145
APPENDIX B - Branch Point Analysis and Contour Integration of Equation 51b	149
APPENDIX C - A Criterion for Estimating the Range of Validity of the Stationary Phase Approximation	157

NOTATION

a	ratio of speeds, c_d/c_s
A, A_i	constants
A_b	beam cross sectional area
Br_1, Br_2	Bromwich integration paths
c	limiting wave speed, $[k'\mu/\rho]^{1/2}$
c_d	dilatation speed, $[(\lambda + 2\mu)/\rho]^{1/2}$
c_p	plate speed, $[E/\rho(1-\nu^2)]^{1/2}$
c_s	shear speed, $[\mu/\rho]^{1/2}$
c_R	Rayleigh surface speed
C_1, C_2, C_3	integration paths
D	plate modulus, $Eh^3/12(1-\nu^2)$
e	constant, $\sqrt{12}$ (for a plate)
E	modulus of elasticity
f_p	point load (force)
f_l	line load (force per unit length)
F	frequency function defined on page 54
F_{p0}	dimensionless point load
F_{l0}	dimensionless line load
g	cutoff frequency
G	frequency function defined on page 73
h	plate thickness
H	function defined on page 73
I	moment of inertia of beam cross section

I_{b_j}, I_{s_j}	integrals representing transient response for w_b and w_s , respectively, defined on page 59
I_j	integrals representing transient response for w of exact theory, defined on page 77
k'	shear correction factor
K, K_e	foundation constants for exact and approximate theories, respectively (force per unit deflection per unit area)
L_j	integration path
N	order of lowest nonzero derivative $d^N \Omega / d\Gamma^N$ at spectrum branch points
p	Fourier transform variable
p_j	poles in p -plane for j^{th} mode
q	transverse shear load per unit area
Q	dimensionless shear load
Q_i	body force per unit volume in i^{th} direction
r	radial coordinate
R	dimensionless radial coordinate, er/h
R_E	(maximum kinetic energy of rotation)/(maximum kinetic energy of translation)
s	Laplace transform variable
s_j	poles in s -plane for j^{th} mode
S_j	branch points in s -plane
t	time
T_a	dimensionless time of occurrence, tc_p/x
T_p	dimensionless predominant period, $2\pi c_p/\omega h$
u_i	displacement in i^{th} direction
\underline{U}	vector displacement with components u_i
\underline{v}	displacement velocity

w	transverse plate deflection
w_b, w_s	transverse plate deflection due to bending and shear, respectively
w_T	total transverse plate deflection, $w_b + w_s$
w_0	total transverse plate deflection under point of loading
W	dimensionless plate deflection, w/h
W_b, W_s	dimensionless plate deflections due to bending, w_b/h , and shear, w_s/h , respectively
x	Cartesian coordinate
x_i	Cartesian coordinate in i^{th} direction
X	real part of Γ
X_a	dimensionless station of occurrence, x/tc_p
y	Cartesian coordinate
Y	imaginary part of Γ
z	Cartesian coordinate
Z	inner root of p_j
α	$[\Gamma^2 - (\pi\Omega/a)^2]^{1/2}$
α'	$[p^2 + (s/a)^2]^{1/2}$
β	$[\Gamma^2 - (\pi\Omega)^2]^{1/2}$
β'	$[p^2 + s^2]^{1/2}$
γ	wave number
Γ	dimensionless wave number, $h\gamma$
Γ'	dimensionless wave number, $h\gamma/e$
δ	ratio of speeds, c/c_p
δ_D	Dirac delta function
ϵ	strain

ε	small quantity, $\varepsilon \ll 1$
ζ	dimensionless Cartesian coordinate, z/h
η, η'	dummy variables
θ	angular coordinate
μ	Lamé constant
Λ_p	dimensionless predominant wave length
λ	Lamé constant
ν	Poisson's ratio
ξ, ξ^0	dimensionless Cartesian coordinate, x/h
ξ'	dimensionless Cartesian coordinate, ex/h
ρ	mass density
σ_{ij}	stress on j^{th} face in i^{th} direction
τ	dimensionless time, tc_s/h
τ'	dimensionless time, et_c/h
τ^0	dimensionless time, tc_p/h
φ	scalar potential
Φ	dimensionless scalar potential
Ψ	vector potential component
$\underline{\Psi}$	vector potential
$\underline{\Phi}$	dimensionless vector potential component
ω	angular frequency
Ω	dimensionless frequency, $\omega h/\pi c_s$ (exact theory) and $\omega h/ec$ (approximate theories)
Re	real part
Im	imaginary part
∇	gradient operator

∇^2	Laplacian operator
$(\bar{\quad})$	Laplace transform
$(\tilde{\quad})$	Fourier transform
$(\quad)^0$	Hankel transform of order zero
$(\quad)_*$	pertaining to real-complex arm intersection

INTRODUCTION

It is well known that in an unbounded, homogeneous, isotropic, linear elastic solid two basically different types of waves (dilatational and equivoluminal) can propagate independently, each with a different speed. Superposition of these waves in various ways determine the dynamic deformation of the elastic solid.

The introduction of a traction free boundary requires the coupling of the two basic waves in order to satisfy the boundary conditions. For example, in the plane strain case of an elastic half space with a traction free boundary, an obliquely incident harmonic plane dilatational (or a vertically polarized shear) wave will, in general, give rise to two reflected waves: a vertically polarized shear wave and a dilatational wave. This process is commonly referred to as mode conversion. The characteristic angles of reflection and amplitudes of the reflected waves are dependent only on the angle of incidence of the incident wave and the two basic wave speeds which are defined by the material properties. If a second stress free boundary parallel to the first is introduced, the same laws of reflection exist for an incident plane wave on this boundary. For instance, in the case of symmetric deformation with respect to the mid-plane of the two boundaries the two plane waves combine to form a single wave that propagates parallel to the boundaries. For this wave to satisfy the traction free boundaries of such a wave guide it is necessary that its phase velocity be dependent on its wavelength. This dependence is called dispersion and is described by the frequency equation. A mathematical treatment of this physical argument describing dispersion has been

accomplished by Harrison (1) for the example cited above. The present work is concerned primarily with related transient problems. In particular, interest is focused on such problems involving a restraining elastic boundary.

The effect of a restraining elastic boundary has been the subject of several recent investigations on the dynamic excitation of beams and plates. Of note are the works of Kenney (2) and Mathews (3) on the steady vibration of a beam on an elastic foundation based on the elementary bending theory (Bernoulli-Euler). Mathews and Kenney also studied the related problem of the traveling load. Crandall (4) treated similar problems later on the basis of the more exact theory of bending due to Timoshenko. Das Gupta (5) considered the influence of an elastic boundary on one face of an infinite plate using the equations of motion from linear elasticity theory. Das Gupta's interest was focused on the Rayleigh surface waves in a plate. He described this surface motion in terms of an equivalent system composed of a rigid base with a thin plate resting on the foundation. Boley (6) in an investigation concerned with a dynamic Saint Venant's Principle, used as an example a mechanical system of two Timoshenko beams connected by springs. This problem relates to the present general interest. Mindlin (7) has made use of a restraining elastic boundary to study, in accord with the exact theory, the development of coupling between uncoupled dilatation and equivoluminal waves. This development occurs in a plate under mixed boundary conditions on its faces (normal displacement, shear stress zero) as these conditions are relaxed to the traction free case. In all of these studies concerned with the influence of the elastically restrained boundary no consideration has

been given the behavior of the various propagation modes under transient loading. Such consideration is the main theme here.

The response of a mechanical system to transient loading requires the superposition of waves with different frequencies and wave lengths to match the loading function and the remaining boundary conditions. In the absence of dispersion the frequency and wave length superpositions may be carried out independently provided the spacial and time variations of the loading function are separable. This is due to the independence of the wave length and frequency. The resulting waves remain unchanged in shape as they propagate. However, in the case of dispersion the aforementioned superpositions may not be carried out independently, because of the relations existing between the frequency, wave speed, and wave length. To illustrate this consider a transient normal point load on a free plate. At the point of application of this load the stress in the plate must have a Fourier spectrum to match the load's functional dependence on time. An infinite number of stress waves having different frequencies are involved and propagate away from their source. Each travels at a different speed depending on its particular frequency, and at a station remote from the source the stress will not have the same Fourier spectrum in time as the original stress at the point of loading. In terms of operational calculus the response is described by a double transform (in space and time).

Efforts to solve transient problems in elasticity which involve dispersion have been impeded by the complex forms of the frequency equations for even the simplest boundary conditions. Closed form solutions are not

possible with the mathematical tools available. Two distinct methods of approximation have been used in the literature:

1. Approximation of formal exact solutions

The double inverse transform which represents the formal solution of a transient problem can be approximated by restricting interest to particular regions of time and space. For the far field (large time and station) the integrals can be estimated by summing the normal mode solutions making use of methods such as stationary phase and saddle point integration. For the near field and short time information ray theory and wave front expansions are possible.

For moderate values of the spacial and time variables these integrals have eluded approximation.

2. Approximation of the governing equations

Returning to the formulation of the governing equations, it is possible with certain restrictions to incorporate boundary conditions into the governing equations. For example, the deflection of a very thin plate (thickness small compared to wave length) in steady-state, low frequency, transverse vibration will be negligibly influenced by the shear distortion and rotatory inertia of the plate elements. The maximum energy in this system is exchanged between the potential energy due to the stretching and compression of the longitudinal plate fibers and the kinetic energy due to the transverse motion of a beam section. The boundary conditions on the plate faces are incorporated by making suitable approximations. In this case all stresses and strains are assumed zero except those parallel to the mid-plane; and they are assumed proportional to the distance from the

mid-plane. Writing the equations of motion results in the classical Lagrange equation. This elementary theory has the dispersive nature of the linear elasticity theory for low frequency-long waves. More refined approximations are possible such as those found in the Timoshenko bending mechanism (8) which includes, in addition to elementary bending, the effects of shear force and rotatory inertia of the plate element on the transverse deflection. Generally, however, these higher order approximations are accompanied by an increased order in the governing differential equations. Provided the order of these equations is not too large, the transient loading problem can be solved exactly. The interpretation of these results must then be restricted in accordance with the limitations of the theory. This method of approximation was pioneered by Davies (9) when he solved the Love equation (10) for the elastic rod which includes the effects of radial inertia on the longitudinal displacement. In this case the frequency spectrum is dispersive and is in agreement with the linear elasticity theory for the rod only for low frequency-long waves. The transient response is therefore accurate only where these waves govern.

The two methods of approach are supplementary but as yet have not been used cooperatively to bring out further understanding of the complex problem of dispersive transient wave propagation. The subject under study here, of an infinite plate bounded on one side by an elastic foundation whose local deformation is proportional to the local interface stress, has afforded a good opportunity to do so. This particular boundary condition generates an unusual frequency spectrum which includes complex and imaginary wave numbers for real frequencies. As will be shown in

the present work, it is possible using approximate theories to develop methods of handling the transient response in problems based on the exact theory of linear elasticity which have similar spectra. It will also be shown that by considering the approximate theories one is able to qualitatively discuss the influence of the various parts of the spectrum on the transient response.

The direct methods of solving transient loading problems for approximate beam and plate theories of the Timoshenko type (Timoshenko (8), Uflyand (11), and Mindlin (12)) have been clearly demonstrated by Miklowitz (13, 14) using only a Laplace transform in time. Miklowitz (15) has established a systematic procedure for handling the multiple branch points existing in the Laplace transform plane that occur in this method of solution. Later Jones (16) used a method of handling these problems which made use of a Fourier transform in the spacial variable and did not require the consideration of the existing branch points.

The former method followed by Miklowitz, though requiring some branch point analysis, is shown here to have distinct advantages for interpreting the various modal contributions.* It is also shown here that the integrals generated in this method are easily transformed to different integrals that retain this interpretation but lend themselves to rapid numerical computation for long time solutions. A direct application of this method can be adapted to the solution of the exact problem where the frequency spectrum is known.

* An inversion path is used which is similar to that used by Miklowitz (15) in a related problem for compressional waves in a rod.

The relation of these two methods of solution is discussed in detail later in terms of the spectrum and associated wave dispersion. In particular the behavior of the complex and imaginary wave numbers and their role in the transient response is considered in both methods. The discovery of such general wave numbers has only recently been made. The existence of large complex wave numbers for real frequency was first established by Adem (17) in 1954 in his study of the Pochhammer frequency equation for axially symmetric waves in an elastic rod. Mindlin and Onoe (18) described in more general detail the nature of similar roots found in the Rayleigh-Lamb frequency equation and higher order approximate theories of the free elastic plate. The influence of these complex modes on the steady state vibration of a free elastic plate in symmetric excitation have been discussed by Gazis and Mindlin (19) and related to the experimental results of Shaw (20). Both experimentally and theoretically a characteristic edge frequency was observed, which arises as a result of coupling between the real extensional mode and the modes corresponding to two complex wave numbers at that frequency. In reference 19 a straight-crested extensional wave is considered to impinge normally on a free edge of a plate. The resulting amplitude of the reflected extensional wave and the "complex waves" necessary to satisfy the boundary condition are shown. At the edge frequency this incident wave gives rise to a maximum "complex wave" amplitude (approximately eight times the incident wave amplitude for Poisson's ratio $\nu = .31$). The amplitude of the displacements from this mode decays exponentially from the edge in agreement with the complex wave number associated with this

frequency. The transient influence of these edge modes, however, has not been investigated.

The higher order approximate theory developed for the lowest three modes of the symmetric excitation of a plate by Mindlin and Medick (21) do not lend themselves to easy transient analysis even though they do contain the desired complex wave numbers. The present work has an advantage in this respect, since the problem of an elastic plate on an elastic foundation gives rise to these complex wave numbers in a lower order theory. These general wave numbers are studied here in detail for the cases of steady and transient wave propagation. Due to the simplicity of the approximate theory, however, there is no coupling between real and "complex waves". Therefore, a characteristic edge mode frequency does not exist for steady waves impinging on a free boundary.

I. GOVERNING EQUATIONS AND STEADY WAVE PROPAGATION CHARACTERISTICS OF AN ELASTIC PLATE ON AN ELASTIC FOUNDATION

A. Exact Theory

The equations of motion for the solid continuum can be written by considering equilibrium of a volume element (figure 1) and making use of Newton's second law, with the result

$$\frac{\partial \sigma_{ij}}{\partial x_j} + Q_i = \rho \frac{d^2 u_i}{dt^2} \quad (1)$$

where σ_{ij} is the stress tensor, Q_i the body forces per unit volume, u_i the displacements at a point defined by the Cartesian coordinates x_i , ρ the material mass density, and t the time. For a displacement component, say $u = u_1$,

$$\frac{d^2 u}{dt^2} = \underline{v} \cdot \nabla \left(\frac{\partial u}{\partial t} \right) + \frac{\partial}{\partial t} \left(\frac{\partial u}{\partial t} \right) \quad (2)$$

where \underline{v} is the position velocity vector and ∇ the gradient operator.

Imposing small strain rates and position velocity (first term on the right hand side of equation 2 small compared to second term) and neglecting the body forces reduces equation 1 to

$$\frac{\partial \sigma_{ij}}{\partial x_j} = \rho \frac{\partial^2 u_i}{\partial t^2} \quad (3)$$

Now assuming an isotropic, homogeneous, linear elastic solid, Hooke's law given by

$$\sigma_{ij} = \lambda \Delta \delta_{ij} + 2\mu \epsilon_{ij} \quad (4)$$

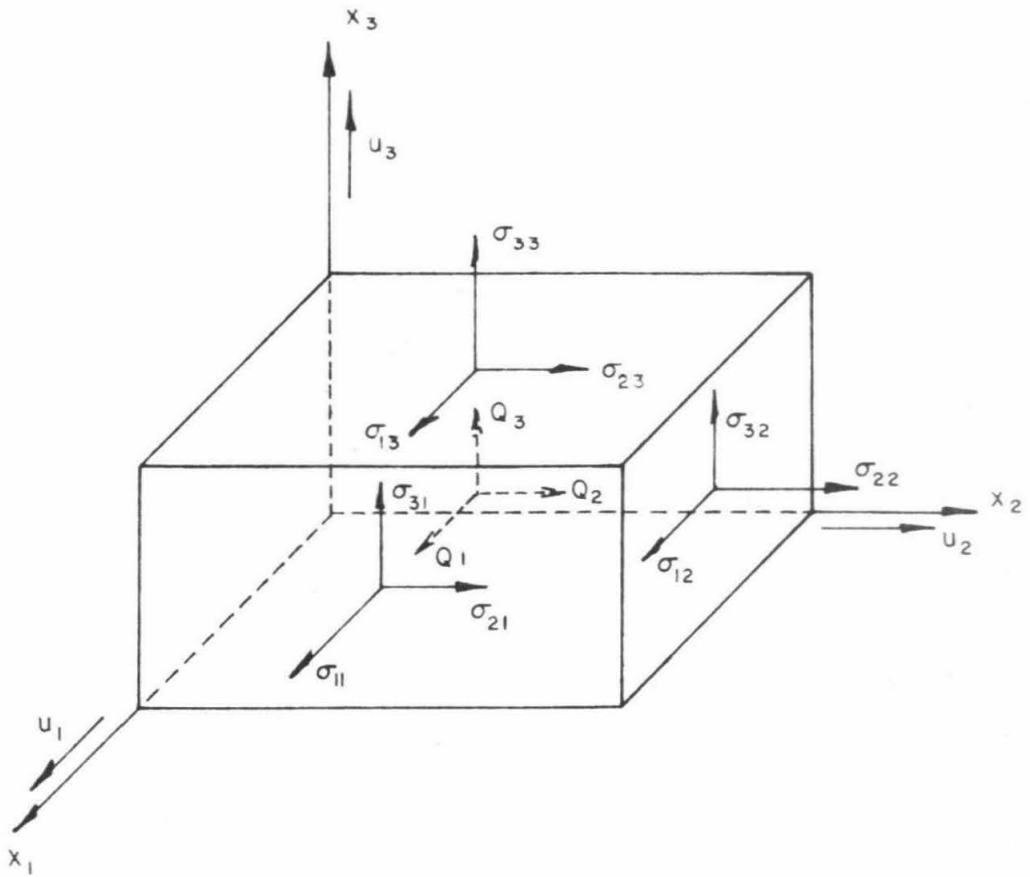


Figure 1. Volume element of solid continuum.

governs. Here ϵ_{ij} are the strains

$$\epsilon_{ij} = \frac{1}{2} \left(\frac{\partial u_i}{\partial x_j} + \frac{\partial u_j}{\partial x_i} \right)$$

and Δ the dilatation

$$\Delta = \epsilon_{ii}.$$

The quantity δ_{ij} is the Kronecker delta, and λ and μ are the Lamé constants

$$\lambda = \frac{\nu E}{(1+\nu)(1-2\nu)}, \quad \mu = \frac{E}{2(1+\nu)}$$

in which E is the modulus of elasticity, and ν is Poisson's ratio.

Substituting equation 4 into equation 3 yields, after some algebra, the displacement equations of motion

$$(\lambda + \mu) \frac{\partial \Delta}{\partial x_i} + \mu \nabla^2 u_i = \rho \frac{\partial^2 u_i}{\partial t^2} \quad (5a)$$

where ∇^2 is the Laplacian $\partial^2 / \partial x_j \partial x_j$. Equation 5a can be written in vector form

$$(\lambda + \mu) \nabla (\nabla \cdot \underline{U}) + \mu \nabla^2 \underline{U} = \rho \frac{\partial^2 \underline{U}}{\partial t^2} \quad (5b)$$

where \underline{U} is the vector displacement with components u_i . By introducing the relation

$$\nabla^2 \underline{U} = \nabla (\nabla \cdot \underline{U}) - \nabla \times \nabla \times \underline{U}$$

equation 5b is sometimes written as

$$(\lambda + 2\mu) \nabla (\nabla \cdot \underline{U}) - \mu \nabla \times \nabla \times \underline{U} = \rho \frac{\partial^2 \underline{U}}{\partial t^2} \quad (5c)$$

Using Lamé's general solution to equation 5b (or equation 5c),

$$\underline{U} = \nabla\varphi + \nabla_x \underline{\Psi} \quad (6)$$

gives the wave equations

$$\nabla^2 \varphi = \frac{1}{c_d^2} \frac{\partial^2 \varphi}{\partial t^2} \quad (7a)$$

$$\nabla^2 \underline{\Psi} = \frac{1}{c_s^2} \frac{\partial^2 \underline{\Psi}}{\partial t^2} \quad (7b)$$

where φ is a scalar potential and $\underline{\Psi}$ a vector potential, both being functions of position and time. The quantities c_d and c_s are the infinite medium, dilatation and equivoluminal wave velocities, respectively, given by

$$c_d^2 = \frac{\lambda + 2\mu}{\rho}, \quad c_s^2 = \frac{\mu}{\rho}$$

Equations 7a and 7b, together with the appropriate boundary and initial conditions, can be used to derive a unique solution to a problem involving a bounded, isotropic, elastic solid. Problems of this nature are of interest here. In particular, for the plate and beam, equations 7a and 7b for plane strain become

$$\nabla^2 \Phi = \frac{1}{a^2} \frac{\partial^2 \Phi}{\partial \tau^2} \quad (8a)$$

$$\nabla^2 \underline{\Psi} = \frac{\partial^2 \underline{\Psi}}{\partial \tau^2} \quad (8b)$$

where

$$\nabla^2 = \frac{\partial^2}{\partial \xi^2} + \frac{\partial^2}{\partial \zeta^2}$$

The Cartesian coordinates for the plate are shown in figure 2. The related displacements and stresses are given by

$$W = \frac{u_z}{h} = \frac{\partial \Phi}{\partial \zeta} + \frac{\partial \Psi}{\partial \xi} \quad (9a)$$

$$\frac{u_x}{h} = \frac{\partial \Phi}{\partial \xi} - \frac{\partial \Psi}{\partial \zeta} \quad (9b)$$

$$\sigma_{\zeta\zeta} = \frac{\sigma_{zz}}{\mu} = \left(1 - \frac{2}{a^2}\right) \frac{\partial^2 \Phi}{\partial \tau^2} + 2 \left(\frac{\partial^2 \Phi}{\partial \zeta^2} + \frac{\partial^2 \Psi}{\partial \zeta \partial \xi} \right) \quad (10a)$$

$$\sigma_{\xi\xi} = \frac{\sigma_{xx}}{\mu} = 2 \frac{\partial^2 \Phi}{\partial \zeta \partial \xi} - \frac{\partial^2 \Psi}{\partial \zeta^2} + \frac{\partial^2 \Psi}{\partial \xi^2} \quad (10b)$$

where

$$\Phi = \frac{\varphi}{h^2}, \quad \Psi = \frac{\psi}{h^2}$$

$$\tau = \frac{tc_s}{h}, \quad \zeta = \frac{z}{h}, \quad \xi = \frac{x}{h}$$

$$a^2 = \frac{c_d^2}{c_s^2} = \frac{2(1-\nu)}{(1-2\nu)}$$

and h is the plate thickness.

Frequency Spectrum

The frequency equation for an infinite plate resting on a foundation has been derived by Das Gupta (5) using the equations from linear elasticity theory. The boundary conditions for this problem require that one face of the plate be traction free and the other face be free of shear

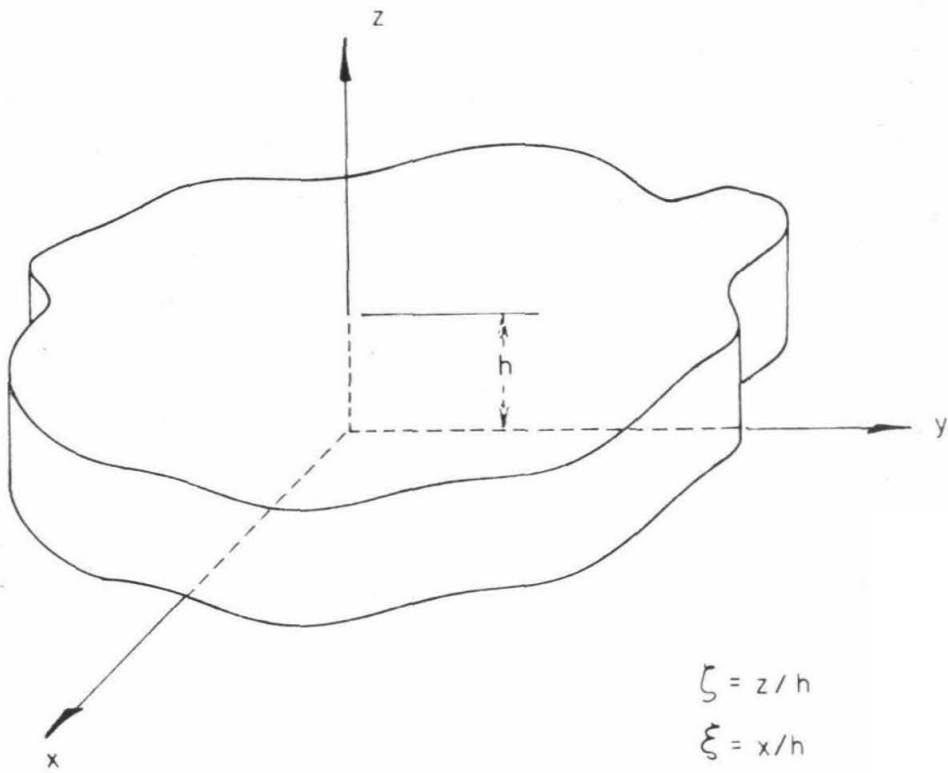


Figure 2. Cartesian coordinates for a plate.

stress but subject to a normal stress proportional to the displacement of that face:

$$\left. \begin{aligned} \sigma_{\xi\xi} &= 0 & \text{at } \xi &= 0, 1 \\ \sigma_{\xi\xi} &= 0 & \text{at } \xi &= 1 \\ \sigma_{\xi\xi} &= \frac{-K_e W}{\mu h} & \text{at } \xi &= 0 \end{aligned} \right\} \quad (11)$$

where K_e is the spring foundation constant with dimensions of force per unit area per unit deflection. Assuming solutions of equations 8a and 8b in the form of straight-crested (plane strain) traveling wave trains, propagating in the positive ξ direction, the potential functions are of the form

$$\Phi = \left[A_1 \cosh a\xi + A_2 \sinh a\xi \right] e^{i(\Gamma\xi - \pi\Omega\tau)} \quad (12a)$$

$$\Psi = \left[A_3 \cosh \beta\xi + A_4 \sinh \beta\xi \right] e^{i(\Gamma\xi - \pi\Omega\tau)} \quad (12b)$$

where

$$a^2 = \Gamma^2 - \left(\frac{\pi\Omega}{a} \right)^2, \quad \beta^2 = \Gamma^2 - (\pi\Omega)^2$$

$$\Gamma = \gamma h = X + iY, \quad \Omega = \omega/\omega_s, \quad \omega_s = \frac{\pi c_s}{h}$$

and γ is the wave number and ω the angular frequency. Substitution into the boundary conditions 11, making use of equations 12a, 12b and 9a, results in a set of four equations in the four unknowns A_1 , A_2 , A_3 and A_4 . A non-trivial solution results by setting the determinant of the coefficients equal to zero. The resulting characteristic equation gives an implicit functional relationship between the wave number and the frequency, which describes the dispersive nature of the system. A convenient form of this equation is given by

$$\begin{aligned} & \frac{\pi^2 h}{\mu} K_e a \Omega^2 \left[\theta_1^2 \tanh \beta - \theta_2 \tanh a \right] \\ &= \frac{(1 + \cosh a)(1 + \cosh \beta)}{\cosh a \cosh \beta} \left[\theta_1^2 \tanh \frac{a}{2} - \theta_2 \tanh \frac{\beta}{2} \right] \left[\theta_1^2 \tanh \frac{\beta}{2} - \theta_2 \tanh \frac{a}{2} \right] \end{aligned} \quad (13)$$

where

$$\theta_1 = 2 \Gamma^2 - (\pi \Omega)^2, \quad \theta_2 = 4a\beta \Gamma^2$$

The most interesting feature of this equation is the symmetry it exhibits of the displacements about the base of the foundation. Consider, for example, a sandwich of two flat plates separated by an elastic layer, figure 3. All displacements can be assumed symmetric about the center plane. For an infinite spring constant equation 13 reduces to the Rayleigh-Lamb frequency equation for symmetric straight-crested waves in a free plate of thickness $2h$. At the other extreme for $K_e = 0$ equation 13 reduces to the Rayleigh-Lamb frequency equation for both symmetric and anti-symmetric waves for a free plate of thickness h . The behavior of the frequency equation for intermediate ranges of K_e must exhibit this transition of modes.

It is interesting to note that for very high frequencies, the term containing the K_e becomes negligible compared with the remaining term. This means that for any finite foundation stiffness the spectrum representing equation 13 must approach the spectrum of a free plate in the limit for very high frequencies. This characteristic can be observed for small foundation stiffnesses at fairly low frequencies.

The frequency spectrum of equation 13 for steady state analysis is described physically only for Ω real. Imposing this condition the cutoff

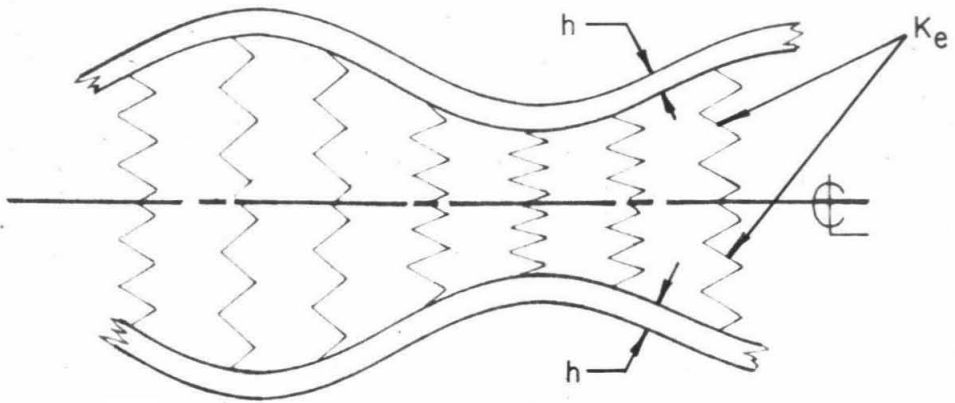


Figure 3. Sandwich of two plates in symmetric wave excitation.

frequencies, which are characteristic of infinitely long waves, can be found by setting $\Gamma = 0$ and are given by

$$\Omega_n = n, \quad n = 1, 2, 3, \dots \quad (14a)$$

and the roots of

$$\frac{\pi\Omega_m}{a} \tan \frac{\pi\Omega_m}{a} = \frac{K_e h}{2\mu}, \quad m=0, 1, 2, \dots \quad (14b)$$

The frequencies given by equation 14a are independent of the foundation stiffness and indicate a thickness-shear motion* at the cutoff which is independent of an applied normal force. Only the cutoff frequencies from equation 14b depend on the foundation stiffness. These cutoff frequencies vary from $\Omega = am$ to $\Omega = a(m + \frac{1}{2})$ as the foundation stiffness increases from zero to infinity. No cutoff frequencies depending on the foundation stiffness are found in the range $a(m + \frac{1}{2}) < \Omega < a(m+1)$ since this would require a negative spring constant which is not permissible physically.

These cutoff frequencies which depend on the foundation hardness are the limiting long wave, symmetric thickness-stretch mode frequencies for the system indicated in figure 3. For very small foundation hardness these cutoff frequencies are given by

$$\text{and } \left. \begin{aligned} \Omega_0 &= \left[\frac{K_e h}{\pi^2 \mu} \right]^{1/2} \quad \text{or} \quad \omega = \left[\frac{K_e}{h \rho} \right]^{1/2} \\ \Omega_m &= ma + \frac{K_e h}{a \mu m \pi^2} \quad m=1, 2, 3, \dots \end{aligned} \right\} \quad (15)$$

* The classification of the various plate motions at the cutoff frequencies have been presented by Mindlin (7). Thickness-shear denotes elemental motions that give rise to transverse shear and are parallel to the mid-plane. Thickness-stretch describes motions normal to the mid-plane.

The first of equation 15 corresponds to the one degree of freedom spring-mass oscillator where the entire plate vibrates as a rigid mass. The second of equation 15 shows a small perturbation due to the spring foundation which slightly increases the m^{th} symmetric thickness-stretch mode cutoff frequency for a plate of thickness h . As the foundation stiffness increases to infinity this cutoff frequency becomes the $(m+1)^{\text{th}}$ symmetric thickness-stretch mode frequency for a plate of thickness $2h$.

The frequency spectrum transition is sketched in figures 4 through 7 showing real and imaginary arms* for four foundation stiffnesses and Poisson's ratio $\nu = .31$ ** (Real arms which have negative slope are actually associated with negative wave numbers and are shown with positive wave numbers for convenience.) Figure 4 shows the symmetric wave branches (solid lines) and antisymmetric wave branches (dotted lines) of the Rayleigh-Lamb frequency equation for a free plate of thickness h . Figure 7 shows the symmetric wave branches of the Rayleigh-Lamb frequency equation for a free plate of thickness $2h$. The dotted portions of the curves in figure 7 indicate their antisymmetric wave origin. The transition mechanism is indicated in figures 5 and 6.

Note the exchange of arms of the different branches in figure 5. This phenomenon has been observed for the symmetric Rayleigh-Lamb

* The terminology used to identify the parts of the spectrum follows that given by Mindlin and Onoe (18): a group of intersecting curves of wave number against real frequency is called a branch, and the real, imaginary, and complex portions of such a branch are its arms. Each real arm is associated with a particular mode of wave transmission.

** This value of Poisson's ratio has been used in order to facilitate comparison to the complete spectrum for a free plate sketched in reference 18. Figures 4 and 7 are reproduced from that reference.

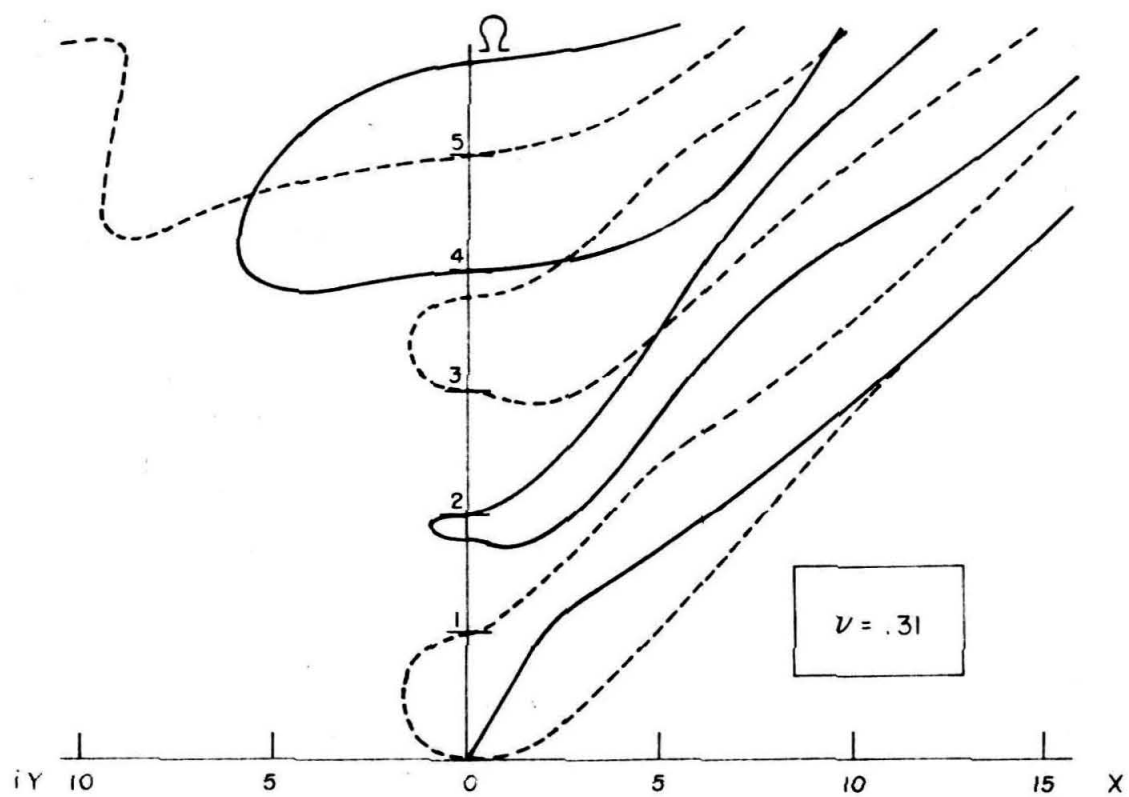


Figure 4. Frequency spectrum for no foundation.

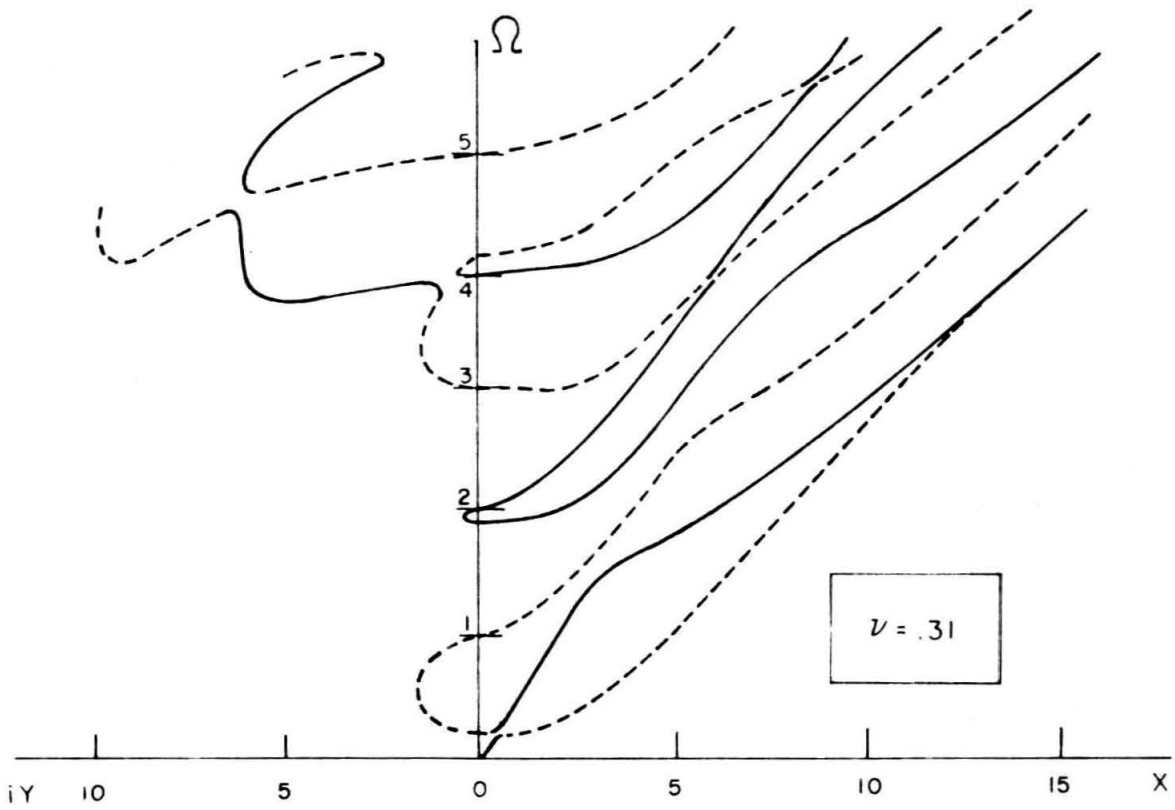


Figure 5. Frequency spectrum for a soft foundation.

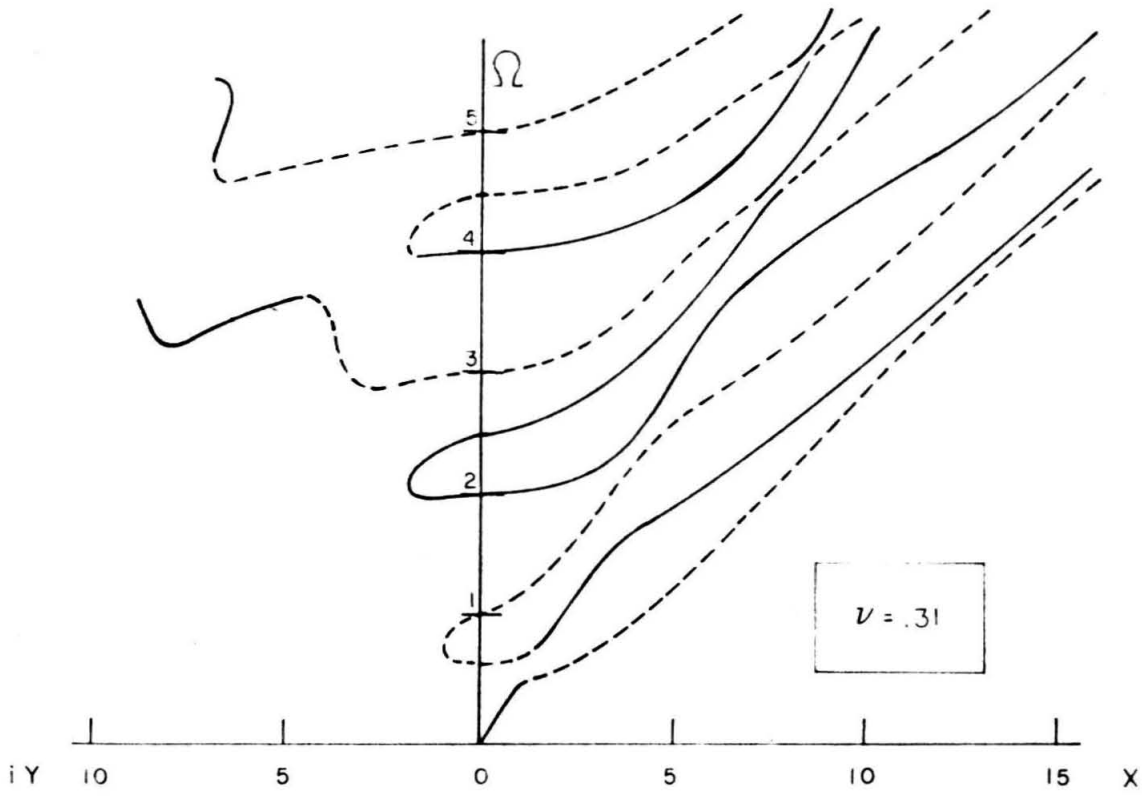


Figure 6. Frequency spectrum for a hard foundation.

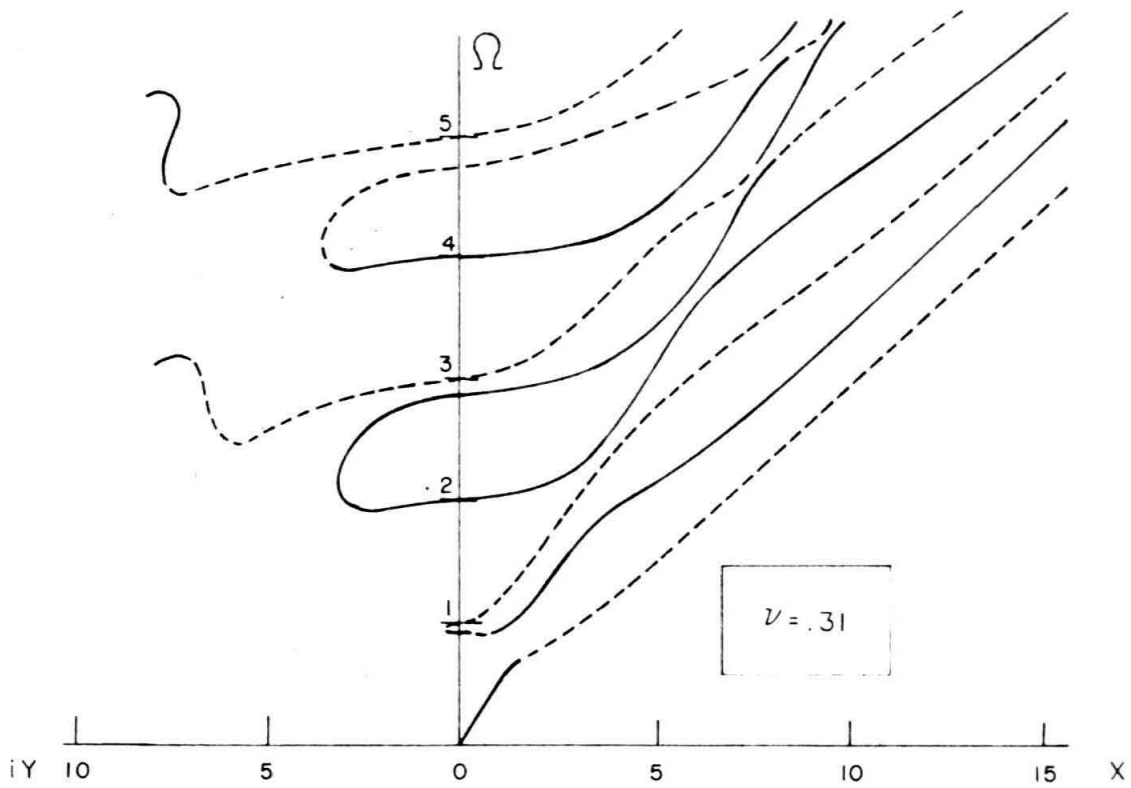


Figure 7. Frequency spectrum for a rigid foundation.

spectrum by Mindlin and Onoe (18) for varying Poisson's ratio, where the effect of increasing Poisson's ratio is similar to that found for increasing spring stiffness. This is in agreement with the qualitative nature of Poisson's ratio. Further comparison between the influence of a foundation and Poisson's ratio is reflected by the cutoff frequency dependence on Poisson's ratio. For example, consider a foundation stiffness $K_e = \infty$. The cutoff frequencies given by equations 14a and 14b are then the cutoff frequencies for the symmetric spectrum for a plate of thickness $2h$. Equation 14a remains unchanged and the associated frequency is independent of Poisson's ratio as it was for the case of a spring foundation. Equation 14b becomes

$$\Omega_m = \frac{ma}{2} \quad m = 1, 2, \dots$$

and shows the frequency dependence on \underline{a} and consequently on Poisson's ratio. Differentiation shows that

$$\frac{d\Omega_m}{dv} > 0$$

This shows that the cutoff frequency Ω_m increases with increasing Poisson's ratio; a dependence on foundation stiffness already established.

The lowest three branches of the spectrum for equation 13 were calculated using an IBM 709 computer and are shown in detail in figures 8 through 12 for five foundation hardnesses and Poisson's ratio $\nu = .35$.^{*} The spectrum is composed of real, imaginary, and complex arms. The real arm emanating from the lowest cutoff frequency, and its associated complex arm, have been shown reflected in the plane $X = 0$ and superimposed on a second complex arm. For

* This Poisson's ratio permits the study of a typical interchanging of two real arms of the same branch without resorting to the investigation of higher modes. The exchange is anticipated for $\nu > 1/3$, since at $\nu = 1/3$, the critical Poisson's ratio, the first two cutoff frequencies of the symmetric Rayleigh-Lamb spectrum are equal.

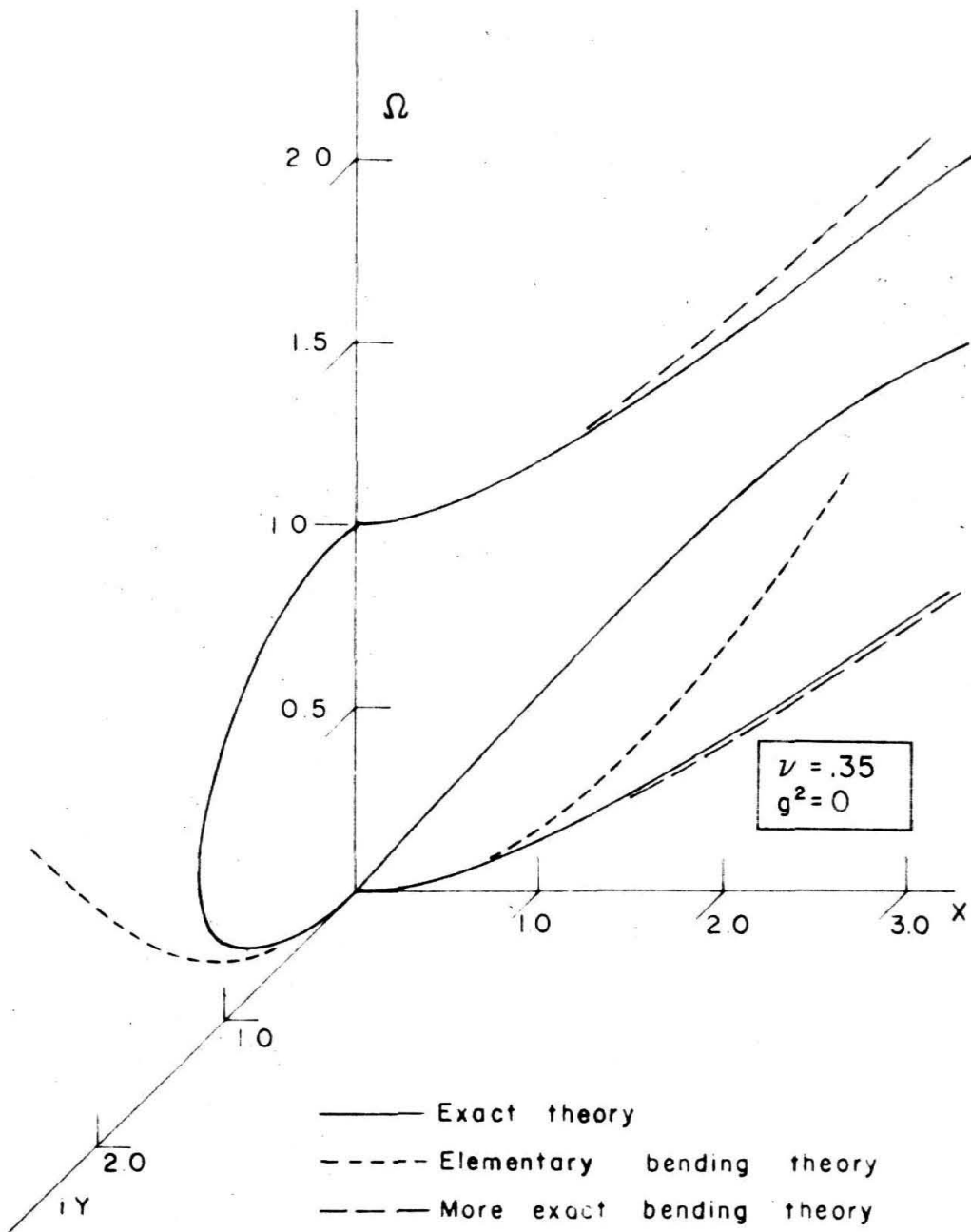


Figure 8. Frequency spectrum for no foundation.

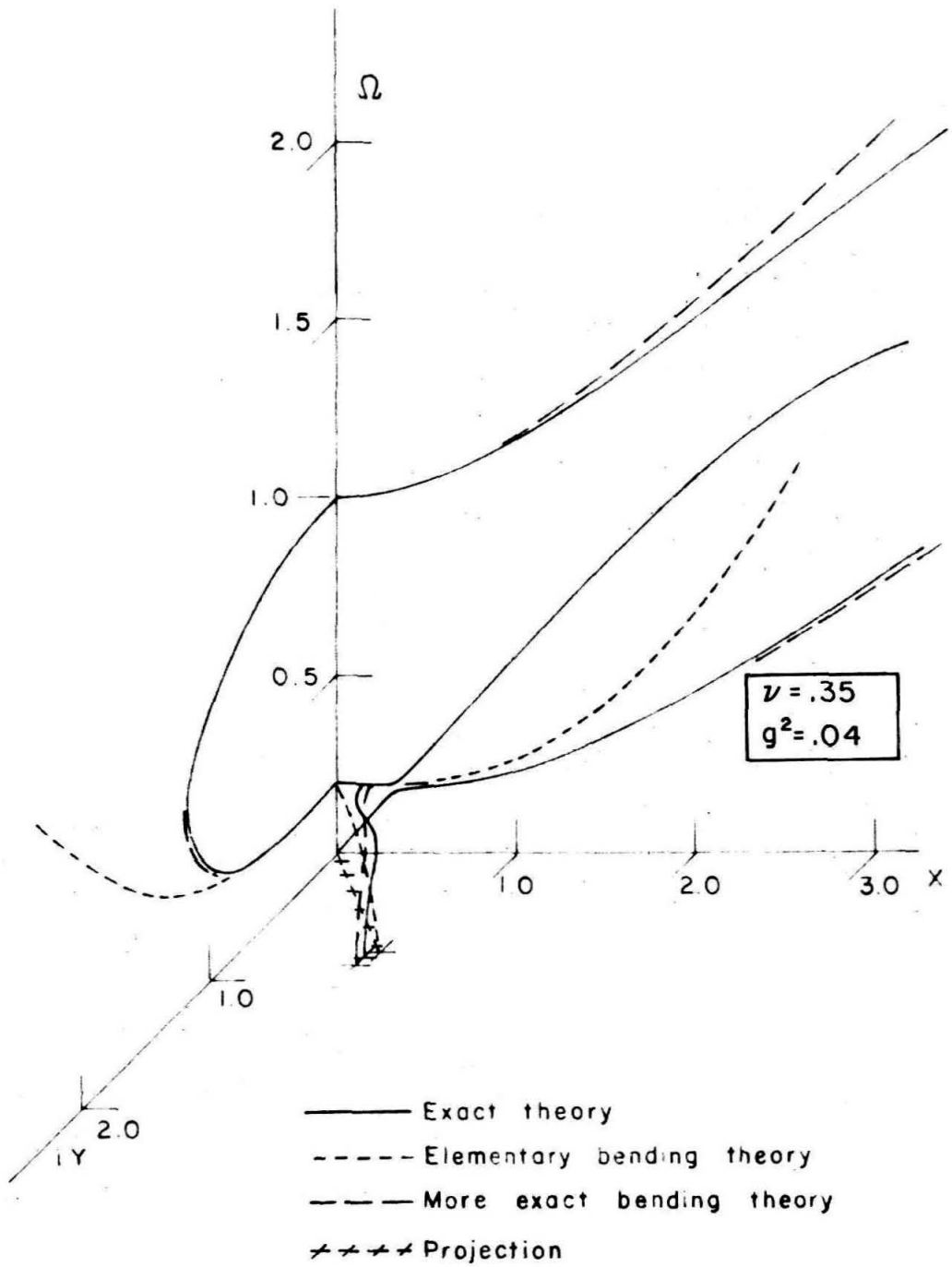


Figure 9. Frequency spectrum for a soft foundation.

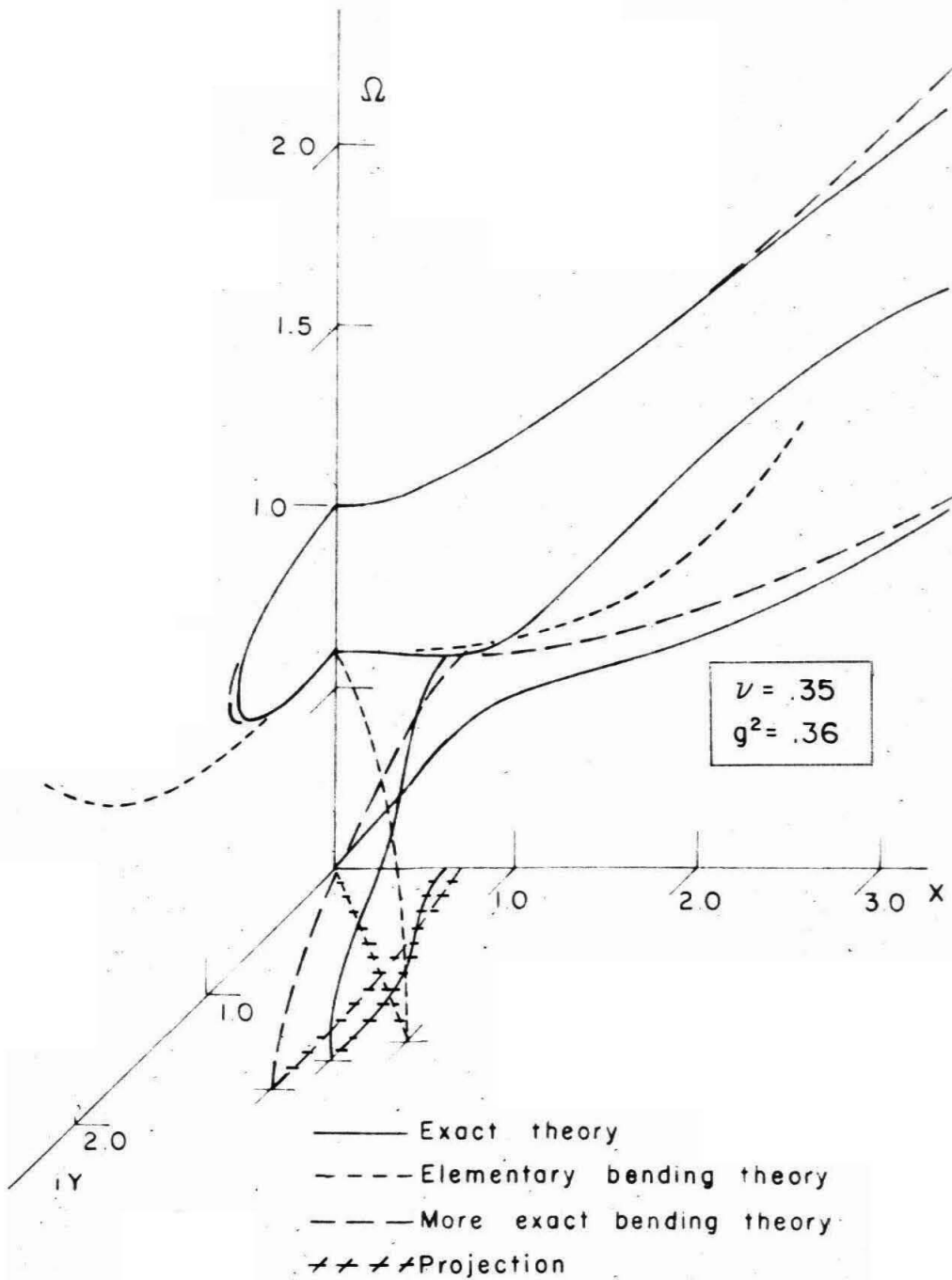


Figure 10. Frequency spectrum for an intermediate foundation stiffness.

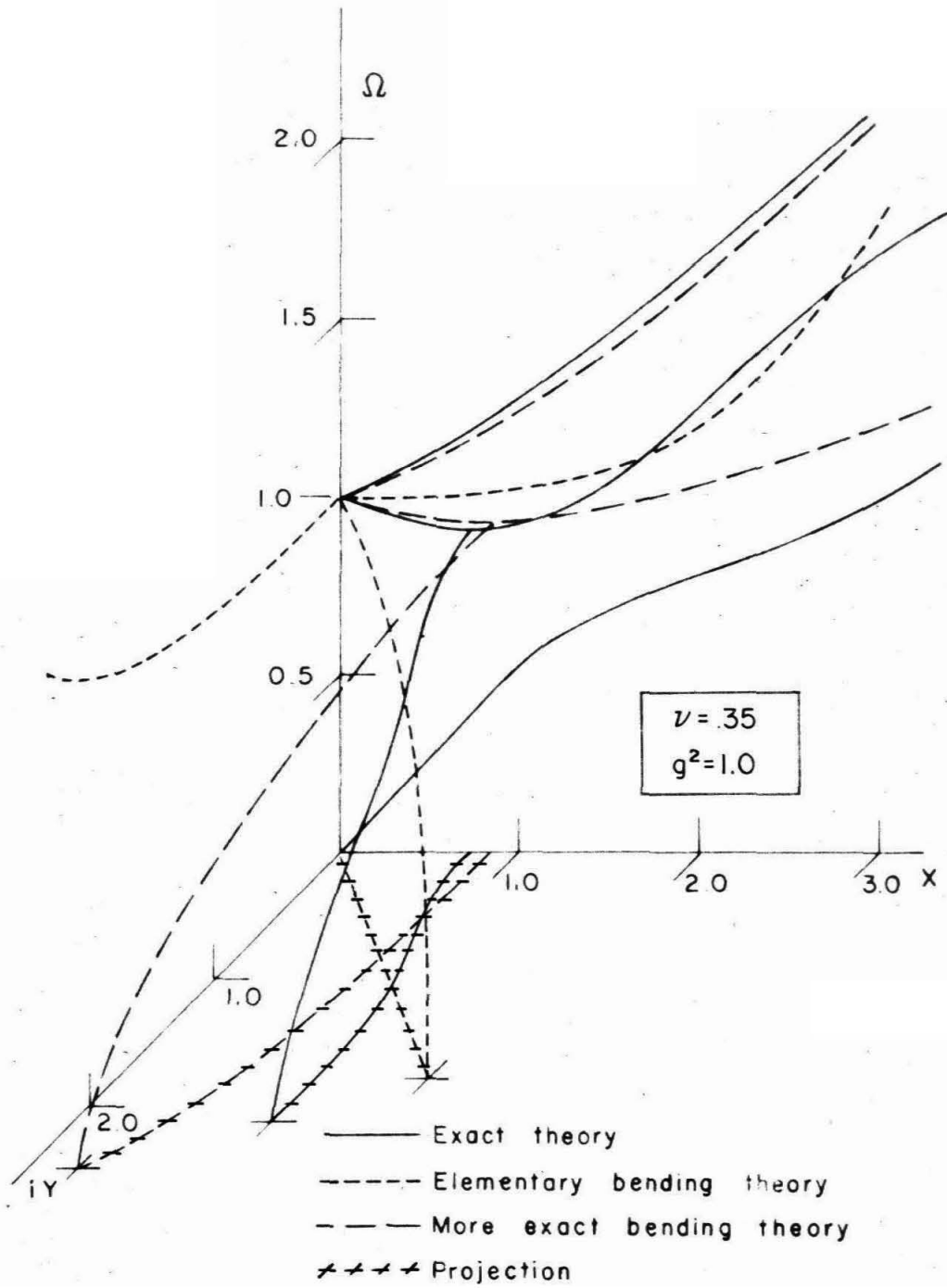


Figure 11. Frequency spectrum for a hard foundation.

simplification in comparing these spectra with the approximate theories, to be discussed later, only the lowest cutoff frequency $\Omega = g$ is listed in each figure. The foundation stiffness corresponding to a given cutoff frequency is found from equation 14b. Figure 8, which is for $g = 0$ ($K_e = 0$), shows the lowest symmetric and the first two antisymmetric modes of a free plate of thickness h . Figure 12 is for an infinite foundation hardness and reflects the lowest three symmetric modes of a plate of thickness $2h$. Figures 9, 10 and 11 show in detail how the transition previously mentioned takes place. For very small foundation stiffness the lowest mode which has its origin at $\Omega = \Gamma = 0$ behaves like a symmetric dilatation mode until a frequency slightly less than the cutoff frequency $\Omega = g$. At this point it bends sharply and now associates itself with what used to be a purely antisymmetric mode (but now a symmetric mode with respect to the base of the foundation). The real arm emanating from the lowest cutoff frequency now has a minimum and an associated complex arm. For increasing wave number the real arm then bends to associate itself with what used to be a purely symmetric mode.

The characteristics of the arms are discussed with generality in Appendix A for frequency equations like 13. The only information required to describe the arm intersections is the order N of the first nonzero derivative at these intersections. Expansion in the neighborhood of the lowest cutoff frequencies shows that $N = 2$ except for the third branch when $g^2 = 1$. In this special case the first derivative is nonzero and no imaginary arm exists. The value of N at the intersection of the complex

arm with the second real arm can be deduced to be $N = 2$ from the corresponding intersection in the symmetric spectrum for a free plate (see reference 18 and figures 8 to 12). Further details may be found in Appendix A.

B. Approximate Theories

1. Elementary Theory

The deflection equation of motion from the classical theory for the bending of a thin plate (Lagrange's equation) is given by

$$D \nabla^2 \nabla^2 w + \rho h \frac{\partial^2 w}{\partial t^2} = q \quad (16)$$

where w is the mid-plane deflection of the plate, D is the plate modulus given by $Eh^3/12(1-\nu^2)$, and q is the transverse loading per unit area. The first term of equation 16 accounts for the shear force due to bending and the second term is due to the transverse inertia of a plate element.

For a plate resting on a foundation of stiffness K , q is given by

$$q = -Kw \quad (17)$$

Substituting equation 17 into equation 16, and writing the result in dimensionless form, gives

$$\nabla^2 \nabla^2 W + \zeta^2 g^2 W + \zeta^2 \frac{\partial^2 W}{\partial \gamma'^2} = 0 \quad (18)$$

where

$$W = w/h, \quad \gamma' = \frac{ect}{h}, \quad c_p^2 = E/\rho(1-\nu^2)$$

$$\zeta^2 = c^2/c_p^2, \quad g^2 = hK/(e^2 \rho c^2), \quad e^2 = 12$$

The $\nabla^2 \nabla^2$ operator is made dimensionless using variables like $\xi' = \frac{ex}{h}$.

The quantity c is an arbitrary velocity at this point, but is introduced to

facilitate comparison of frequency spectra.

Equation 18 is the same for a Bernoulli-Euler beam (classical theory) on an elastic foundation if the $\nabla^2 \nabla^2$ operator is replaced by $\partial^4 / \partial \xi^4$ and the following parameters are redefined:

$$c_p^2 = \frac{E}{\rho}, \quad K = \frac{hK_b}{A_b}, \quad e^2 = \frac{A_b h^2}{I} \quad (19)$$

where K_b is the spring constant of the beam foundation with dimensions force per unit length per unit deflection, A_b the beam cross section, I the moment of inertia of this section about the neutral axis of bending, and h/e the radius of gyration of the beam cross section.

Frequency Spectrum

In the usual manner the frequency spectrum for equation 18 is found by assuming a solution in the form of a straight-crested traveling wave train

$$W = A e^{i(\Gamma' \xi' - \Omega \tau')} \quad (20)$$

where Γ' , the dimensionless wave number, and Ω , the dimensionless frequency, are given by

$$\Omega = \frac{h\omega}{ec}, \quad \Gamma' = \frac{\gamma h}{e} = \frac{1}{e} (X + iY) \quad (21)$$

and A is a constant.

Substituting equation 20 into equation 18 gives the frequency equation

$$\Gamma'^4 = \zeta^2 (\Omega^2 - g^2) \quad (22)$$

Since interest is confined to only real values of Ω , the four roots of equation 22 may be real or imaginary for $\Omega^2 > g^2$ and are complex for

$\Omega^2 < g^2$. Only two distinct roots exist since the remaining two are the negative of the first two. The two roots considered will be those which are positive real and positive imaginary for $\Omega^2 > g^2$, corresponding to waves traveling in the positive ξ^1 -direction and standing waves decaying exponentially in the positive ξ^1 -direction, respectively. These branches may be traced without ambiguity to frequencies below g by examining equation 22 in the neighborhood of its branch point, $\Omega = g$. Here, $d^4\Omega / d\Gamma'^4$ is the first nonzero derivative, i.e., $N = 4$. Reference to Appendix A shows that the complex arm associated with the real arm falls in the first Γ' -quadrant and makes an angle of $\pi/4$ with the Γ' -axes. The complex arm related to the imaginary arm is in the second Γ' -quadrant, and when reflected in the plane $X = 0$ falls on the other complex arm. The frequency spectra for equation 22 may be compared with those from the exact theory by noting, for a plate of thickness h , the dimensionless frequencies are equivalent and $\Gamma'^2 = 12 \Gamma'^2$ if $c^2 = \frac{\pi^2}{12} c_s^2$. Using this equivalence equation 22 is plotted in figures 8 through 12 for $\nu = .35$ as indicated. The cutoff frequencies are the same as those given by equation 14b provided the foundation stiffness in the classical theory has been adjusted by using the relation

$$\frac{K}{K_e} = \frac{\frac{\pi g}{a}}{\tan \frac{\pi g}{a}} \quad (23)$$

It is well known that the classical theory is a good approximation only for low frequencies and long waves. Therefore, comparison of the elementary theory with the exact spectrum must necessarily be confined to this region. The introduction of a finite cutoff frequency and a complex arm, with the

addition of an elastic foundation, is the important feature here. This cutoff frequency is again due to the uniform oscillation of the plate on the foundation and is given by

$$\omega = \left[\frac{K}{h\rho} \right]^{1/2} \quad (24)$$

If small frequency, wave number, and foundation hardness are imposed on equation 13, the lowest mode of equation 13 which possesses a cutoff frequency approaches equation 22 for a plate. This limit is indicated in figure 9. Furthermore, the correction factor for the foundation hardness, equation 23, approaches one. For cutoff frequencies higher than $a/2$ the classical theory has no exact theory counterpart, because K_e would have to be negative according to equation 14b.

2. More Exact Theory of Bending

A more accurate deflection equation of motion than equation 16 was contributed by Uflyand (11), whose plate theory is the analog of the Timoshenko beam theory, and which includes in a similar manner the effects of shear force and rotatory inertia of the plate element on the deflection. A more complete analysis of this theory, including a statement of admissible end conditions, was presented later by Mindlin (12). The governing equations for the case of zero in-plane rotation, as given in a recent paper by Miklowitz (22) are

$$D \nabla^2 w_b + k' \mu h w_s - \rho \frac{h^3}{12} \frac{\partial^2 w_b}{\partial t^2} = 0 \quad (25a)$$

$$k' \mu \nabla^2 w_s + \frac{q}{h} - \rho \frac{\partial^2}{\partial t^2} (w_s + w_b) = 0 \quad (25b)$$

where w_b and w_s are the coupled deflections ($w_T = w_s + w_b$) resulting from bending and shear, respectively, figure 13. The quantity k' is a shear correction factor. ∇^2 is the two-dimensional operator for cylindrical symmetry, $\frac{1}{r} \frac{\partial}{\partial r} (r \frac{\partial}{\partial r})$ or the one-dimensional operator $\partial^2 / \partial x^2$.

Equation 25a is the equation of rotational equilibrium for the plate element where the first term is the moment due to bending, the second term is the moment due to the transverse shear, and the last term is the moment due to the rotatory inertia. Equation 25b is the equation of transverse equilibrium where the first term is the force due to transverse shear on a plate element, and the last term is the force due to the transverse inertia. The plate shear force (per unit length) and moments (per unit length) are given by

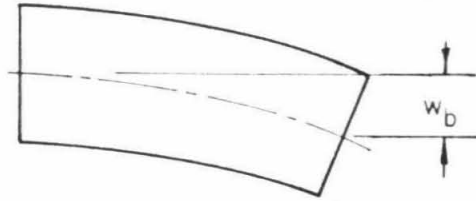
$$S = \int_{-\frac{h}{2}}^{\frac{h}{2}} \sigma_{rz} dz$$

$$M_r = \int_{-\frac{h}{2}}^{\frac{h}{2}} \sigma_r z dz$$

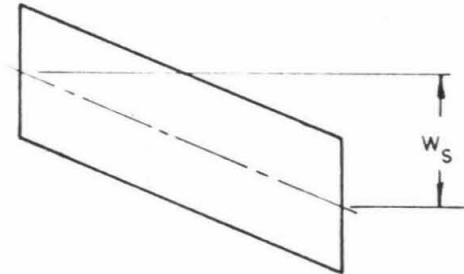
$$M_\theta = \int_{-\frac{h}{2}}^{\frac{h}{2}} \sigma_\theta z dz$$

for cylindrical symmetry

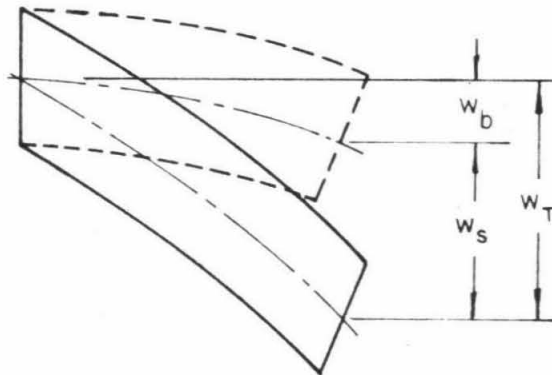
and



(a) bending deflection



(b) shear deflection



(c) total deflection

Figure 13. Coupled deflections resulting from bending and shear for the more exact theory of bending.

$$\left. \begin{aligned}
 S &= \int_{-\frac{h}{2}}^{\frac{h}{2}} \sigma_{xz} dz \\
 M_x &= \int_{-\frac{h}{2}}^{\frac{h}{2}} \sigma_x z dz
 \end{aligned} \right\} \text{for plane strain}$$

where z is the plate thickness coordinate. The shear force- and moment-displacement relations are given by

$$\left. \begin{aligned}
 S &= -k' \mu h \frac{\partial w_s}{\partial r} \\
 M_r &= -D \left[\frac{1}{r} \frac{\partial w_b}{\partial r} + \nu \frac{\partial^2 w_b}{\partial r^2} \right] \\
 M_\theta &= -D \left[\frac{\partial^2 w_b}{\partial r^2} + \frac{\nu}{r} \frac{\partial w_b}{\partial r} \right]
 \end{aligned} \right\} \text{for cylindrical symmetry}$$

and

$$\left. \begin{aligned}
 S &= -k' \mu h \frac{\partial w_s}{\partial x} \\
 M_x &= -D \frac{\partial^2 w_b}{\partial x^2}
 \end{aligned} \right\} \text{for plane strain}$$

The primary limiting assumptions made in the derivation of equations 25a and 25b are:

1. Straight line elements normal to the mid-plane of the unstressed plate remain straight when the plate is deflected.

2. Variations of the transverse shear and inertia over the cross section are neglected.

This assumes that only the lowest antisymmetric thickness-shear mode of the plate motion is considered. In this assumption shear distortion over the plate thickness is taken into account only through an average. This results in a theory applicable to cases involving only moderately high frequencies and moderately short waves.

Again the transverse loading is assumed to be of the form

$$q = -K(w_s + w_b)$$

where K is defined the same as in equation 17. The dimensionless forms of equations 25a and 25b are

$$\nabla^2 W_b + \mathcal{G}^2 W_s - \int^2 \frac{\partial^2 W_b}{\partial \gamma'^2} = 0 \quad (26a)$$

$$\nabla^2 W_s - g^2 (W_s + W_b) - \frac{\partial^2}{\partial \gamma'^2} (W_s + W_b) = 0 \quad (26b)$$

where

$$W_s = w_s/h, \quad W_b = w_b/h$$

$$c^2 = k' \frac{\mu}{\rho}, \quad \mathcal{G}^2 = \frac{c^2}{c_p^2} = \frac{k'}{2} (1-\nu)$$

The remaining terms are the same as defined for equation 18. Also if the ∇^2 operator is replaced by $\partial^2/\partial \xi'^2$ and the constants are defined by equation 19, equations 26a and 26b describe the motion of a Timoshenko beam on an elastic foundation.

The beam shear force and moment are given by

$$S = \iint_{A_b} \sigma_{xz} dA_b$$

$$M = \iint_{A_b} \sigma_x z dA_b$$

and the shear force- and moment-displacement relations are

$$S = -k' \mu A_b \frac{\partial w_s}{\partial x}$$

$$M = -EI \frac{\partial^2 w_b}{\partial x^2}$$

Frequency Spectrum

Assuming a solution in the form of straight-crested waves,

$$W_s = A_1 e^{i(\Gamma' \xi' - \Omega \tau')} \quad (27a)$$

$$W_b = A_2 e^{i(\Gamma' \xi' - \Omega \tau')} \quad (27b)$$

and substituting into equations 26a and 26b results in two algebraic equations in A_1 and A_2 . The nontrivial solution ($A_1 \neq 0 \neq A_2$) gives the frequency equation

$$\begin{vmatrix} \delta^2 & \delta^2 \Omega^2 - \Gamma'^2 \\ \Omega^2 - g^2 - \Gamma'^2 & \Omega^2 - g^2 \end{vmatrix} = 0 \quad (28)$$

This can be regarded as a biquadratic in Γ' as a function of Ω

$$\Gamma'_j{}^2 = \frac{1}{2} \left(\Omega^2 (1 + \delta^2) - g^2 \right) - (-1)^j \left[\left(\frac{\Omega^2 (1 + \delta^2)^2 - g^2}{2} \right)^2 - \delta^2 (g^2 - \Omega^2) (1 - \Omega^2) \right]^{1/2} \quad j=1, 2 \quad (29)$$

Again the dimensionless frequency and wave number are defined by

equation 21.

In general there must be four roots of equation 29, but as in the case of equation 22 only two distinct roots exist corresponding to $j=1$ and $j=2$. The roots Γ'_1 and Γ'_2 can be either real, imaginary, or complex depending on the particular parameters δ^2 and g^2 and on the value of Ω . The frequencies at which real and imaginary arms of the Γ'_j become complex correspond to the zeros of the radical in equation 29 and are given by

$$\Omega_{j*}^2 = \frac{1}{(1-\delta^2)} \left[(g^2 - 2 \frac{2}{1-\delta^2}) - (-1)^j \frac{2\delta^2}{1-\delta^2} \sqrt{1-g^2(1-\delta^2)} \right] \quad (30)$$

Since only real positive frequencies are being considered there may be zero, one, or two such transitions. Figure 14 shows this dependence as a function of δ^2 and g^2 . Regions I and II have no transitions, region III has one Ω_{*} , and region IV has two different Ω_{*} 's. General interest will be confined to III and to values of $g^2 < 1 + \delta^2$ where the one transition occurs on a real Γ' arm. This choice is dictated by the limits of Poisson's ratio of engineering interest, and the greater accuracy of the approximate theory for a softer foundation.

The branches of equation 29 which will be studied are chosen to be those, which for large Ω , have positive wave numbers. These modes can be traced for decreasing Ω by studying equation 29 in the neighborhood of the branch points as in Appendix A. It is found that the lower branch ($j=1$) has a complex arm that extends into the first Γ' -quadrant. The upper branch has two zeros on the Ω -axis at $\Omega = 1$ and $\Omega = g$. A positive imaginary arm connects these two cutoff frequencies. The arm emanating from the lower of these cutoff frequencies extends into the negative Γ' -plane. This branch has a complex arm which is the reflection in the

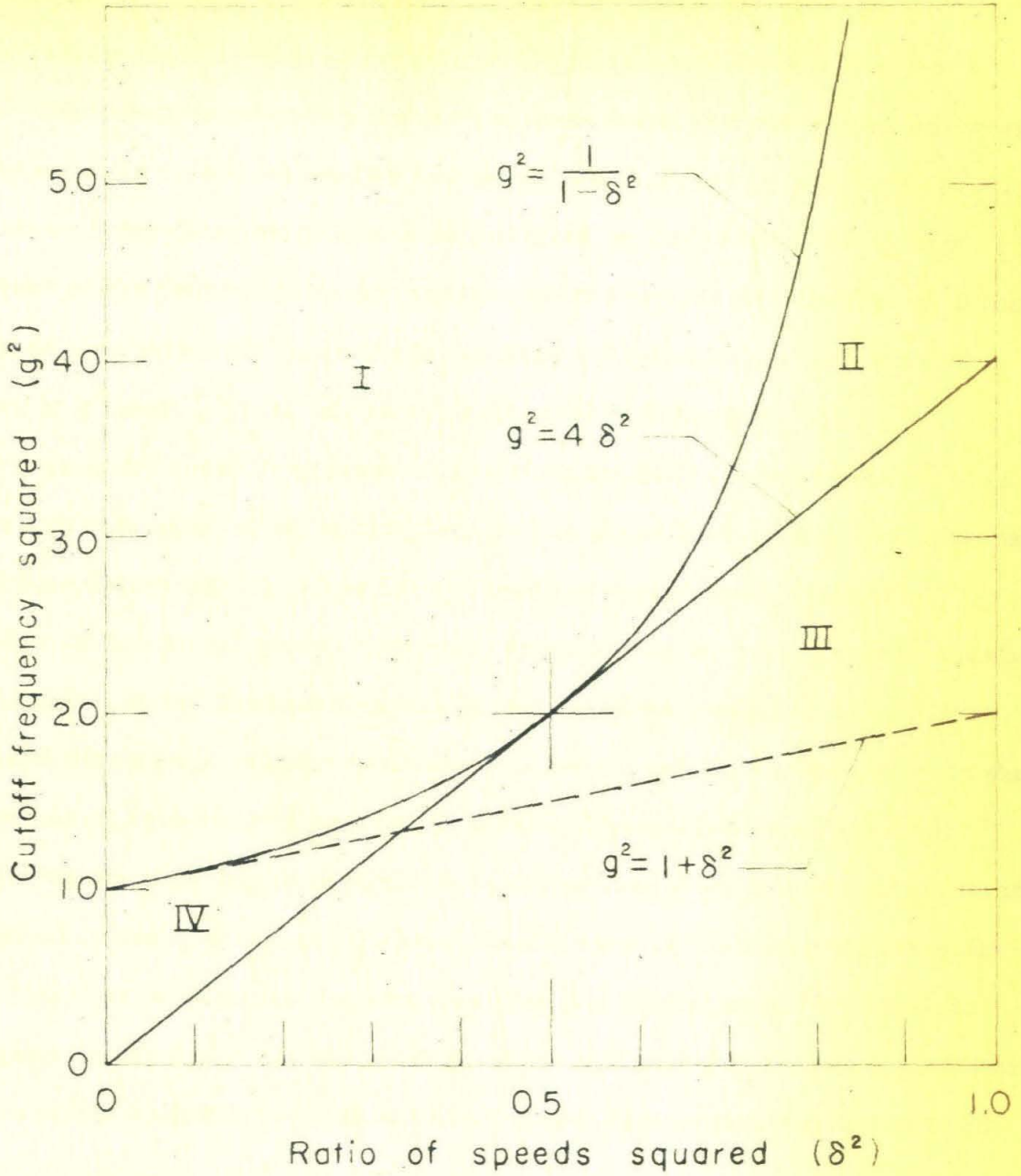


Figure 14. Regions governing number of complex branching points, Ω_* , for more exact theory of bending.

plane $X=0$ of the complex arm from the lower branch.

Figures 8 through 12 show this spectrum as indicated, again with arms having negative wave numbers being shown reflected in the plane $X=0$. The cutoff frequency which is independent of the foundation stiffness has been made to correspond to the other two theories by setting $k' = \frac{\pi^2}{12}$. The other cutoff frequency has been adjusted by correcting the spring constant of the foundation in accordance with equation 23. In figure 12 the complex arm intersection in the imaginary Γ' -plane results from the values of g^2 and ξ^2 that fall in the region IV of figure 14.

Again the cutoff frequency due to the foundation hardness is related to the uniform oscillation of the plate and is given by equation 24. For very small foundation hardness the lowest mode of equation 29 approaches equation 22 for small wave numbers. As in the case of Lagrange's equation no additional cutoff frequencies are found which depend on the foundation stiffness since no symmetric thickness-stretch motion was assumed in the derivation of equations 16 and 25a and 25b. The existence of a second cutoff frequency is due to the inclusion of the transverse shear effect on the deflection in the more exact theory. The elemental motion which results from transverse shear is the same as that due to the lowest symmetric thickness-shear mode for the configuration of figure 3. It is not surprising, therefore, to find this frequency to be independent of the foundation hardness.

Though the highest mode of this theory always associates itself with the third mode of equation 13, the lower mode splits its affiliation between the two remaining exact modes. This is expected since nowhere in the

approximate theory is symmetric thickness-stretch motion considered. Consequently this arm is closest to the exact mode which has the most bending character. The influence of bending is quite large for small foundation hardness and consequently the approximate bending mode agrees well with the two exact modes where they have bending behavior. It is interesting to note that for very stiff foundations the lowest symmetric mode of the exact theory still tends to approach the bending mode of the more exact theory for a plate on a foundation. For very short waves the severe bending of the outer fibers of an exact beam may account for this behavior.

Note that whereas the complex modes of the spectrum from equation 29 have a real mode with which to couple for frequencies below Ω_* , no such mode exists for either approximate theory. Therefore, when a wave in this frequency range reaches an edge, mode conversion is unnecessary to satisfy boundary conditions in the approximate case. It will be possible using these simpler equations to study the influence of these complex modes under transient loading.

It is not surprising to find that the biquadratic form of equation 29 describes a spectrum which has these characteristics. This behavior has been shown to be very much like the second and third symmetric modes of the Rayleigh-Lamb frequency equation. These lowest three symmetric modes are approximated by a bicubic equation very closely up to wave numbers slightly greater than Γ'_* by Mindlin and Medick (21). In this range the lowest mode is almost linear and in principle can be factored out of the bicubic to leave a biquadratic to describe the upper two modes.

This similarity suggests that the influence of Poisson's ratio on the variable cutoff frequency is equivalent to the effect on this frequency of a spring coupling between the inner fibers of a plate with the outer fibers as suggested previously. Since an infinite K_e gives these symmetric modes for a plate thickness $2h$ an equivalent spring constant, K_p , which will correlate the cutoff frequencies of the two spectra is given through (see equation 14)

$$g_p^2 = \frac{a^2}{4} = \frac{(1-\nu)}{2(1-2\nu)}$$

where g_p is related to K_p and h_p by

$$g_p^2 = \frac{h_p K_p}{e^2 \rho c^2}$$

The quantity K_p is the equivalent spring constant, and h_p is the equivalent thickness of the outer plate (or fibers) figure 15a. This comparison has been made by Boley (6) using a similar model.

The value of h_p may be chosen to make the approximate spectrum match more closely that of the exact plate which is being modeled. For example, if the slopes of the arms for the two theories are made the same at $\Gamma = 0$ for the critical Poisson's ratio, $\nu = \frac{1}{3}$, then

$$g_p^2 = 1, \quad c^2 = \frac{16c_s^2}{\pi^2} \quad \text{or } k' = \frac{16}{\pi^2} = 1.62, \quad h_p/h = 8 \sqrt{3}/\pi^2 = 1.40$$

since $d\omega/\omega d\gamma = h_p/2e$ for the approximate theory (from equation 29) and $d\omega/\omega d\gamma = 2h/\pi^2$ for the exact theory (18). The resulting spectrum is shown in figure 16.

The similarity of the frequency spectrum described by the symmetric

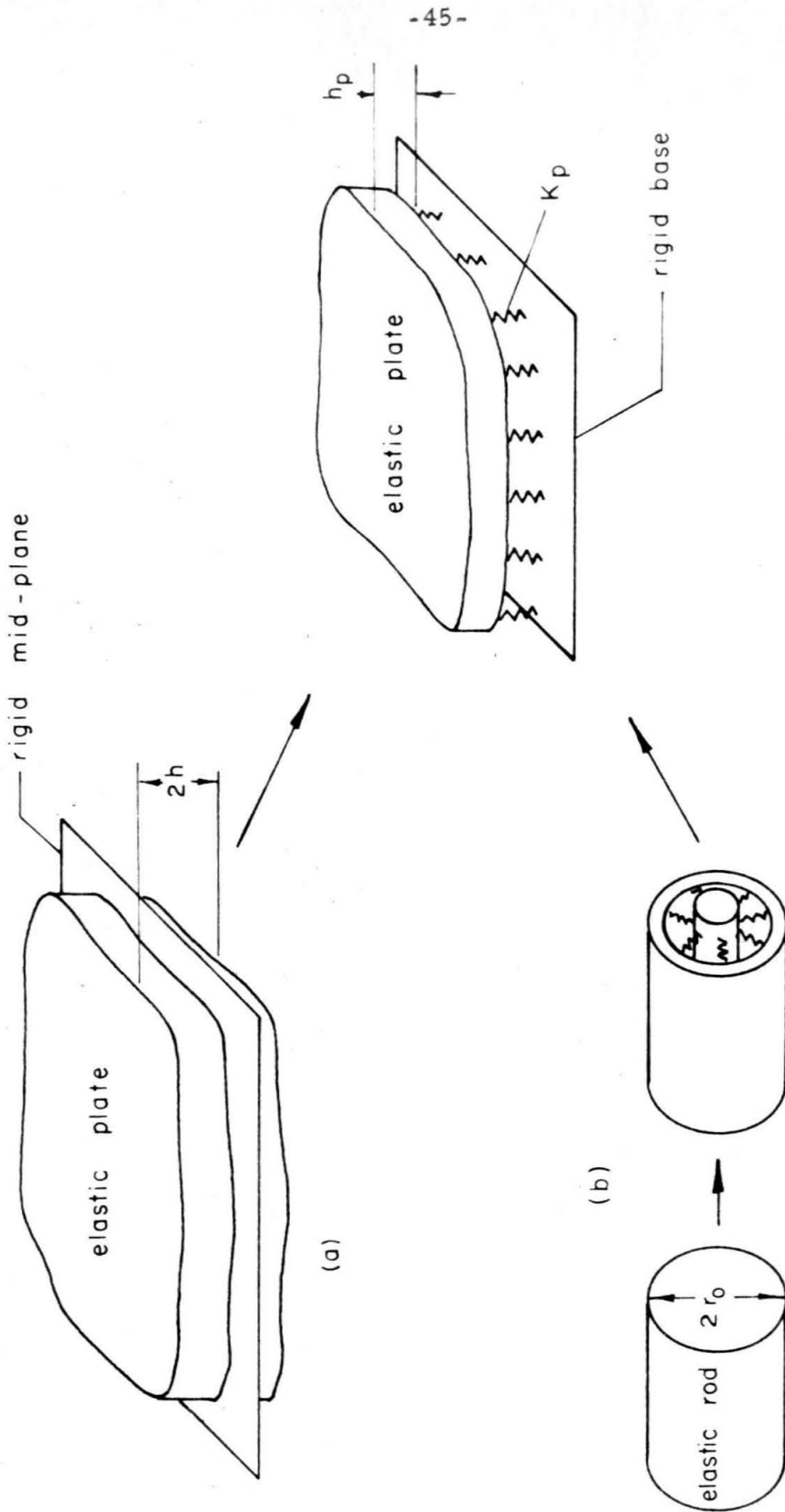


Figure 15. Flat plate on foundation model for symmetric excitation of: (a) flat plate, (b) circular rod.

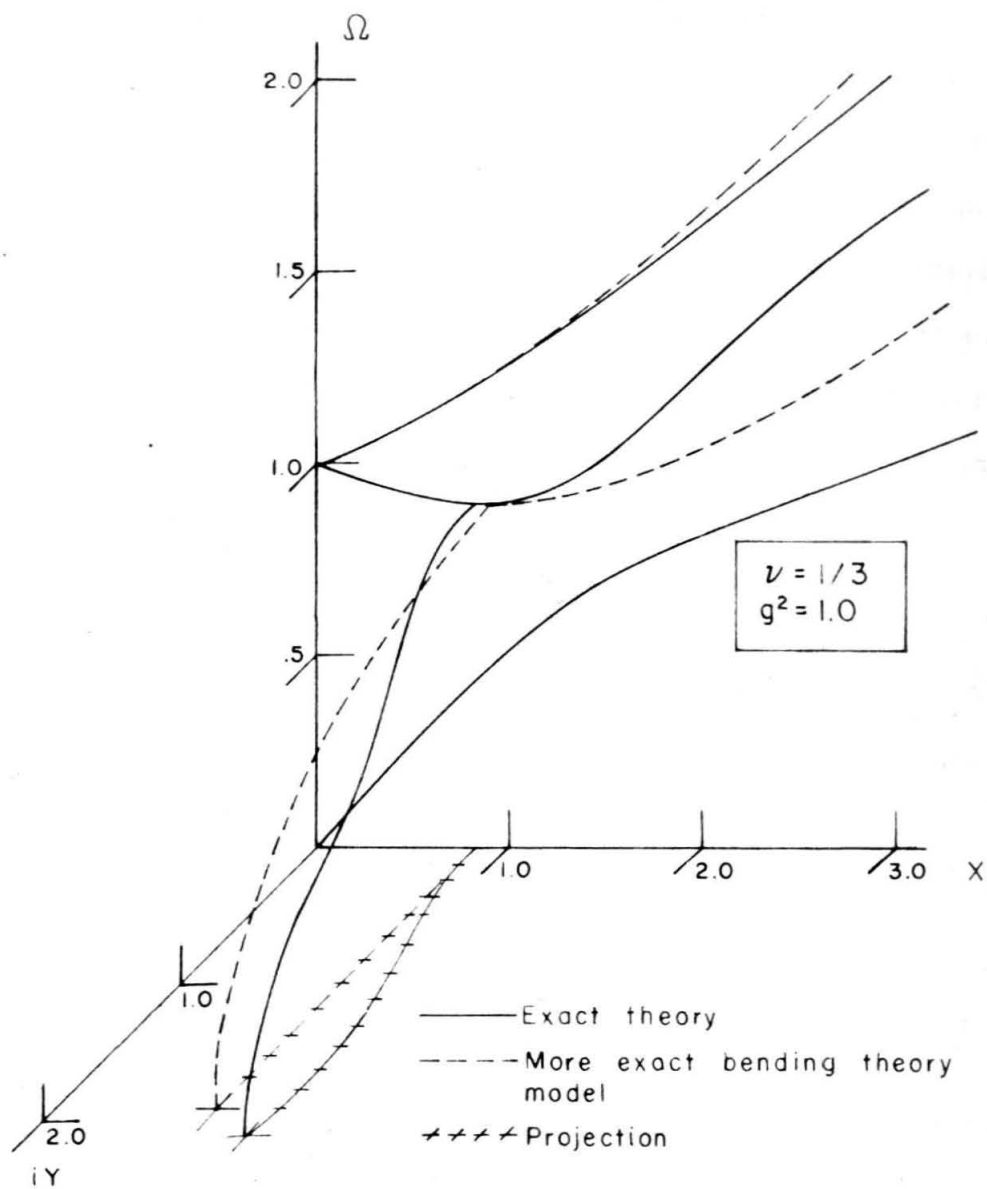


Figure 16. Frequency spectrum for symmetric excitation of a flat plate at the critical Poisson's ratio.

Pochhammer frequency equation to the symmetric Rayleigh-Lamb spectrum suggests a simple model to describe the behavior of a circular rod in symmetric excitation. Consider a thin cylindrical shell connected to a rigid center rod by an elastic sublayer. Taking into account the built in spring character of the thin shell, this system can be further modeled, approximately, by a plate on an elastic foundation, figure 15b. In order to establish the equivalent plate parameters and spring constants, reference is again made to the frequency spectra of the two systems. The symmetric Pochhammer frequency equation is given by (23)

$$(\Gamma_c^2 - \beta_c^2)^2 a_c \frac{J_0(a_c)}{J_1(a_c)} + 4 \Gamma_c^2 a_c^2 \beta_c \frac{J_0(\beta_c)}{J_1(\beta_c)} = 2(\Gamma_c^2 + \beta_c^2) a_c^2$$

where

$$a_c^2 = \left(\frac{\nu_1 \Omega_c}{a} \right)^2 - \Gamma_c^2, \quad \beta_c^2 = (\nu_1 \Omega_c)^2 - \Gamma_c^2$$

$$\Omega_c = \omega / \omega_{s_c}, \quad \omega_{s_c} = \nu_1 c_s / r_o, \quad \Gamma_c = \gamma r_o$$

and r_o is the rod radius, and $\nu_1 = 3.8317$ is the first zero of $J_0(\nu_1) = 0$.

The two cutoff frequencies for the second branch are (23)

$$\Omega_c = 1$$

$$\Omega_c = a \frac{\nu_2}{\nu_1}$$

where ν_2 is the first root of

$$a^2 \nu_2 \frac{J_0(\nu_2)}{J_1(\nu_2)} = 2$$

For a plate made of the same material as the rod being modeled, the adjustment of the cutoff frequencies gives

$$c^2 = \frac{\nu_1^2}{12} \frac{h_p^2}{r_o^2} \quad \text{or} \quad k' = \frac{\nu_1^2}{12} \frac{h_p^2}{r_o^2}$$

$$g_p^2 = a \frac{\nu_2}{\nu_1}$$

The critical Poisson's ratio, $\nu = .2833$, is found by setting

$$g_p^2 = 1 = a \frac{\nu_2}{\nu_1}$$

Again matching the slopes at this Poisson's ratio gives

$$k' = \frac{16a^2}{\nu_3} = 1.35, \quad \frac{h_p}{r_o} = \frac{4\sqrt{12}a}{\nu_1 \nu_3} = 1.05$$

where $\frac{1}{\omega} \frac{d\omega}{d\gamma} = \frac{2ar_o}{\nu_1 \nu_3}$ for the exact theory (23) and $\nu_3^2 = a^2 \nu_1^2 - 4a^2 + 4$.

A comparison of these frequency spectra is shown in figure 17.

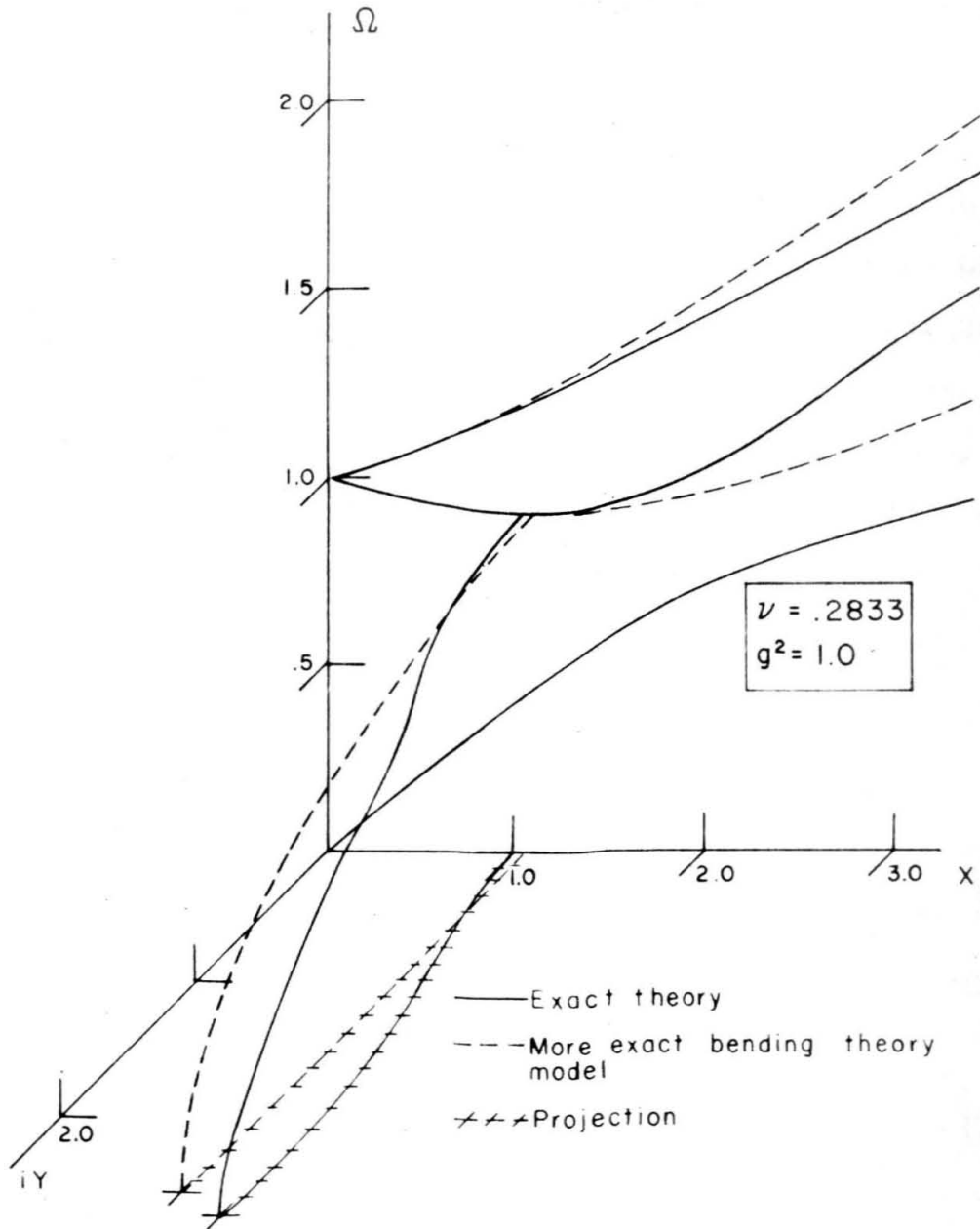


Figure 17. Frequency spectrum for axially symmetric excitation of a circular rod at the critical Poisson's ratio.

II. TRANSIENT RESPONSE OF AN ELASTIC PLATE ON AN ELASTIC FOUNDATION

A. Approximate Theory (more exact bending theory)

In this section two types of transient problems are considered for which equations 25a and 25b are applicable. In the first use is made of the plane strain form of these equations in treating the problem of a plate resting on an elastic foundation subjected to a line loading, figure 18a. In the second the related problem of point load excitation is treated using the cylindrically symmetric forms of equations 25a and 25b, figure 18b. In each case the loading is a step function in time. The linearity of the governing equations permits other forcing functions to be considered through the Duhamel integral.

1. Statement of Problems and Formal Solutions

a. Line Load

For this case the dimensionless transverse loading is given by

$$Q = \frac{q}{2\rho c^2} = Q_\ell(\xi', \tau') - g^2(W_b + W_s) \quad (31)$$

where

$$Q_\ell(\xi', \tau') = F_\ell(\tau') \delta_D(\xi') \quad (32)$$

$F_\ell(\tau')$ being the step function

$$F_\ell(\tau') = \begin{cases} 0 & \tau' < 0 \\ F_{\ell 0} & \tau' > 0 \end{cases}$$

$\delta_D(\xi')$ is the Dirac delta function defined by

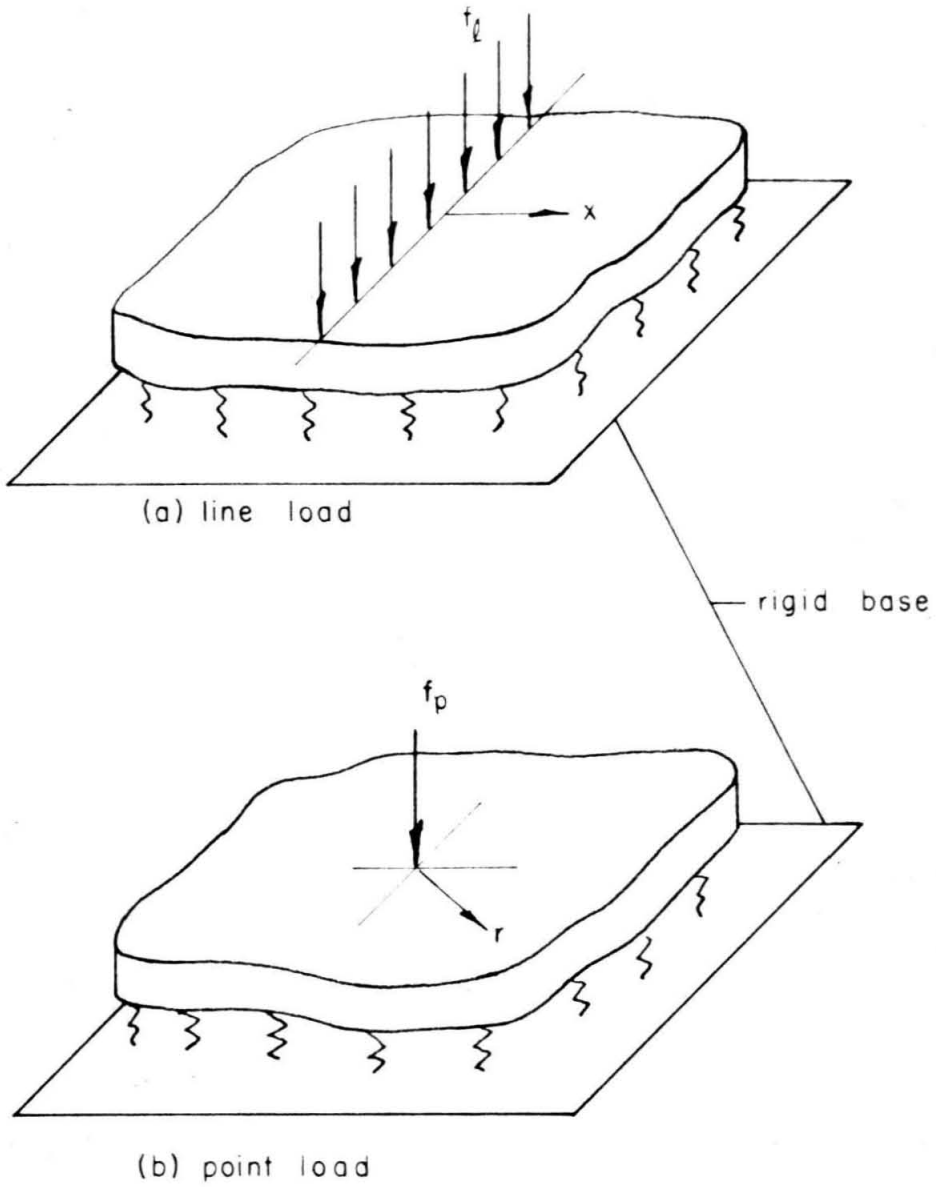


Figure 18. Transient loadings considered.

$$\int_{-\infty}^{\infty} \delta_D(\xi') d\xi' = 1$$

$$\delta_D(\xi') = 0, \quad \xi' \neq 0$$

The dimensionless line loading magnitude is given by

$$F \ell_0 = \frac{f \ell}{e \rho c^2 h}$$

where $f \ell$ is the line loading with dimensions of force per unit length. The remaining constants have been defined previously.* The plate is assumed to be initially at rest and undisturbed at infinity for all time:

$$W_s = W_b = \frac{\partial W_s}{\partial \gamma'} = \frac{\partial W_b}{\partial \gamma'} = 0 \quad \text{at} \quad \gamma' = 0 \quad (33)$$

$$\lim_{\xi' \rightarrow \pm \infty} (W_s, W_b, \frac{\partial W_s}{\partial \xi'}, \frac{\partial W_b}{\partial \xi'}, \text{ etc.}) = 0 \quad (34)$$

Substitution of equation 31 into equation 25b and rewriting equation 26a gives two coupled, nonhomogeneous linear differential equations, which in dimensionless form, are

$$\frac{\partial^2 W_b}{\partial \xi'^2} + \delta^2 W_s - \delta^2 \frac{\partial^2 W_b}{\partial \gamma'^2} = 0 \quad (35a)$$

$$\frac{\partial^2 W_s}{\partial \xi'^2} - g^2 (W_s + W_b) - \frac{\partial^2}{\partial \gamma'^2} (W_s + W_b) = -Q \ell (\xi', \gamma') \quad (35b)$$

* The line load solution is directly applicable to the solution for a beam subjected to a point load if the constants are redefined in accordance with equation 19 and

$$Q = \frac{h q}{A_b e^2 \rho c^2}, \quad F \ell_0 = \frac{f_b}{A_b e \rho c^2}$$

where f_b has dimensions of force.

Taking the Laplace transform of equations 35a and 35b using the initial conditions, equation 33, gives

$$\frac{d^2 \bar{W}_b}{d \xi'^2} + \delta^2 \bar{W}_b - \delta^2 s^2 \bar{W}_b = 0 \quad (36a)$$

$$\frac{d^2 \bar{W}_s}{d \xi'^2} - (s^2 + g^2)(\bar{W}_s + \bar{W}_b) = -\bar{Q}_\ell(\xi', s) \quad (36b)$$

where the bar over the variable denotes the Laplace transform, i.e.,

$$\bar{W}_b(\xi', s) = \int_0^\infty e^{-s\gamma'} W_b(\xi, \gamma') d\gamma'$$

Taking now the Fourier transform of equations 36a and 36b subject to the boundary conditions, equation 34, gives

$$-p^2 \tilde{\bar{W}}_b + \delta^2 \tilde{\bar{W}}_s - \delta^2 s^2 \tilde{\bar{W}}_b = 0 \quad (37a)$$

$$-p^2 \tilde{\bar{W}}_s - (s^2 + g^2)(\tilde{\bar{W}}_s + \tilde{\bar{W}}_b) = -\tilde{\bar{Q}}_\ell(p, s) \quad (37b)$$

where the tilde over a variable denotes the Fourier transform, i.e.,

$$\tilde{\bar{W}}_b(p, s) = \int_{-\infty}^{\infty} e^{ip\xi'} \bar{W}_b(\xi', s) d\xi'$$

Solution of the two algebraic equations 37a and 37b for the double transformed variables gives

$$\tilde{\bar{W}}_b = \frac{\tilde{\bar{Q}}_\ell(p, s)}{F(s^2, p^2)} \quad (38a)$$

$$\tilde{\bar{W}}_s = (s^2 + p^2 / \delta^2) \frac{\tilde{\bar{Q}}_\ell(p, s)}{F(s^2, p^2)} \quad (38b)$$

where

$$F(s^2, p^2) = s^4 + s^2 \left[p^2 \left(1 + \frac{1}{\zeta^2} \right) + 1 + g^2 \right] + g^2 + \frac{p^2}{\zeta^2} (g^2 + p^2) \quad (39)$$

This characteristic equation is the same as frequency equation 28 provided $s = -i\Omega$ and $p = \Gamma'$. The inversions (formal solutions) of equations 38a and 38b are

$$W_b(\xi', \gamma') = \frac{1}{4\pi^2 i} \int_{Br_1} e^{s\gamma'} ds \int_{-\infty}^{\infty} e^{i\xi'p} \frac{\tilde{Q}(p, s) dp}{F(s^2, p^2)} \quad (40a)$$

$$W_s(\xi', \gamma') = \frac{1}{4\pi^2 i} \int_{Br_1} e^{s\gamma'} ds \int_{-\infty}^{\infty} e^{i\xi'p} \frac{(s^2 + p^2 / \zeta^2) \tilde{Q}(p, s) dp}{F(s^2, p^2)} \quad (40b)$$

where Br_1 is the well-known Bromwich contour taken to the right of all singularities of \tilde{W}_b and \tilde{W}_s in the s -plane.

Transformation of the particular loading condition 32 gives

$$\tilde{Q}_L(p, s) = \frac{F \ell_0}{s}$$

b. Point Load

In this case the transverse loading is assumed to be of the form

$$Q = \frac{q}{2\rho c^2} = Q_p(R, \gamma') - g^2 (W_s + W_b) \quad (41)$$

where

$$Q_p(R, \gamma') = F_p(\gamma') \frac{\int_D(R)}{R} \quad (42)$$

$F_p(\gamma')$ being the step function

$$F_p(\gamma') = \begin{cases} 0 & \gamma' < 0 \\ F_{p0} & \gamma' > 0 \end{cases}$$

Here the Dirac delta function is given by

$$\int_0^{\infty} \delta_D(R) dR = \frac{1}{2}$$

$$\delta_D(R) = 0, \quad R \neq 0$$

and $R = er/h$ is the dimensionless radial coordinate in the plane of the plate. The dimensionless point load is

$$F_{p0} = \frac{f_p}{\pi \rho c^2 h^2}$$

where f_p has dimensions of force.

The initial and boundary conditions are

$$W_b = W_s = \frac{\partial W_b}{\partial \gamma'} = \frac{\partial W_s}{\partial \gamma'} = 0 \quad \text{at } \gamma' = 0 \quad (43)$$

$$\lim_{R \rightarrow \infty} (W_b, W_s, \frac{\partial W_b}{\partial R}, \frac{\partial W_s}{\partial R}, \text{ etc.}) = 0 \quad (44)$$

Substituting equation 41 into the cylindrically symmetric forms of equations 25a and 25b results in two equations analogous to equations 36a and 36b

$$\frac{1}{R} \frac{\partial}{\partial R} \left(R \frac{\partial W_b}{\partial R} \right) + \delta^2 W_s - \delta^2 \frac{\partial^2 W_b}{\partial \gamma'^2} = 0 \quad (45a)$$

$$\frac{1}{R} \frac{\partial}{\partial R} \left(R \frac{\partial W_s}{\partial R} \right) - g^2 (W_s + W_b) - \frac{\partial^2}{\partial \gamma'^2} (W_s + W_b) = -Q_p(R, \gamma') \quad (45b)$$

Again taking the Laplace transform and using equation 43 gives

$$\frac{1}{R} \frac{d}{dR} \left(R \frac{d\bar{W}_b}{dR} \right) + \zeta^2 \bar{W}_s - \zeta^2 s^2 \bar{W}_b = 0 \quad (46a)$$

$$\frac{1}{R} \frac{d}{dR} \left(R \frac{d\bar{W}_s}{dR} \right) - (g^2 + s^2) (\bar{W}_s + \bar{W}_b) = -\bar{Q}_p(R, s) \quad (46b)$$

Taking the Hankel transform and using equation 44 gives

$$-p^2 \bar{W}_b^0 + \zeta^2 \bar{W}_s^0 - \zeta^2 s^2 \bar{W}_b^0 = 0 \quad (47a)$$

$$-p^2 \bar{W}_s^0 - (s^2 + g^2) (\bar{W}_s^0 + \bar{W}_b^0) = -\bar{Q}_c^0(p, s) \quad (47b)$$

where the superscript "0" denotes the Hankel transform of order zero, i. e.,

$$\bar{W}_b^0(p, s) = \int_0^\infty R J_0(pR) \bar{W}_b(R, s) dR$$

Equations 47a and 47b may be seen to have the same form as equations 37a and 37b. Hence the formal solutions are

$$W_b(R, \gamma') = \frac{1}{2\pi i} \int_{Br_1} e^{s\gamma'} ds \int_0^\infty p J_0(pR) \frac{\bar{Q}_p^0(p, s) dp}{F(s^2, p^2)} \quad (48a)$$

$$W_s(R, \gamma') = \frac{1}{2\pi i} \int_{Br_1} e^{s\gamma'} ds \int_0^\infty p J_0(pR) (s^2 + p^2 / \zeta^2) \frac{\bar{Q}_p^0(p, s) dp}{F(s^2, p^2)} \quad (48b)$$

Transformation of the loading function $Q_p(\gamma', R)$ gives

$$\bar{Q}_p^0(s, p) = \frac{F p^0}{s}$$

2. Evaluation of Formal Solutions

Evaluations of the double transforms given by equations 40a, 40b, 48a, and 48b may be carried out by performing the indicated integrations in either order.* Future reference to the order of inversion will be denoted by "Method 1" for Fourier or Hankel transform inversion carried out first and "Method 2" for Laplace transform inversion first. It is convenient to express the function $F(s^2, p^2)$ in the following two equivalent forms:

$$F(s^2, p^2) = (s^2 + s_1^2)(s^2 + s_2^2) \quad (49)$$

and

$$= \frac{1}{\delta^2} (p^2 - p_1^2)(p^2 - p_2^2)$$

where

$$s_j^2 = \frac{1}{2} \left[p^2 \left(1 + \frac{1}{\delta^2} \right) + 1 + g^2 \right] + \frac{(-1)^j}{2} \left\{ \left[p^2 \left(1 - \frac{1}{\delta^2} \right) - 1 + g^2 \right]^2 + 4p^2 \right\}^{1/2}$$

$$p_j^2 = -\frac{1}{2} \left[s^2 (1 + \delta^2) + g^2 \right] + \frac{(-1)^j}{2} \left\{ \left[s^2 (1 + \delta^2) + g^2 \right]^2 - 4\delta^2 (g^2 + s^2)(1 + s^2) \right\}^{1/2}$$

$$s_1^2 s_2^2 = \frac{1}{\delta^2} (p^2 + P_{01}^2)(p^2 + P_{02}^2)$$

$$P_{0j} = \left[\frac{1}{2} g^2 (1 + (-1)^j i Z_0) \right]^{1/2}$$

and

$$Z_0 = \left[\frac{4\delta^2}{g^2} - 1 \right]^{1/2}$$

* Justification of this inversion in the order of integration results from the fact that the integrand is continuous in s and p and the individual infinite integrations converge uniformly for all parameters γ' and ξ' (24).

a. Line Load

The particularly simple forms of the integrands of equations 40a and 40b for the loading assumed yields a closed form result for the first integration performed.

Method 1

Consider first the inversion of the Fourier transform. Integration of the transform along the real p-axis can be accomplished using the Cauchy integral theorem and residue theory. Integration along an infinite arc in the upper (lower) half of the p-plane vanishes for ξ' greater than (less than) zero. This can be shown by applying Jordan's lemma, noting that for large p the integrand behaves like $1/p^k$ where $k > 0$ (24). The formal solution reduces to

$$\frac{2\pi}{\delta^2 F \ell_0} W_b(\xi', \tau') = \frac{1}{2} \int_{Br_1} \frac{e^{ip_2 \xi'}}{p_2(p_2^2 - p_1^2)} + \frac{e^{ip_1 \xi'}}{p_1(p_1^2 - p_2^2)} e^{s\tau'} \frac{ds}{s} \quad (50a)$$

$$\frac{2\pi}{\delta^2 F \ell_0} W_s(\xi', \tau') = \frac{1}{2} \int_{Br_1} \frac{[s^2 + p_2^2 / \delta^2] e^{ip_2 \xi'}}{p_2(p_2^2 - p_1^2)} + \frac{[s^2 + p_1^2 / \delta^2] e^{ip_1 \xi'}}{p_1(p_1^2 - p_2^2)} e^{s\tau'} \frac{ds}{s} \quad (50b)$$

where the branches p_j in equation 49 are selected according to $\text{Im } p_j > 0$ for agreement with $\text{Re } s > 0$ on Br_1 . It is thus assured that p_1 and p_2 in equations 50a and 50b are in the upper half of the p-plane. Similarly for $\xi' < 0$, $\text{Im } p_j < 0$ dictates the selection of the branches of p_j on Br_1 , and the solution is seen to be symmetric in ξ' . The remaining inversion must be carried out by means of a contour integration in the complex s-plane due to the multivalued character of p_1 and p_2 . The details of this inversion

are given in Appendix B for the integral of equation 50b. The results may be applied to equation 50a by simply neglecting the factor due to $(s^2 + p_j^2 / \delta^2)$ in each term. The inversion contour employed is shown in figure 19. The results of the integration for $0 < g^2 < 1$ are as follows:

For $\gamma' < \delta \xi'$

$$W_b(\xi', \gamma') = W_s(\xi', \gamma') = 0$$

For $\delta \xi' < \gamma' < \xi'$

$$\frac{2\pi}{\delta^2 F \ell_0} W_b(\xi', \gamma') = \frac{I_{b_0}}{2} + I_{b_1} + I_{b_2} + I_{b_3} + I_{b_6} + I_{b_7} \quad (51a)$$

$$\frac{2\pi}{\delta^2 F \ell_0} W_s(\xi', \gamma') = \frac{I_{s_0}}{2} + I_{s_1} + I_{s_2} + I_{s_3} + I_{s_6} + I_{s_7} \quad (51b)$$

For $\delta \xi' < \gamma'$

$$\frac{2\pi}{\delta^2 F \ell_0} W_b(\xi', \gamma') = \sum_{i=0}^5 I_{b_i} \quad (52a)$$

$$\frac{2\pi}{\delta^2 F \ell_0} W_s(\xi', \gamma') = \sum_{i=0}^5 I_{s_i} \quad (52b)$$

where the I_{s_i} are given by

$$I_{s_0} = \pi \operatorname{Re} \left\{ \frac{\left[-P_{02}^2 / \delta^2 \right] e^{-P_{02} \xi'}}{(-2iZ_0) P_{02}} \right\}$$

$$I_{s_1} = - \int_1^{\infty} \frac{\left[-\eta^2 + P_{12}^2 / \delta^2 \right]}{(-2iZ_1) P_{12}} \cos(\eta \gamma' - P_{12} \xi') \frac{d\eta}{\eta}$$

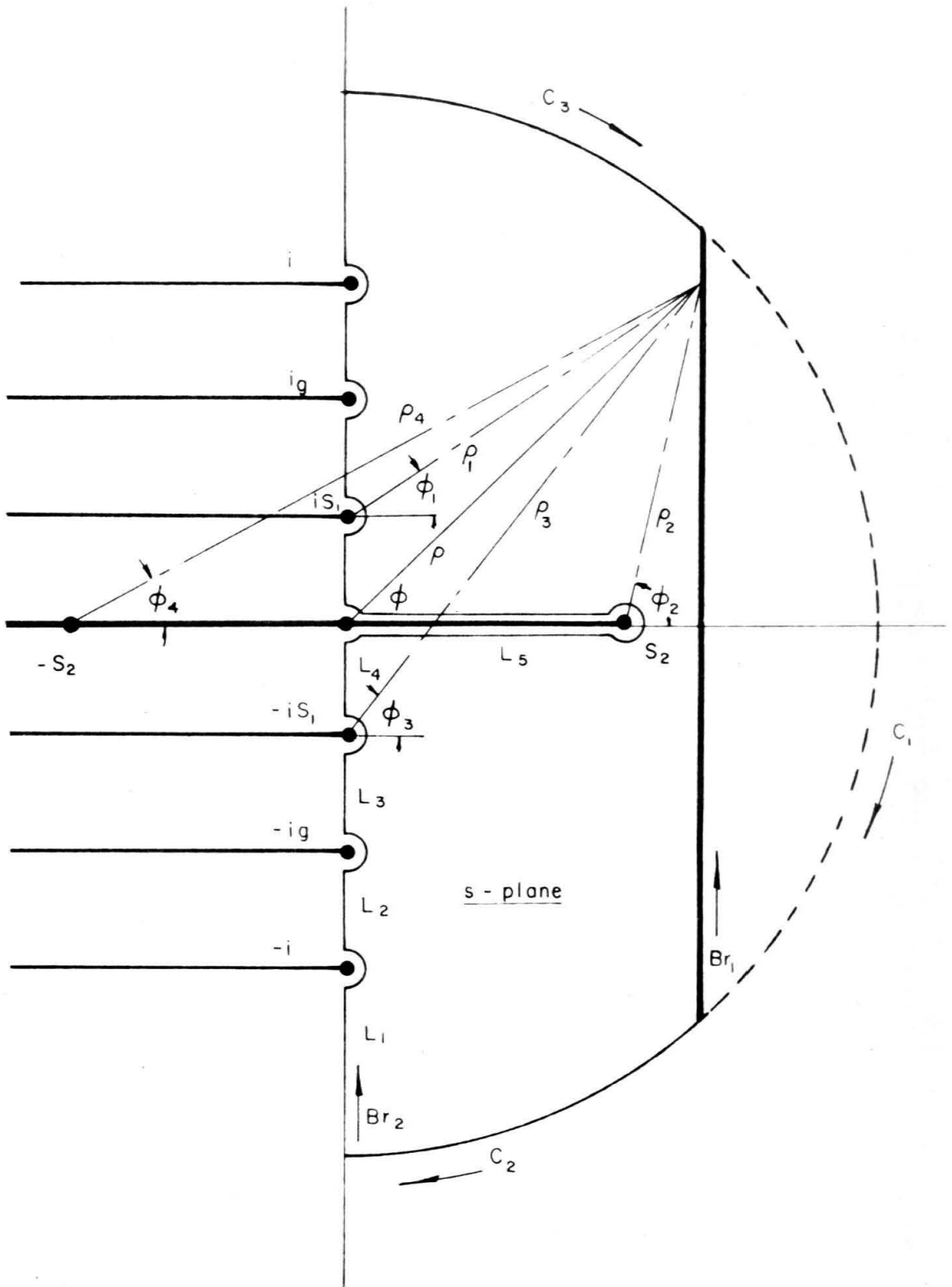


Figure 19. Inversion contour for second integration of Method 1.

$$I_{s_2} = \int_g^1 \frac{[-\eta^2 - P_{12}^2 / \delta^2] e^{-P_{12} \xi'}}{(-2Z_1)P_{12}} \sin \eta \gamma' \frac{d\eta}{\eta}$$

$$I_{s_3} = \int_{S_1}^g \frac{[-\eta^2 + P_{12}^2 / \delta^2]}{(-2Z_1)P_{12}} \cos(\eta \gamma' + P_{12} \xi') \frac{d\eta}{\eta}$$

$$I_{s_4} = 2 \operatorname{Im} \int_0^{S_1} \frac{[-\eta^2 + P_2^2 / \delta^2] e^{-iP_2 \xi'}}{(-2iZ_1)P_2} \sin \eta \gamma' \frac{d\eta}{\eta}$$

$$(\operatorname{Re} P_2 > 0)$$

$$I_{s_5} = - \int_{S_1}^{\infty} \frac{[-\eta^2 + P_{11}^2 / \delta^2]}{(2Z_1)P_{11}} \cos(\eta \gamma' - P_{11} \xi') \frac{d\eta}{\eta}$$

$$I_{s_6} = \operatorname{Re} \int_0^{S_1} \left\{ \frac{[-\eta^2 + P_2^2 / \delta^2] e^{-i(P_2 \xi' + \eta \gamma')}}{(-2iZ_1)P_2} \right. \quad (\operatorname{Re} P_2 > 0)$$

$$\left. + \frac{[\eta^2 - P_3^2 / \delta^2] e^{\eta \gamma' - P_3 \xi'}}{(2Z_2)P_3} \right\} \frac{d\eta}{\eta} \quad (\operatorname{Re} P_3 > 0)$$

$$I_{s_7} = \operatorname{Re} \int_{S_1}^{S_2} \frac{[\eta^2 - P_3^2 / \delta^2] e^{\eta \gamma' - P_3 \xi'}}{(2Z_2)P_3} \frac{d\eta}{\eta}$$

and

$$P_{0j} = \left[\frac{g^2}{2} (1 + (-1)^j i Z_0) \right]^{1/2}$$

$$Z_0 = \left[\frac{4\delta^2}{g^2} - 1 \right]^{1/2}$$

$$P_{1j} = \frac{1}{2} \eta^2 (1 + \delta^2) - \frac{g^2}{2} - (-1)^j Z_1 \quad 1/2$$

$$P_2 = \left| \frac{1}{2} \eta^2 (1 + \delta^2) - \frac{g^2}{2} - i Z_1 \right|^{1/2}$$

$$P_3 = \left| \frac{1}{2} \eta^2 (1 + \delta^2) + \frac{g^2}{2} + i Z_2 \right|^{1/2}$$

$$Z_1 = \frac{1 - \delta^2}{2} \left| (\eta^2 - s_1^2)(\eta^2 + s_2^2) \right|^{1/2}$$

$$Z_2 = \frac{1 - \delta^2}{2} \left| (\eta^2 + s_1^2)(\eta^2 - s_2^2) \right|^{1/2}$$

$$s_j^2 = \frac{1}{(1 - \delta^2)} \left\{ (-1)^j \left(2 \frac{\delta^2}{1 - \delta^2} - g^2 \right) + \frac{2\delta^2}{1 - \delta^2} \sqrt{1 - g^2(1 - \delta^2)} \right\}$$

The I_{b_i} 's are equal to the I_{s_i} 's when the square bracketed terms are set equal to one.

If a case is treated for $1 < g^2 < 1 + \delta^2$ the limits of I_{s_1} and I_{s_2} must be changed such that l becomes g and g becomes l .

The integrals I_{s_6} and I_{s_7} may be written in an equivalent form by considering the integral

$$\int_{Br_1} \frac{(s^2 + p_1^2 / \delta^2) e^{i p_1 \xi'} e^{s \gamma'}}{p_1(p_1^2 - p_2^2)} \frac{ds}{s}$$

over Br_2 , figure 19, for $\delta \xi' < \gamma' < \xi'$. Noting that the integral along Br_1 has already been shown to be zero, the integrals along Br_2 may be combined directly with I_{s_6} and I_{s_7} to give the same solution as found for $\gamma' > \xi'$. It follows then that the solution for $\gamma' > \xi'$ is also valid for $\delta \xi' < \gamma'$. Inspection of these integrals shows that each corresponds to the contribution of a particular portion of the frequency spectrum, including the complex and imaginary arms. This will be discussed in more detail later.

Method 2

Now consider the inversion of the Laplace transform first. In the s -plane simple poles occur at $\pm is_1$, $\pm is_2$ and zero. Residue theory, as in Method 1, gives the first inversion as

$$\frac{2\pi W_b(\xi', \gamma')}{\delta^2 F_{l0}} = \frac{1}{\delta^2} \int_{-\infty}^{\infty} \left[1 + \frac{s_1^2}{s_2^2 - s_1^2} \cos s_2 \gamma' + \frac{s_2^2}{s_1^2 - s_2^2} \cos s_1 \gamma' \right] \frac{e^{i \xi' p} dp}{s_1^2 s_2^2} \quad (53a)$$

$$\frac{2\pi W_s(\xi', \gamma')}{\delta^2 F_{l0}} = \frac{1}{\delta^2} \int_{-\infty}^{\infty} \left[\frac{p^2}{\delta^2} + \frac{(p^2 / \delta^2 - s_2^2) s_1^2}{s_2^2 - s_1^2} \cos s_2 \gamma' + \frac{(p^2 / \delta^2 - s_1^2) s_2^2}{s_1^2 - s_2^2} \cos s_1 \gamma' \right] \times \frac{e^{i \xi' p} dp}{s_1^2 s_2^2} \quad (53b)$$

The first term in each of these integrals can be evaluated directly yielding the static solution. Again restricting interest to the positive ξ' -axis, so that the integration around the large arc in the upper half of the p -plane vanishes, these terms can be evaluated by adding the residues at iP_{01} and iP_{02} . Here the P_{0j} are defined by $\text{Re } P_{0j} > 0$. The final form of the solution is

$$\frac{2\pi}{\delta^2 F_{\ell 0}} W_b(\xi', \gamma') = 2\pi \text{Re} \left[\frac{e^{-P_{02} \xi'}}{(-2iZ_0)P_{02}} \right] + \frac{2}{\delta^2} \int_0^{\infty} \left[\frac{\cos s_2 \gamma'}{s_2^2 (s_2^2 - s_1^2)} + \frac{\cos s_1 \gamma'}{s_1^2 (s_1^2 - s_2^2)} \right] \cos p \xi' dp \quad (54a)$$

$$\frac{2\pi}{\delta^2 F_0} W_s(\xi', \gamma') = 2\pi \text{Re} \left[\frac{-P_{02}^2 / \delta^2 e^{-P_{02} \xi'}}{(-2iZ_0)P_{02}} \right] + \frac{2}{\delta^2} \int_0^{\infty} \left[\frac{(p^2 / \delta^2 - s_2^2)}{s_2^2 (s_2^2 - s_1^2)} \cos s_2 \gamma' + \frac{(p^2 / \delta^2 - s_1^2)}{s_1^2 (s_1^2 - s_2^2)} \cos s_1 \gamma' \right] \cos p \xi' dp \quad (54b)$$

where $\xi' > 0$ and $\gamma' > 0$. The leading term in each expression is the static solution in agreement with those in equations 52a and 52b.

b. Point Load

Method 1

Again a first integration in equations 48a and 48b can be obtained in closed form. Consider first the Hankel inversion. Writing the Bessel function in terms of Hankel functions

$$2J_0(pR) = H_0^{(1)}(pR) + H_0^{(2)}(pR)$$

equation 48a can be written in the form

$$W_b(R, \gamma') = \frac{F_{p0}}{4\pi i} \int_{Br_1} e^{s\gamma'} \frac{ds}{s} \left\{ \int_0^\infty \frac{pH_0^{(1)}(pR) dp}{F(s^2, p^2)} + \int_0^\infty \frac{pH_0^{(2)}(pR) dp}{F(s^2, p^2)} \right\} \quad (55)$$

Consider the integration of the first term by completing the contour in the upper half of the p -plane as indicated in figure 20. A branch cut has been made on the negative real axis due to the logarithmic singularity of the Hankel function at the origin. Making use of the asymptotic form

$$H_0^{(1)}(pR) \sim \left(\frac{2}{\pi pR} \right)^{1/2} e^{i(pR - \pi/4)}$$

and noting that the order of the integrand is $1/p^k$, $k > 0$, for large p , the integral along the infinite arc can be shown to vanish by applying Jordan's lemma. Again as in the analogous method for the line load problem, the branches of p_j are selected according to $\text{Im } p_j > 0$ on Br_1 . The contour integration therefore gives

$$\int_0^\infty \frac{\eta H^{(1)}(\eta R)}{F(s^2, \eta^2)} d\eta = \int_0^\infty \frac{\eta H^{(1)}(\eta e^{i\pi} R)}{F(s^2, \eta^2)} d\eta - \frac{i\pi \zeta^2}{p_2 - p_1} \zeta \left[H_0^{(1)}(p_1 R) - H_0^{(1)}(p_2 R) \right] \quad (56)$$

where the last two terms are the residues at p_1 and p_2 . Substituting equation 56 into equation 55 and using the identity

$$H_0^{(1)}(ze^{i\pi}) = -H_0^{(2)}(z)$$

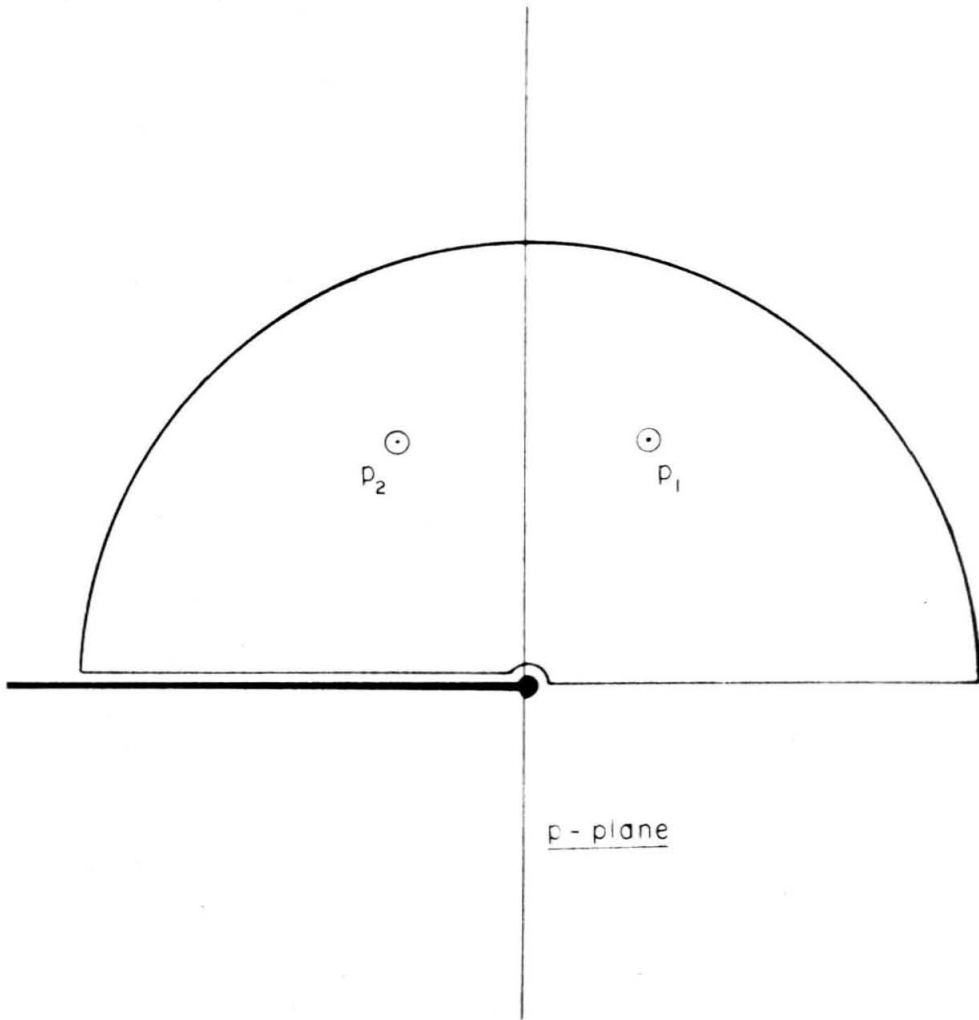


Figure 20. Inversion contour for first integration of Method 1 applied to the point load problem.

yields the solution

$$\frac{W_b(R, \gamma')}{\delta^2 F_{p0}} = \frac{1}{4} \int_{Br_1} \left[\frac{H_0^{(1)}(p_2 R)}{(p_2^2 - p_1^2)} + \frac{H_0^{(1)}(p_1 R)}{(p_1^2 - p_2^2)} \right] e^{s\gamma'} \frac{ds}{s} \quad (57)$$

Similarly it can be shown from equation 48b that

$$\frac{W_s(R, \gamma')}{\delta^2 F_{p0}} = \frac{1}{4} \int_{Br_1} \left[\frac{(s^2 + p_2^2 / \delta^2) H_0^{(1)}(p_2 R)}{(p_2^2 - p_1^2)} + \frac{(s^2 + p_1^2 / \delta^2) H_0^{(1)}(p_1 R)}{(p_1^2 - p_2^2)} \right] e^{s\gamma'} \frac{ds}{s} \quad (58)$$

Method 2

Consider now the inversion of equations 48a and 48b by integrating out the Laplace variable first. Using the same arguments that led to equations 53a and 53b it can be shown that

$$\frac{2W_b(R, \gamma')}{\delta^2 F_{p0}} = \frac{2}{\delta^2} \int_0^\infty \left[1 + \frac{s_1^2}{s_2^2 - s_1^2} \cos s_2 \gamma' + \frac{s_2^2}{s_1^2 - s_2^2} \cos s_1 \gamma' \right] \frac{p J_0(pR) dp}{s_1 s_2} \quad (59a)$$

$$\begin{aligned} \frac{2W_s(R, \gamma')}{\delta^2 F_{p0}} = \frac{2}{\delta^2} \int_0^\infty & \left[\frac{p^2}{\delta^2} + \frac{s_1^2}{s_2^2 - s_1^2} (p^2 / \delta^2 - s_2^2) \cos s_2 \gamma' \right. \\ & \left. + \frac{s_2^2}{s_1^2 - s_2^2} (p^2 / \delta^2 - s_1^2) \cos s_1 \gamma' \right] \frac{p J_0(pR) dp}{s_1 s_2} \quad (59b) \end{aligned}$$

The first term in each of these integrals can be evaluated in closed form by following the same integration procedure applied in equation 56. Here

the residues to be evaluated are at P_{01} and P_{02} . The final forms of the solution become

$$\frac{W_b(R, \gamma')}{\zeta^2 F_{p0}} = -2\text{Re} \left[\frac{K_0(P_{02}R)}{(2iZ_0)} \right] + \frac{1}{\zeta^2} \int_0^\infty \left[\frac{\cos s_2 \gamma'}{s_2^2 (s_2^2 - s_1^2)} + \frac{\cos s_1 \gamma'}{s_1^2 (s_1^2 - s_2^2)} \right] p J_0(pR) dp \quad (60a)$$

$$\begin{aligned} \frac{W_s(R, \gamma')}{\zeta^2 F_{p0}} = & -2\text{Re} \left[\frac{[-P_{02}^2 / \zeta^2] K_0(P_{02}R)}{(2iZ_0)} \right] \\ & + \frac{1}{\zeta^2} \int_0^\infty \left[(p^2 / \zeta^2 - s_2^2) \frac{\cos s_2 \gamma'}{s_2^2 (s_2^2 - s_1^2)} + (p^2 / \zeta^2 - s_1^2) \frac{\cos s_1 \gamma'}{s_1^2 (s_1^2 - s_2^2)} \right] \\ & \times p J_0(pR) dp \quad (60b) \end{aligned}$$

where $\text{Re } P_{02} > 0$, and K_0 is the zero order modified Bessel function of the second kind.

This solution is valid for $\gamma' > 0$. The first term in each expression is the static solution, which could have been found directly from equations 57 and 58 by evaluating the residue at the origin, $s = 0$.

3. Correspondence Between Line Load and Point Load Solutions

Noting that the particular $\tilde{Q}_\ell(p, s)$ chosen is even in p as is the function $F(s^2, p^2)$, the Fourier transform inversion path for the line load problem may be considered to be the positive real p -axis. This gives, from equation 40a, the cosine transform solution for this symmetric loading problem,

$$W_b(\xi', \gamma') = \lim_{\epsilon \rightarrow 0} \frac{F \ell_0}{2\pi^2 i} \int_{Br_1} \frac{e^{s\gamma'} ds}{s} \int_{\epsilon}^{\infty} \frac{\cos \xi' p}{F(s^2, p^2)} dp \quad (61)$$

Here the limiting process is introduced with no loss of generality.

Differentiating equation 61 with respect to ξ' , substituting $R \cosh \eta$ for ξ' , and integrating with respect to η from zero to infinity yields

$$\int_0^{\infty} \left. \frac{\partial W_b(\xi', \gamma')}{\partial \xi'} \right|_{\xi' = R \cosh \eta} d\eta = \lim_{\epsilon \rightarrow 0} \left(-\frac{F \ell_0}{4\pi i} \right) \int_{Br_1} \frac{e^{s\gamma'} ds}{s} \int_{\epsilon}^{\infty} \frac{p dp}{F(s^2, p^2)} \times \left[\frac{2}{\pi} \int_0^{\infty} \sin(pR \cosh \eta) d\eta \right] \quad (62)$$

where the limit process and the orders of integration have been exchanged in light of the integrand's continuity and the integrals' uniformity of convergence (24). Making use of the Mehler-Sonine form of the Bessel function (25)

$$\frac{2}{\pi} \int_0^{\infty} \sin(pR \cosh \eta) d\eta = J_0(pR)$$

where $\text{Re } pR > 0$, equation 62 becomes

$$\int_0^{\infty} \left. \frac{\partial W_b(\xi', \gamma')}{\partial \xi'} \right|_{\xi' = R \cosh \eta} d\eta = \lim_{\epsilon \rightarrow 0} \left(-\frac{F \ell_0}{4\pi i} \right) \int_{Br_1} \frac{e^{s\gamma'} ds}{s} \int_{\epsilon}^{\infty} \frac{p J_0(pR) dp}{F(s^2, p^2)} \quad (63)$$

The limit can now be taken, and comparison of equation 63 with equation 48a shows the correspondence between the two solutions:

$$W_b(R, \gamma') \Big|_{\text{Point load}} = -2 \int_0^{\eta_0} \frac{\partial W_b(\xi', \gamma')}{\partial \xi'} \Big|_{\substack{\xi' = R \cosh \eta \\ \text{line load}}} d\eta \quad (64a)$$

similarly

$$W_s(R, \gamma') \Big|_{\text{Point load}} = -2 \int_0^{\eta_0} \frac{\partial W_s(\xi', \gamma')}{\partial \xi'} \Big|_{\substack{\xi' = R \cosh \eta \\ \text{line load}}} d\eta \quad (64b)$$

where $F_{l0} = F_{p0}$ and

$$e^{\eta_0} = \frac{\gamma'}{\xi R} + \sqrt{\left(\frac{\gamma'}{\xi R}\right)^2 - 1}$$

The upper limit of integration, η_0 , results from the condition $W_b(\xi', \gamma') = W_s(\xi', \gamma') = 0$ for $\gamma' < \xi \xi'$ found in Appendix B. The choice of the positive sign in the quadratic solution for e^{η_0} is required by $\eta_0 > 0$.

This correspondence is indicated by Ewing, Jardetsky, and Press (26) for the half space, surface point and line load problems.

B. Exact Theory

In this section the line load problem is solved for the case of an infinite foundation stiffness. This simplification permits a clearer parallel to be drawn between approximate and exact problems. The method can be applied to the more difficult boundary value problems, which include a finite foundation stiffness or point loading, with only the addition of algebraic obfuscation.

1. Statement of Problem and Formal Solution

A transverse line loading is assumed to be of the form

$$Q = \frac{\sigma_{\zeta\zeta}}{\mu} = Q_{\ell}(\xi, \tau) \text{ at } \zeta = 1 \quad (65)$$

where

$$Q_{\ell}(\xi, \tau) = F_{\ell}(\tau) \delta_D(\xi)$$

$F_{\ell}(\tau)$ being the step function

$$F_{\ell}(\tau) = \begin{cases} 0 & \tau < 0 \\ F_{\ell 0} & \tau > 0 \end{cases}$$

and $\delta_D(\xi)$ is as defined previously in equation 32. The dimensionless line loading is now

$$F_{\ell 0} = \frac{f_{\ell}}{\mu h}$$

where f_{ℓ} is again the line loading per unit length.

The plate is assumed to be initially at rest and undisturbed at infinity for all time:

$$\Phi = \Psi = \frac{\partial \Phi}{\partial \tau} = \frac{\partial \Psi}{\partial \tau} = 0 \quad \text{at } \tau = 0 \quad (66)$$

$$\lim_{\xi \rightarrow \pm \infty} (\Phi, \Psi, \text{ etc.}) = 0 \quad (67)$$

Subject to these conditions the Laplace and Fourier transformations of the governing equations 7a and 7b lead to the following equations:

$$\frac{\partial^2 \tilde{\Phi}}{\partial \zeta^2} = a'^2 \tilde{\Phi}$$

$$\frac{\partial^2 \tilde{\Psi}}{\partial \zeta^2} = \beta'^2 \tilde{\Psi}$$

where

$$a'^2 = \frac{s^2}{a^2} + p^2$$

$$\beta'^2 = s^2 + p^2$$

The solutions of these equations are given by

$$\tilde{\Phi} = A_1 \cosh a' \zeta + A_2 \sinh a' \zeta$$

and

$$\tilde{\Psi} = A_3 \cosh \beta' \zeta + A_4 \sinh \beta' \zeta$$

The transformed boundary stresses 10 are

$$\tilde{\sigma}_{\zeta\zeta} = p^2 \left(1 - \frac{2}{a^2}\right) \tilde{\Phi} + 2 \frac{\partial^2 \tilde{\Phi}}{\partial \zeta^2} + ip \frac{\partial \tilde{\Psi}}{\partial \zeta} = F \ell_0 / s \quad \text{at } \zeta = 1$$

$$\tilde{\sigma}_{\zeta\xi} = 2ip \frac{\partial \tilde{\Phi}}{\partial \zeta} - \frac{\partial^2 \tilde{\Psi}}{\partial \zeta^2} - p^2 \tilde{\Psi} = 0 \quad \text{at } \zeta = 0, 1$$

and the transformed deflection from equation 9a is

$$\tilde{W} = \frac{\partial \tilde{\Phi}}{\partial \zeta} + ip \tilde{\Psi}$$

Substituting these expressions into the transformed boundary conditions

11 with $K_e = \infty$ (or $W = 0$ at $\zeta = 0$) and using equations 12a and 12b results

in a set of algebraic equations for the A_i . Solving for the A_i gives the

following results:

$$A_1 = \frac{F \ell_0}{s} \frac{(\beta'^2 + p^2)}{G(s^2, p^2)} \frac{\tanh \beta'}{\cosh \alpha'}$$

$$A_2 = A_3 = 0$$

and

$$A_4 = \frac{F \ell_0 (2i p \alpha')}{s G(s^2, p^2)} \frac{\tanh \alpha'}{\cosh \beta'}$$

where

$$G(s^2, p^2) = (\beta'^2 + p^2)^2 \sinh \beta' \cosh \alpha' - 4p^2 \alpha' \beta' \sinh \alpha' \cosh \beta' \quad (68)$$

As pointed out by Miklowitz (27) in his study on the related symmetric loading problem, $G(s^2, p^2)$ is the Rayleigh-Lamb frequency equation for symmetric waves in a plate of thickness $2h$, if the Laplace transform variable s^2 is replaced by $-\Omega^2 \pi^2$. (Refer to equation 13 with $K_e = \infty$.) This makes the present plate foundation problem equivalent to that of the symmetric excitation of a plate of thickness $2h$, as noted in reference 27. A generalization of this equivalence is an underlying theme in the present work, particularly in Part I. The formal solution for the vertical displacement, W , is

$$W(\xi, \tau, \zeta) = \frac{F \ell_0}{4\pi^2 i} \int_{Br_1} \frac{e^{s\tau}}{s} ds \int_{-\infty}^{\infty} \frac{e^{i\xi p}}{G(s^2, p^2)} H(s^2, p^2, \zeta) dp \quad (69)$$

where

$$H(s^2, p^2, \zeta) = \alpha' \left[(\beta'^2 + p^2) \sinh \beta' \sinh \alpha' \zeta - 2p^2 \sinh \alpha' \sinh \beta' \zeta \right]$$

2. Evaluation of Formal Solution

The evaluations of the integrals indicated in equation 69 are accomplished using the same methods applied previously to the approximate problems with, however, greater algebraic complexity. The integrations can again be performed in either order with the first through simple residue theory.

The integrand is even in α' and β' and consequently does not have branch point character due to these functions even though α' and β' themselves are multivalued. Physically this can be interpreted as reflecting the finiteness of the domain in ζ as argued in reference 27.

Method 1

For sufficiently large p the integrand behaves like $1/p$. Making use of Method 1, by inverting the Fourier transform first, integration along an infinite arc in the upper half p -plane vanishes for $\xi > 0$. It remains only to evaluate the residues that arise from the zeros of $G(s^2, p^2)$.* For a given s an infinite set of p_n exists for which $G(s^2, p_n^2) = 0$, $n = 0, 1, 2, \dots$. These zeros correspond to the modes of symmetric wave transmission of the Rayleigh-Lamb frequency equation provided $s = -i\pi\Omega$. Again $\text{Im } p_n > 0$ on Br_1 is required for $\xi > 0$, and this assures that no zeros fall on the real p -axis. The remaining integration is given by

$$\frac{2\pi}{F\ell_0} W(\xi, \tau, \zeta) = \int_{\text{Br}_1} \frac{e^{s\tau}}{s} ds \sum_{n=0}^{\infty} \frac{e^{ip_n\xi} H(s^2, p_n^2, \zeta)}{\left[\frac{\partial}{\partial p} G(s^2, p^2) \right]_{p=p_n}} \quad (70)$$

* The zero at $\beta'=0$ does not give rise to a simple pole, since $H(s^2, p^2)$ also has a zero there.

where the p_n are functions of s given by $G(s^2, p_n^2) = 0$.

To invert the remaining transform consideration must be given to the singularities of the integrand in equation 70. Consider an inversion path which completes Br_1 to the left and follows the imaginary s -axis except for indentations to the right at possible branch points and poles of the integrand. Existence of poles and branch points in the right half s -plane is not permitted, since the solution is expected to be bounded in time. (The branch point $s = S_2$ in the right half of the s -plane found in the approximate case exists only for times less than the arrival time of the second wave. For large time and far stations such a branch point can be shown, through Watson's lemma, to contribute at most a term of order $1/\sqrt{t}$; hence stability is assured there (15).)

The determination of possible branch points for the exact problem unfortunately is not as easy as in the case of the approximate problem where merely an inspection of the algebraic expressions reveals the multivalued character. Any branch points must be a result of the particular function p_n , since the integrand is still even in α' and β' . Using the fact that $s = -i\pi\Omega$ and referring to Appendix A, the only points on the imaginary s -axis at which branch points occur are where $ds/dp_n = 0$. In the neighborhood of such a point (denoted by the pair s_*, p_{n*}) the p_n are given by

$$p_n - p_{n*} \sim \sqrt{s - s_*}$$

Note that this is in agreement with the results from the approximate theory.

The denominator of the integrand in equation 70 may be written as

$$\left[\frac{\partial G}{\partial p} (s^2, p^2) \right]_{p=P_n} = 2p_n \left[\frac{\partial G}{\partial \eta} (s^2, \eta) \right]_{\eta=P_n^2} \quad (71)$$

When p_{n^*} is zero the branch character is conveniently removed from the derivative and is contained only in the leading p_n . When p_{n^*} is not zero the apparent complication can be handled by considering the two conjugate complex arms together as demonstrated in the example that follows.

Inversion for Modes $n = 1$ and $n = 2$

The inversion path in figure 19 is used with the exception that the path around the branch cut on the real axis is replaced by a small indentation at the origin. The cutoff frequencies correspond to $s = \pm i\pi$ and $s = \pm i\pi g$, and the minimum in the first mode is assumed to be at $s = \pm i\pi S_1$ (S_1 not defined the same as for equations 52a and 52b). Subject to the condition that $\text{Im } p_n > 0$ on Br_1 and referring again to Appendix A and the computed spectra of figure 12, for example, the p_1 and p_2 are easily traced along the paths. Their arguments are indicated in Table I.

Path	Arg p_1	Arg p_2
L_1	0	0
L_2	0	$\frac{\pi}{2}$
L_3	0	π
L_4	$0 < \arg p_1 < \frac{\pi}{2}$	$\frac{\pi}{2} < \arg p_2 < \pi$

Table I

The argument of the term $\left[\frac{\partial G}{\partial p} (s^2, p^2) \right]_{p=P_1, P_2}$ follows directly from equation 71 for $|s| > \pi S_1$. For $|s| < \pi S_1$

$$\left[\frac{\partial}{\partial p} G(s^2, p^2) \right]_{p=p_1} = - \overline{\left(\left[\frac{\partial G}{\partial p} (s^2, p^2) \right]_{p=p_2} \right)^*}$$

where

$$\operatorname{Re} \left[\frac{\partial G}{\partial \eta} (s^2, \eta) \right]_{\eta=p_1^2} = \operatorname{Re} \left[\frac{\partial}{\partial (p^2)} G(s^2, p^2) \right]_{p=p_1} > 0$$

Analytic continuation to the upper half s -plane gives the result that integrations, along paths corresponding to those in the lower half plane, contribute the complex conjugates of the integrations from the lower half plane. It is therefore only necessary to consider integral contributions in the lower half plane taking twice the real part of each integral. The following set of integrals result for the vertical displacement W :

$$\frac{-2\pi}{F \ell_0} W(\xi, \tau, \zeta) = \sum_{i=0}^5 I_i \tag{72}$$

$$I_0 = \pi \operatorname{Im} \left\{ \frac{e^{ip_1 \xi} H(0, p_1^2, \zeta)}{p_1 \frac{\partial G}{\partial \eta} (0, \eta) \Big|_{\eta=p_1^2}} \right\} \quad (\operatorname{Im} p_1 > 0)$$

$$I_1 = \int_{\pi}^{\infty} \frac{H(-\eta'^2, p_2^2, \zeta)}{p_2 \frac{\partial G}{\partial \eta} (-\eta'^2, \eta) \Big|_{\eta=p_2^2}} \cos(p_2 \xi - \eta' \tau) \frac{d\eta'}{\eta'} \quad (p_2 \text{ real and } > 0)$$

$$I_2 = - \int_{\pi g}^{\pi} \frac{H(-\eta'^2, p_2^2, \zeta) e^{ip_2 \xi}}{(-ip_2) \frac{\partial G}{\partial \eta} (-\eta'^2, \eta) \Big|_{\eta=p_2^2}} \sin \eta' \tau \frac{d\eta'}{\eta'} \quad \begin{matrix} (p_2 \text{ imaginary}) \\ \operatorname{Im} p_2 > 0 \end{matrix}$$

* The wavy line denotes the complex conjugate.

$$I_3 = - \int_{\pi S_1}^{\pi g} \frac{H(-\eta'^2, p_2^2, \zeta)}{(-p_2) \frac{\partial G}{\partial \eta} (-\eta'^2, \eta) \Big|_{\eta=p_2^2}} \cos(-p_2 \xi + \eta' \tau) \frac{d\eta'}{\eta'} \quad (p_2 \text{ real and } < 0)$$

$$I_4 = 2 \operatorname{Im} \int_0^{\pi S_1} \frac{H(-\eta'^2, p_1^2, \zeta) e^{ip_1 \xi}}{p_1 \frac{\partial G}{\partial \eta} (\eta'^2, \eta) \Big|_{\eta=p_1^2}} \sin \eta' \tau \frac{d\eta'}{\eta'} \quad (\operatorname{Im} p_1 > 0)$$

$$I_5 = \int_{\pi S_1}^{\infty} \frac{H(-\eta'^2, p_1^2, \zeta)}{p_1 \frac{\partial G}{\partial \eta} (-\eta'^2, \eta) \Big|_{\eta=p_1^2}} \cos(p_1 \xi - \eta' \tau) \frac{d\eta'}{\eta'} \quad (p_1 \text{ real and } > 0)$$

where η' is a dummy variable. This solution is valid for $\tau / \sqrt{\xi^2 + (\zeta - 1)^2} > a$ which corresponds to $t / \sqrt{x^2 + (z-h)^2} > 1/c_d$.

The results indicated in equation 72 may be compared integral by integral with the results of the approximate theory presented in equations 52a and 52b. These integrals in turn establish a direct relationship of the various portions of the exact frequency spectrum to their contribution to the transient response. The term I_0 is only the partial static deflection. The total static deflection as well as the entire transient response must include the contributions from the remaining modes.

The example considered here has demonstrated the similarity in the exact and approximate theories, and a related method of solving transient wave propagation problems. A similar approach can be applied to other modes provided complex arms are taken in conjugate complex pairs.

Method 2

Since the integrand of equation 69 is of order $1/s^k$, $k > 0$, integration along an infinite arc to the left of Br_1 in the s -plane will vanish. The integral along Br_1 is simply equal to the sum of the residues of the integrand at simple poles corresponding to the zeros of $G(s^2, p^2)$ and a zero at the origin. Since p is real (imposed by the Fourier transform path of integration), these zeros of $G(s^2, p^2)$ are the roots of the Rayleigh-Lamb frequency equation where $s_n = \pm i\pi\Omega_n$, and they fall on the imaginary s -axis. Evaluation of the residues gives

$$\frac{2\pi W}{F_{l0}}(\xi, \tau, \zeta) = 2 \int_0^\infty \cos \xi p dp \left\{ \begin{array}{l} \frac{\frac{\partial}{\partial(\eta^2)} H(\eta^2, p^2, \zeta)}{\frac{\partial}{\partial(\eta^2)} G(\eta^2, p^2)} \Big|_{\eta^2=0} \\ - \sum_{n=0}^{\infty} 2 \frac{H(-\pi^2 \Omega_n^2, p^2, \zeta)}{\pi^2 \Omega_n^2 \frac{\partial}{\partial \eta} G(\eta, p^2)} \Big|_{\eta = -\Omega_n^2 \pi^2} \cos(\pi \Omega_n \tau) \end{array} \right\} \quad (73)$$

Here it has been noted that in the neighborhood of $s = 0$ the quantities $H(s^2, p^2, \zeta)$ and $G(s^2, p^2)$ are proportional to s^2 . Again the denominator is studied for possible branch points in the Ω_n . Using arguments similar to those of Skalak (28), that there are no points of infinite slope $d\Omega_n/dp = \infty$, it can be shown that no branch points fall on the real p -axis. This is discussed in greater detail later drawing on the results of Appendix A.

The first term in the integral of equation 73 is the static solution, and the terms of the series represent traveling wave contributions from the various modes of wave transmission described by the Rayleigh-Lamb

frequency equation. In his work on the symmetric loading problem related to equation 73, Miklowitz (27) evaluated the lowest mode waves for the far field with the method of stationary phase.

C. Discussion of Methods and Their Relation to Certain Wave Features

The relatively simple algebraic properties of the approximate theories permits a significant degree of flexibility for computation and approximation. The interpretation of the results may be applied to the exact problem. It is seen by examining the forms of the transient solutions that the similarity in the frequency spectra is reflected in the transient response. The important feature here is not necessarily the numerical values but rather the behavior of the response resulting from the various arms that make up the frequency spectrum. For this purpose the results from the approximate theory demonstrate clearly the influence and behavior of the complex and imaginary arms, as well as the real arms. A direct correlation exists between the integral solutions presented in the previous sections in Part II and the frequency spectra presented in Part I. Each of the integrals of equations 52a, 52b, 54a, 54b, 57, 58, 60a, 60b, 72, and 73 can be seen to correspond directly to the contributions from one of the arms of the frequency spectrum. In each case the $p_n(s)$, where s is proportional to $-i\Omega$, is the functional dependence of wave number on frequency which described such an arm. For example, compare equation 49 with equation 28.

1. Comparison of Methods 1 and 2

Two distinct forms of solution result depending on the order of inversion of the double transform. Method 1, which inverts the Fourier

transform in the spacial variable first, has been used by Folk, Fox, Shook, and Curtis (29) and Jones (30), for example, in problems involving solutions based on the exact linear elasticity theory. In these references the second inversion was approximated by the methods of stationary phase and saddle point integration. Detailed branch point study was not employed, since the lowest symmetric mode does not have a branch point and the higher modes were not investigated in the vicinity of their branch points. The relative simplicity of the lower order approximate theories of the Timoshenko beam type has permitted more detailed study of this method by other authors. For examples, see Miklowitz (14, 22) and Boley and Chao (31). In the approximate theories the principle advantage arising from this order of inversion has been the analytic separation of the solution into time regions delineated by the arrival of two distinct waves. Method 2, which inverts the Laplace transform in the time variable first, has been used by Skalak (28) and Miklowitz (27), for example, in problems using the exact linear elasticity theory. Again the details of the second inversion were not considered, and the use of the approximations was made as in the former case. This method has been applied by Jones (16) and Boley (32, 6) for the Timoshenko beam theory. The main benefit in applying this order of inversion lies in the simplification of the details required to reduce the solution to real integrals.

For the sake of discussion compare the forms of equations 52a with 54a. In the former case where Method 1 has been used the correspondence between the integrals and the frequency spectrum is through the condition that the frequency is real. This results in integrals which have complex, imaginary, or real wave numbers, p_j , which may be identified with the

corresponding branches of the spectra shown, for example, in figure 9. Where Method 2 has been used, equation 54a, the resulting integrals contain only real wave numbers (as a function of real frequency) in agreement with the undeformed Fourier inversion path. All branch points of the integrals in equation 54a fall above or below the integration path but not on it. This result may be interpreted in terms of the conformal mapping properties between the wave number and frequency planes discussed in Appendix A. Subject to the condition that along real arms of the frequency spectrum there are no points where $d\Gamma/d\Omega = 0$, following the procedures of Appendix A shows that no branching points can be found which result in complex frequencies. Points where $d\Omega/d\Gamma = \infty$ ($\frac{d\Gamma}{d\Omega} = 0$) correspond to waves which travel at an infinite group velocity and are physically unacceptable in a hyperbolic system of governing equations. Such points do not occur in either the approximate or the exact frequency spectra, where the steepest slope, $d\Omega/d\Gamma$, corresponds to waves traveling at the plate speed, c_p , and the dilatation speed, c_d , respectively.

Though the solutions of both methods necessarily result in the same ultimate response, the interpretation of the individual integrals in each must be considered independently. To illustrate this, the integrals of Method 1 which are related to the real arms of the frequency spectrum, I_1 , I_3 and I_5 , have stationary phase points corresponding to waves traveling away from the source in agreement with the infinity condition. Only the integral I_3 has negative phase velocities in agreement with the computed spectrum for real frequencies. In terms of the frequency spectrum the

infinity condition is contained in $\text{Im } p_n > 0$ which is the same as $\text{Im } p_n > 0$ on Br_1 and Br_2 , figure 19.

The integrals resulting from the use of Method 2 can be each re-written using the trigonometric identity

$$\cos p_n \xi' \cos s \gamma' = \frac{1}{2} \cos(p_n \xi' + s \gamma') + \frac{1}{2} \cos(p_n \xi' - s \gamma')$$

Thus the integrals from Method 2 can be separated into two types of integrals: the first with positive traveling wave groups (away from the source) and the second with negative traveling groups (toward the source). This may be interpreted to mean that two groups of waves traveling in opposite directions and infinite in extent are superimposed to give the transient response. These waves necessarily cancel for stations which the front of the transient wave has not yet reached. Only the outward traveling waves have points of stationary phase and offer the principle contribution to the result for the far field. The negative traveling waves give rise to integrals governed by the Riemann-Lebesgue lemma (33) which decay as $(1/\gamma')$, whereas the stationary phase integrals (33) are of the order $(1/\sqrt{\gamma'})$.

It can be shown by a change of integration parameters, without resorting to algebraic computation, that the integrals of the outward traveling waves for both Methods 1 and 2 are equivalent. This means that integrals of negative traveling waves from Method 2 are equivalent to the contributions from the integrals of Method 1 which correspond to the complex and imaginary arms of the frequency spectrum. Integrals governed by the Riemann-Lebesgue lemma, which do not have points of stationary phase but arise in wave propagation problems, have been

discussed by Havelock (34) and termed "nonwave". Their function in the solution is to satisfy boundary and initial conditions. Consider as an example the integrand of one of the negative traveling wave integrals from Method 2 for fixed time, γ' , and positive station, ξ' . A point of stationary phase does not exist. However, if the integrand is plotted for negative values of the variable of integration, the wave number p , then such a critical point does exist as sketched in figure 21. This means that the integration which involves only the positive p -axis is an integration over the canceling portion of a stationary phase integral. The more negative this stationary phase point is, the less is the contribution from the oscillatory integrand in the positive region. The position of this stationary phase point corresponds directly to the stationary phase point for its positive traveling wave counterpart, but it is negative. Therefore in the case of the approximate theory, where the head of the wave is at large wave numbers, the contribution from such a negative traveling wave will be small in the vicinity of the wave front. For a fixed time this contribution is larger for stations closer to the origin. This result agrees with the integral forms of I_{s_2} and I_{s_4} of equation 52a, which have negative real exponents proportional to ξ' .

2. Extensions of Method 1 and Approximations

a. Wave Front Approximations

Working directly with equations 50a and 50b after the inversion of the Fourier transform, it is possible to make a wave front expansion which will serve as a check on the results from numerical integration. This is made possible using Method 1 since the wave front is clearly defined

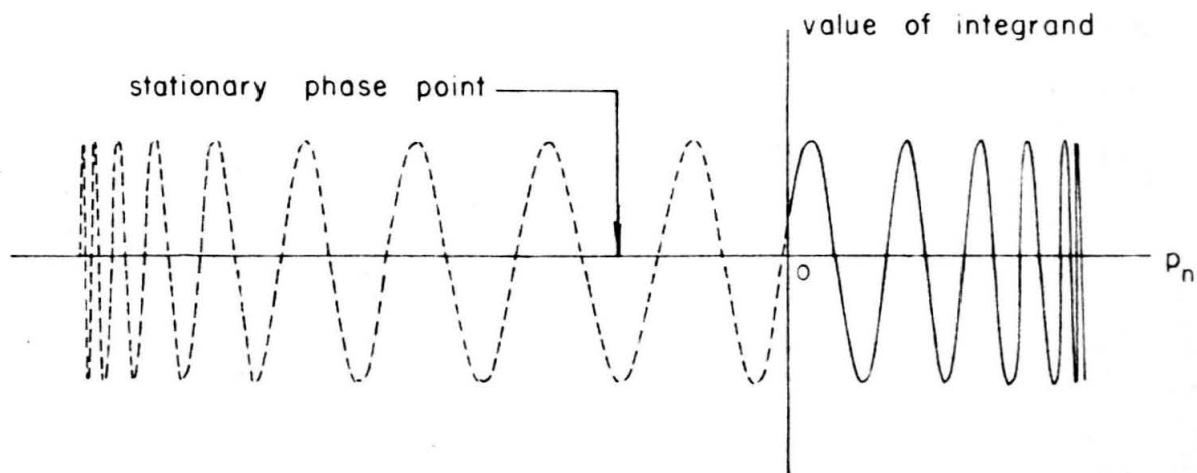


Figure 21. Sketch of integrand for negative traveling wave integral.

through the fact that the Bromwich contour, Br_1 , lies to the right of all singularities. Since Br_1 lies at an arbitrary positive distance from the imaginary axis, this distance may be made large and the integrand approximated for large $|s|$ accordingly. Termwise integration of the resulting Gamma function integrals gives the wave front expansion good for small times after the wave front arrival. Expansions for equations 50a and 50b, where the first three terms in the expansion have been included, are at the first wave front, $\gamma' > \delta \xi'$,

$$\frac{2\pi W_b}{\delta^2 F_{\ell 0}} \approx \frac{\pi (\gamma' - \delta \xi')^3}{6\delta (1 - \delta^2)} \left\{ 1 - \frac{\delta \xi'}{8(1 - \delta^2)} (\gamma' - \delta \xi') - \frac{1}{20(1 - \delta^2)} \left[\frac{1}{2} + g^2 - \frac{2\delta^2}{1 - \delta^2} \right] \right\} (\gamma' - \delta \xi')^2$$

$$\frac{2\pi W_s}{\delta^2 F_{\ell 0}} \approx - \frac{\pi (\gamma' - \delta \xi')^3}{6\delta (1 - \delta^2)^2} \left\{ 1 - \frac{\delta \xi'}{8(1 - \delta^2)} (\gamma' - \delta \xi') - \frac{1}{20(1 - \delta^2)} \left[\frac{1}{2} + g^2(1 + \delta^2) - \frac{3\delta^2}{1 - \delta^2} \right] \right\} (\gamma' - \delta \xi')^2$$

and at the second wave front, $\gamma' > \xi'$,

$$\frac{2\pi W_b}{\delta^2 F_{\ell 0}} \approx - \frac{\pi (\gamma' - \xi')^3}{6(1 - \delta^2)} \left\{ 1 - \frac{\xi'}{8} \left(g^2 - \frac{\delta^2}{1 - \delta^2} \right) (\gamma' - \xi') - \frac{1}{20} \left[\frac{1}{2} \left(g^2 - \frac{\delta^2}{1 - \delta^2} \right) + \frac{1}{1 - \delta^2} \right] \left(g^2 - \frac{2\delta^2}{1 - \delta^2} \right) (\gamma' - \xi')^2 \right\}$$

$$\frac{2\pi W_s}{\delta^2 F_{\ell 0}} \approx \frac{\pi (\gamma' - \xi')}{\delta^2} \left\{ 1 - \frac{\xi'}{4} \left(g^2 - \frac{\delta^2}{1 - \delta^2} \right) (\gamma' - \xi') - \left[\frac{1}{2} \left(g^2 - \frac{\delta^2}{1 - \delta^2} \right) - \frac{\delta^2}{(1 - \delta^2)^2} \right] (\gamma' - \xi')^2 \right\}$$

Here the expansions at the second wave front are due to the second terms in the integrands of equations 50a and 50b. The results of this expansion show the continuity of the displacement at the wave front arrivals. At the arrival of the second wave the shear displacement has a discontinuous slope which indicates a jump in shear stress. This result is in agreement with and due to the shear nature of the source loading function. Notice that the derivative of this term at the shear wave front does indeed result in a jump in dimensionless load of $Q = -F_0/2$ in agreement with the input function.

b. Stationary Phase Approximations

Integrals I_{s_1} , I_{s_2} and I_{s_5} , equation 52b, are of the stationary phase type. Through the use of the stationary phase method, but subject to its limitations, evaluation of these integrals is simplified considerably. Unfortunately in the present work the limitations are rather severe. A criterion for estimating the range of parameters over which the stationary phase approximation of an integral is valid is developed in Appendix C. It is based on the higher order derivatives involved with the approximation of the integrand and the truncation of integration due to its limits. Specific numerical examples related to the problems studied numerically later are considered in Appendix C. The results indicate that the applicability of this form of approximation is limited to extremely far fields. Several detrimental features of the integrals in the present work influence this difficulty:

1. The close proximity of the stationary phase point to the integral limit does not permit the highly oscillatory nature of the integrand to take

place before the limit is reached. As a result the stationary phase approximation includes contributions that should not be incorporated. This close proximity may be seen easily in terms of the frequency spectrum when ξ'/τ' is small. The points of stationary phase are defined by the points on the real arms where the slope is equal to ξ'/τ' , i.e., $d\Omega/d\Gamma' = \xi'/\tau'$ (the group velocity). Since the real branches have zero slope at the cutoff frequencies and the minimum at Ω_* , the points of stationary phase approach these three frequencies for small ξ'/τ' (the tail of the wave). These frequencies are in turn the limits of the integrals.

2. The integrals I_{s_1} , I_{s_2} , and I_{s_5} are improper at their finite limits. Consequently when the stationary phase points are near these limits the coefficient of the exponential term is no longer slowly varying.

3. The third derivative of the phase and the first derivative of the amplitude function are not negligible compared to the lower derivatives.

In each case if the field of interest is chosen far enough from the source, the error in the stationary phase method of approximation can be made negligible.

c. Alternate Path of Integration

The path of integration along the imaginary axis of the Laplace transform plane has been taken to illustrate the influence of the various portions of the frequency spectrum. These integrals are not easily integrated numerically as a result of the oscillatory nature of their integrands. This difficulty becomes worse for long time evaluation due to the increased frequency of this oscillation.

The original path of integration can be deformed as indicated in figure 22. The resulting infinite real integrals may still be related to the various integrals of equations 52a and 52b by using the Cauchy integral theorem. This correspondence is indicated in figure 22 where the integration paths are labeled as in figure 19. A quarter residue is included in path L_1 .

This path deformation is prompted by the advantage of exponentially decaying integrands. For long time this decay causes the greatest contributions to occur in the neighborhood of the branch points, in agreement with the discussion of the stationary phase method of approximation. One would expect this also on the basis of Watson's lemma (24), which may be applied to integrals arising from paths such as those in figure 22.

Again only the lower half plane is considered, and along a given path the net contribution is twice the real part. The multivalued character of p_j and its inner root require the branch cuts shown in figure 22. If the two terms of equations 50a and 50b are taken together, the zeros of the inner root that fall on the real axis are not branch points of the composite integrand. Using the results of Appendix B, where analytic continuation was used to establish the branches of p_j and its inner root, Z , on the imaginary s -axis, the arguments of these functions have been established on the new paths. These results are indicated in figure 22. (Note that the points $s = -i$ and $s = -ig$ are not branch points of p_1 .) The corresponding integrals may be evaluated numerically with the aid of complex arithmetic. The merits of this direct method of integration are somewhat offset by the greater numerical effort required to evaluate each integrand. Though

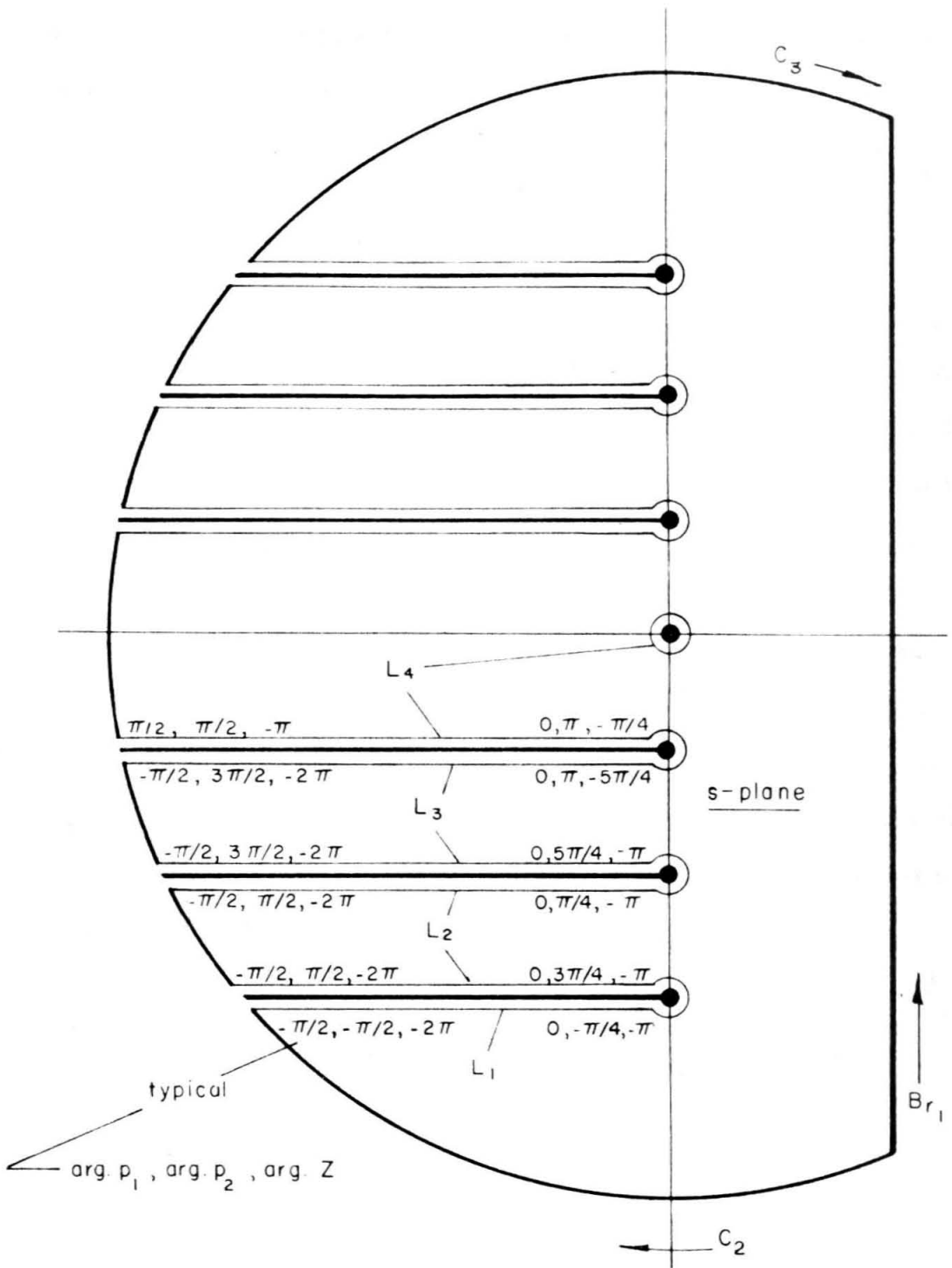


Figure 22. Deformation of integration path of figure 19.

integration along the imaginary axis may require a finer mesh to maintain accuracy, the integrand involves considerably less computation time. For long time, however, the direct method becomes superior because of the aforementioned difficulty of an oscillatory integrand along the imaginary axis.

As pointed out earlier for very long time the integrals along the paths of figure 22 are of the type amenable to approximation using Watson's lemma. This method is applied by expanding the integrand in the neighborhood of the branch point retaining the exponential term. Term by term integration leads to an asymptotic expansion valid for long time.

Unfortunately the limitations of this method, as in the case of stationary phase, relegate its possible use in the present work to times greater than the range of interest. The cause of this difficulty is the close proximity of the branch points, which gives rise to severe restrictions on the necessary expansions. For example, a crude estimate of the range of validity can be made by expanding the p_j in the neighborhood of a branch point of their inner root, $s = -iS_1$. The result is

$$p_j \simeq \left\{ \frac{1}{2} \left[S_1^2 (1 + \delta^2) - g^2 \right] - (-1)^j \frac{1 - \delta^2}{2} \sqrt{2S_1(S_1^2 + S_2^2)} \sqrt{\eta} + O(\eta) \right\}^{1/2}$$

where $s = -iS_1 - \eta$. For the case of $\delta^2 = .28375^*$ and $g^2 = .9079^*$ this expansion is numerically

$$p_j \simeq \left[.071 - (-1)^j .55 \sqrt{\eta} + O(\eta) \right]^{1/2}$$

In order to expand further, η must satisfy the inequality

$$\eta \leq .0166$$

* These values of δ^2 and g^2 relate to one of the numerical examples studied in detail later.

This rather small value of η is what causes difficulty and results from the close proximity of the zero of the inner root to the zero of the p_j .

Consider now an exponential integral of the Watson's lemma form

$$I = \int_0^{\infty} f(\eta) e^{-\eta \gamma'} d\eta$$

where $f(\eta)$ is slowly varying. If $f(\eta)$ is assumed constant, say unity, the error introduced by truncating this integral at $\eta = \eta_0$ is given by

$$\text{Error} \simeq e^{-\eta_0 \gamma'}$$

Since the necessary expansion cannot be carried out beyond $\eta = .0166$, the truncation error will be approximately given by

$$\text{Error} \simeq e^{-.0166 \gamma'}$$

For an error of 10% this would require $\gamma' \simeq 140$ ($t \simeq 260 \frac{h}{c_p}$).

This estimate is very crude but shows how the nearness of the zeros of the p_j to the zeros of its inner root causes a simple expansion to be impossible for an adequate range of integration for exponential decay to take place. For times sufficiently large, however, this method may be applied.

D. Discussion of Results from Numerical Computation

The transient response of a plate on an elastic foundation has been computed using the integrals I_{s_i} and I_{b_i} of equations 52a and 52b for the

more exact theory of bending.*

The value $\xi^2 = .28375$ has been assumed. This corresponds to $k' = \pi^2/12$ and $\nu = .31$ and in turn causes the cutoff frequency, which is independent of the foundation stiffness, to be equal to the cutoff frequency of the third symmetric mode of an exact plate of thickness $2h$ with Poisson's ratio $\nu = .31$. Two values of g^2 have been used; $g^2 = .9079$ and $g^2 = .04$, representing a stiff and soft foundation, respectively. The former value makes the cutoff frequency at $\Omega = g$ equal to the corresponding cutoff frequency of the symmetric mode for the exact plate of thickness $2h$ and Poisson's ratio $\nu = .31$; the latter value has been arbitrarily selected to study the influence of the foundation stiffness.

For reference the frequency spectra for these two foundation stiffnesses are shown in figures 23a and 23b. The corresponding frequency spectra from the exact theory (equation 13) are also shown in these figures for spring constants adjusted by equation 23. In figure 23a the exact spectrum is for an infinite foundation stiffness in agreement with the choice of g^2 .

* All numerical evaluation of integrals was carried out on an IBM 709 electronic computer using a nine point Gaussian quadrature (35). Each interval step was compared with the results from an eight point integration over the same interval. This permitted an estimate of the error, which was maintained between 10^{-4} and 10^{-6} by adjusting the interval. Infinite integrals were truncated when the contribution over a specified interval (at least one wavelength for oscillating integrands) was 10^{-4} that of the previous integrations of that same integral.

In order to facilitate numerical evaluation, improper integrals were made regular in the neighborhood of their improper limit by a change of variables (32).

The numerical results were checked in the neighborhood of the wave fronts and found to agree with the wave front expansions within the specified error of 10^{-4} .

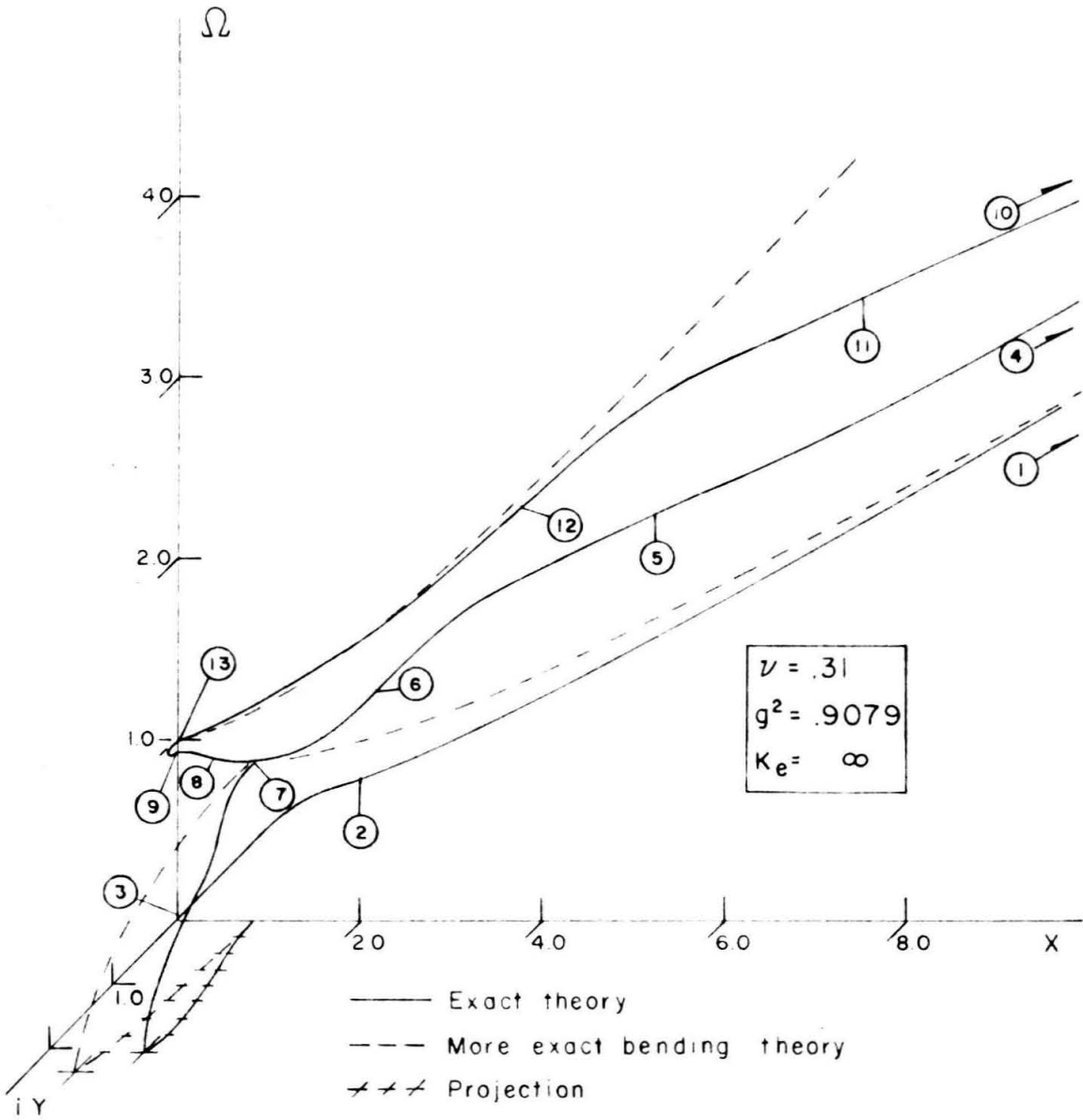


Figure 23a. Frequency spectrum for a hard foundation.

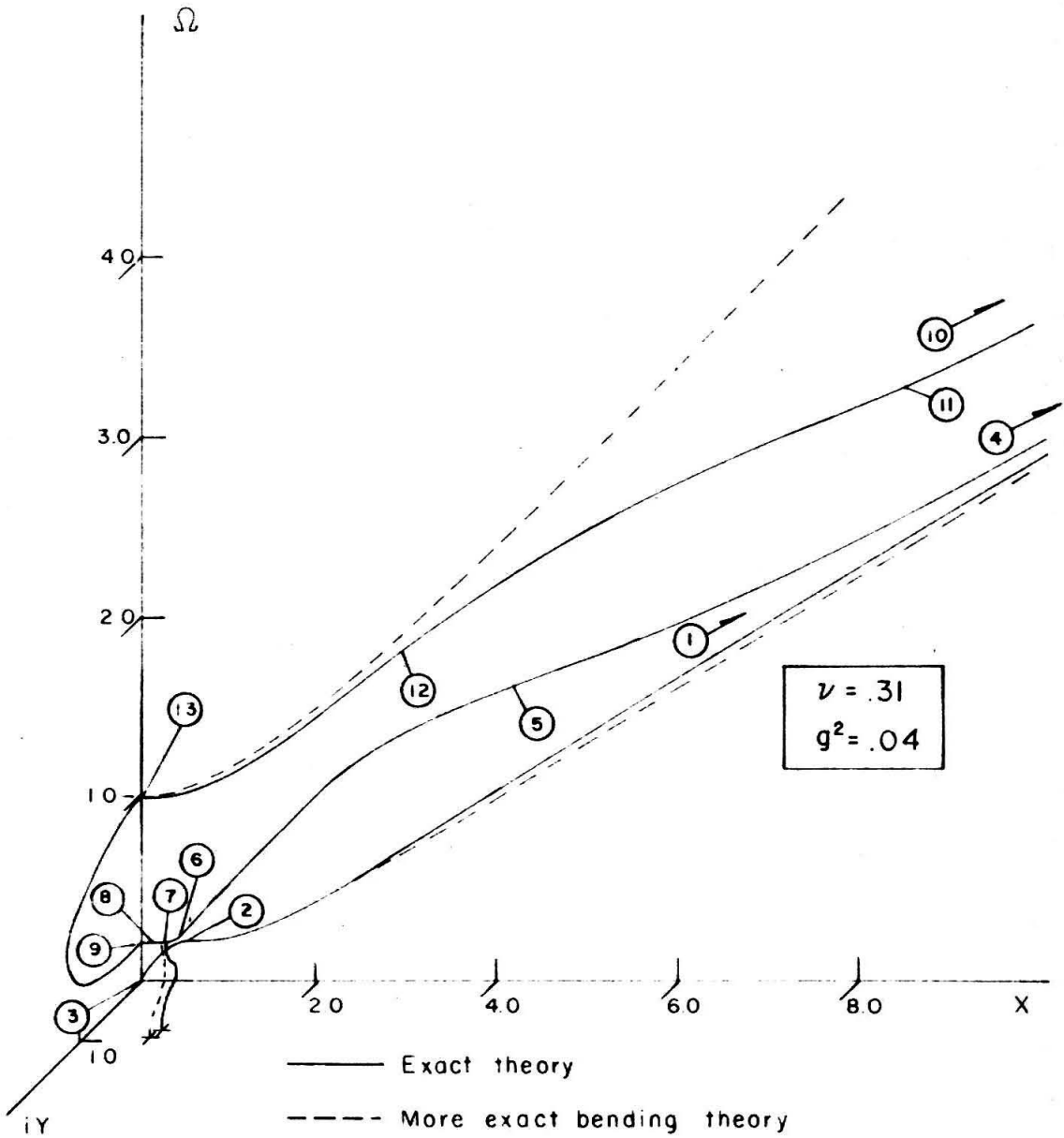


Figure 23b. Frequency spectrum for a soft foundation.

The transient solution is presented in two different ways:

1. The response is computed for a fixed station with time as the variable, as would be recorded from a strain gage, for example. It is possible, making use of stationary phase arguments, to predict the predominant period character of such a time record from the frequency spectrum. The greatest contribution at any station x and time t will be from wave groups having a group velocity $c_g = x/t$. These waves are characterized by their frequency (or predominant period), which on a time recording may be determined from the observed period of oscillation where such a recording has harmonic character. Noting that the group velocity is given by $d\omega/d\gamma$ for real arms of the spectrum, the predominant period can be related to the time of occurrence. These relations are shown in figures 24a and 24b and are derived from the spectra of figures 23a and 23b, respectively.

$$\text{Predominant period } T_p = \frac{2\pi c_p}{\omega h} = \frac{2\pi}{e \zeta} \frac{1}{\Omega}$$

$$\text{Time of occurrence } T_a = \frac{t c_p}{x} = \frac{1}{e \zeta} \frac{1}{\frac{d\Omega}{dX}}$$

The correspondence between the pairs of curves for the exact theory is indicated by the encircled numbers. To illustrate this relation consider the points (1), (4) and (10). In figure 23a the slopes of the associated modes are the high frequency limiting group velocities at these points. Figure 24a shows these speeds to be the Rayleigh surface wave speed c_R for (1) and the shear speed c_s for (4) and (10). The cutoff frequencies, (9) and (13), and the minimum of the second mode, (7), are points of

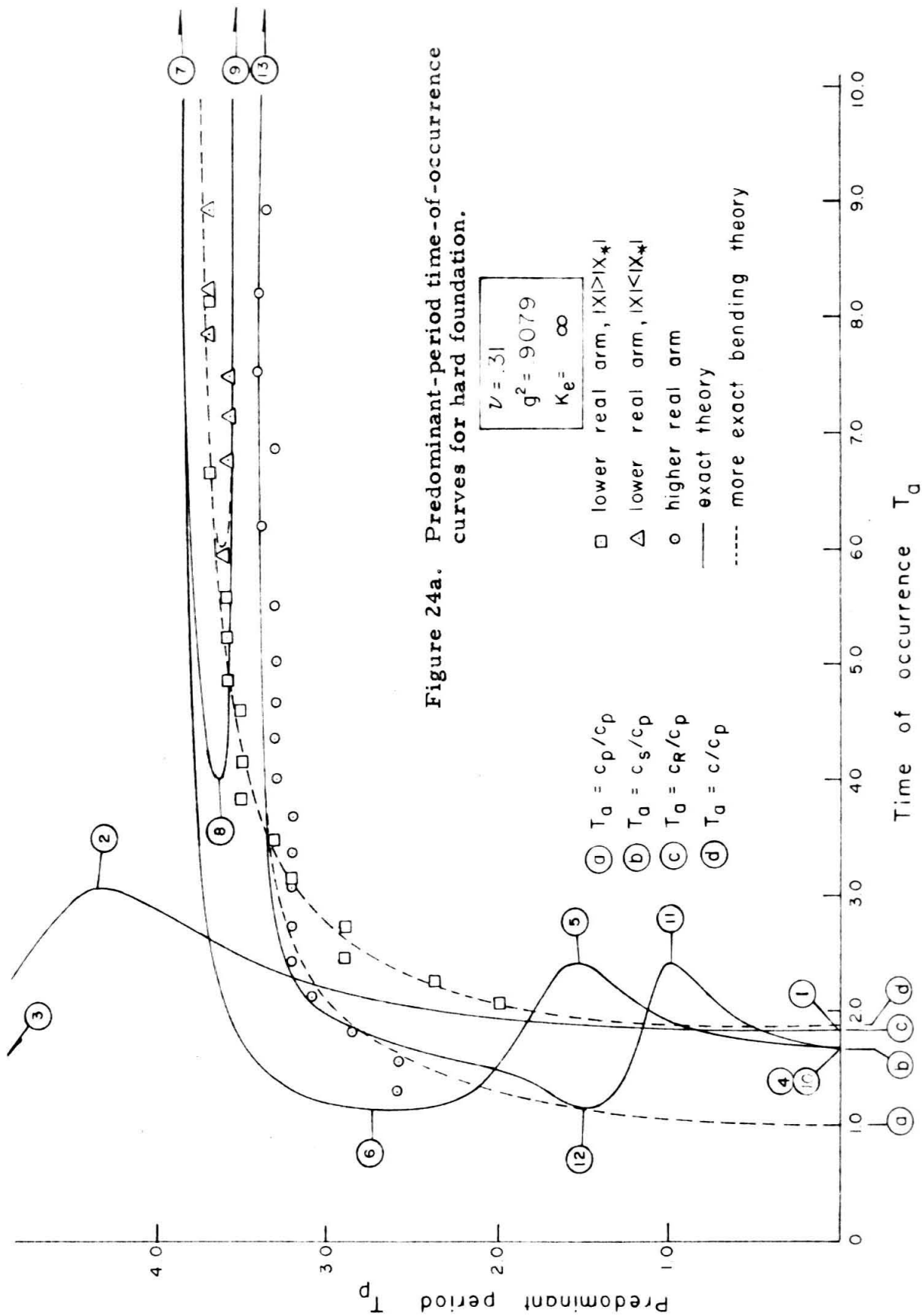


Figure 24a. Predominant-period time-of-occurrence curves for hard foundation.

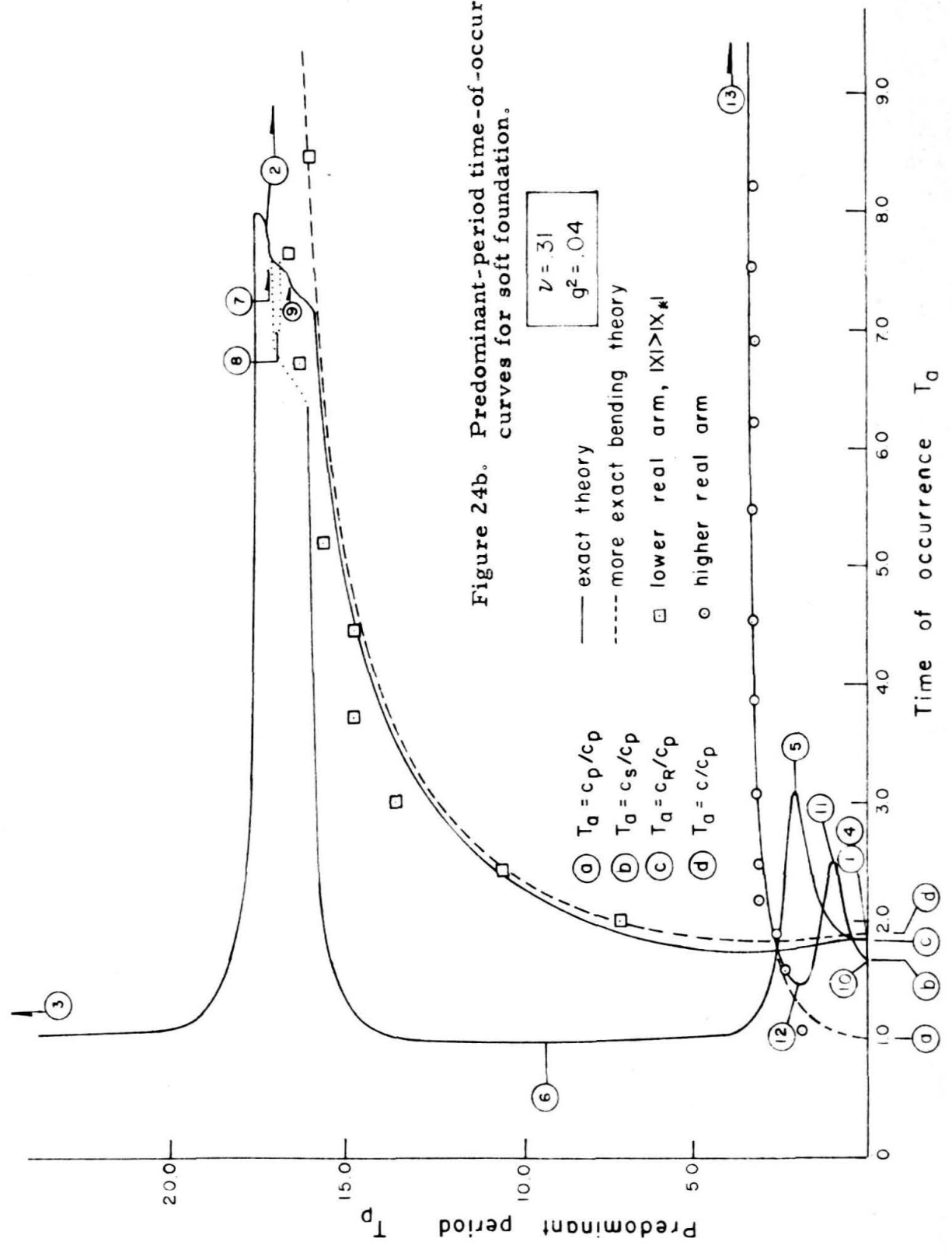


Figure 24b. Predominant-period time-of-occurrence curves for soft foundation.

zero slope for their modes, figure 23a, and correspond to a vanishing group velocity. Their influence is felt at infinite time as indicated in figure 24a. The point (3) in figure 23a is not a cutoff frequency but is the low frequency limit of the lowest mode, which has its maximum slope there. Though this limit cannot be shown in figure 24a, the limiting speed is the plate speed, c_p . The remaining points shown indicate inflection points in figure 23a and reflect points of higher order stationary phase. These points appear as extrema in figure 24a.

2. The response is computed at a fixed time with the station as the variable. Such a record of displacements would be observed in a photograph. Again using the arguments of stationary phase, it is possible to relate the observed predominant wave length to the station at which it occurs. These relations are depicted in figures 25a and 25b and correspond to figures 23a and 23b, respectively.

$$\text{Predominant wave length} \quad \lambda_p = \frac{2\pi}{\gamma h} = \frac{2\pi}{e \Gamma^1}$$

$$\text{Station of occurrence} \quad X_a = \frac{x}{tc_p} = e \delta \frac{d\Omega}{dX}$$

The related points of the exact theory are again indicated. Further reference to these two sets of curves will be made in later discussion.

The response records from numerical computation are shown in figures 26a, b through 46a, b.* The times have been normalized such that $\gamma^0 = tc_p/h = \gamma^1/e\delta$, and the stations are given by $\xi^0 = x/h = \xi^1/e$.

*The origin of time in these records corresponds to the time of arrival of the fastest waves represented in the more exact theory of bending (speed c_p).

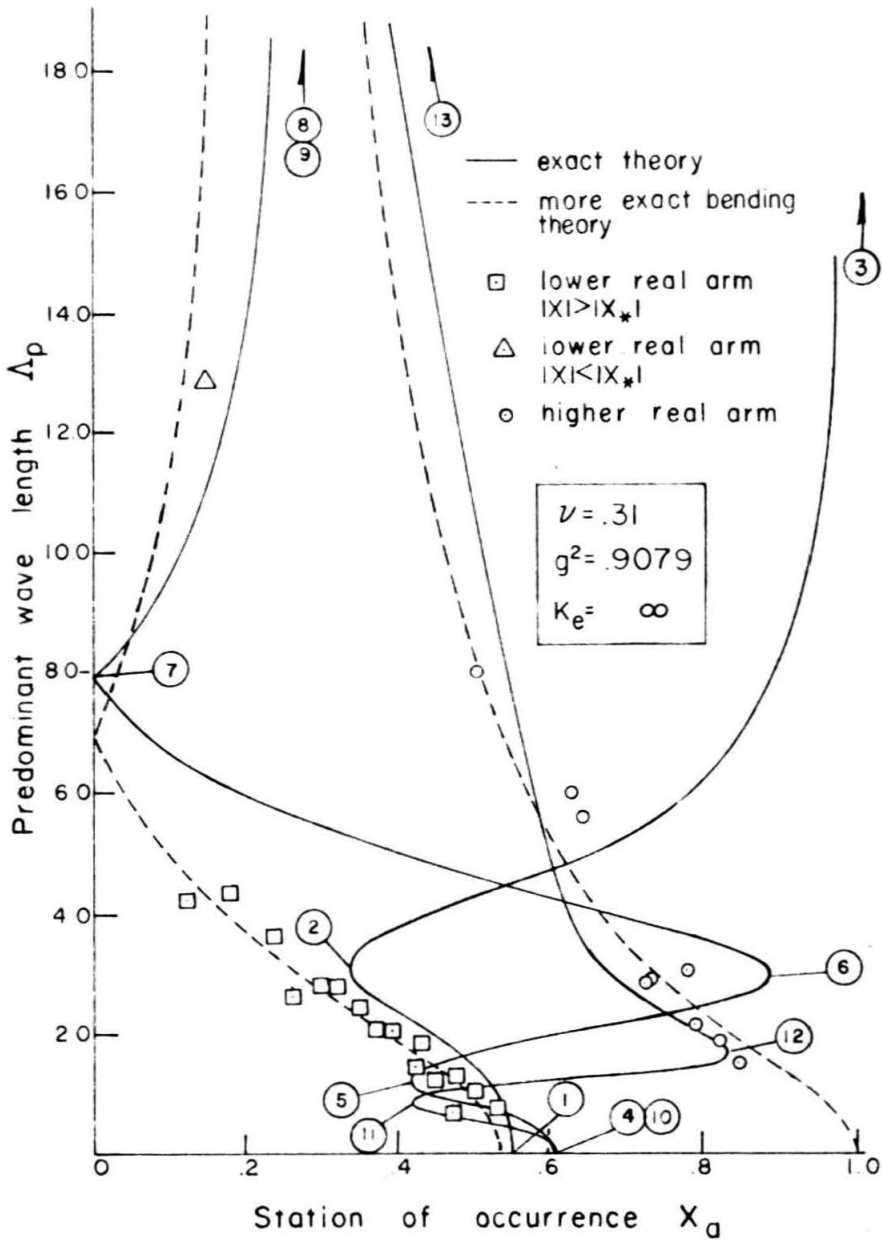


Figure 25a. Predominant wave-length station-of-occurrence for hard foundation.

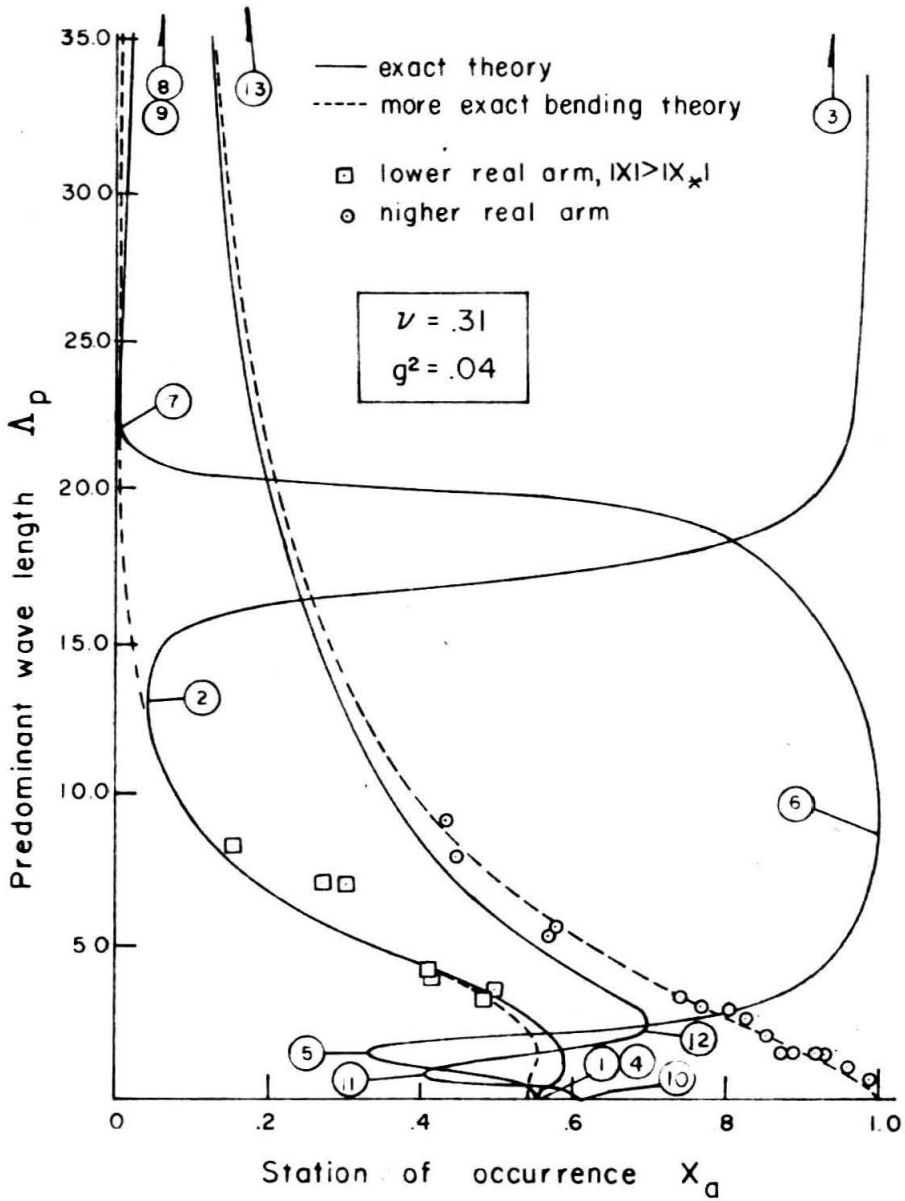
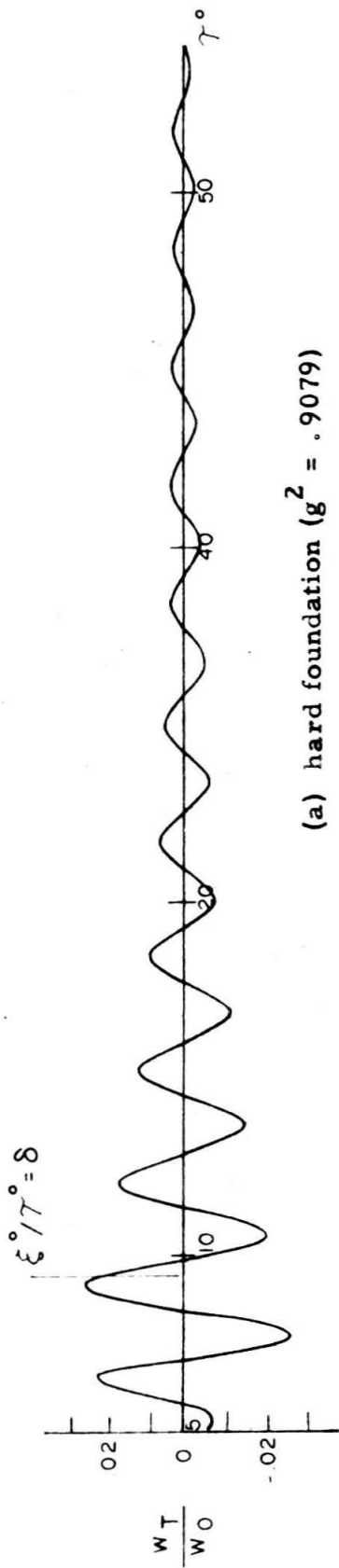
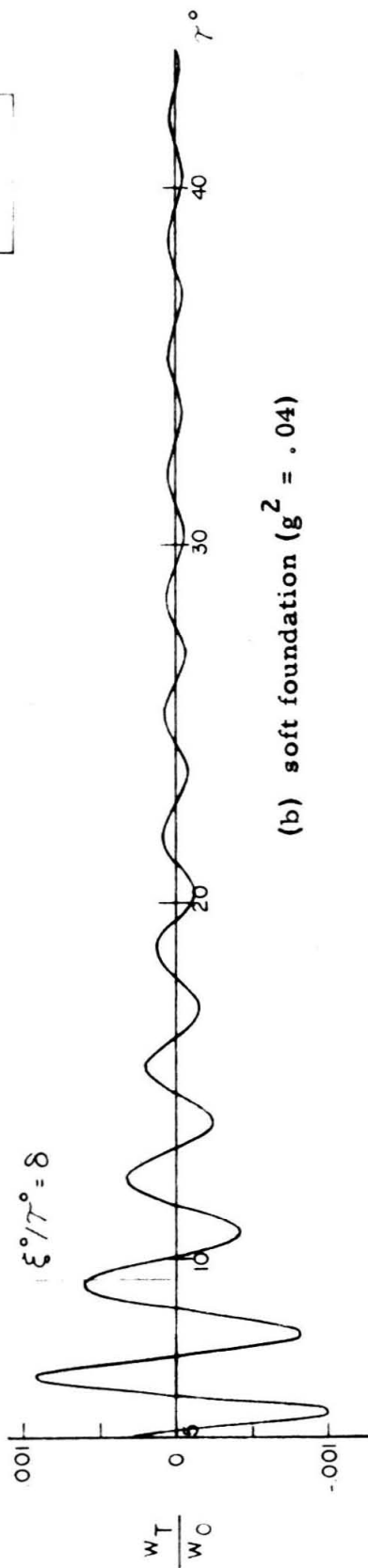


Figure 25b. Predominant wave-length station-of-occurrence curves for soft foundation.



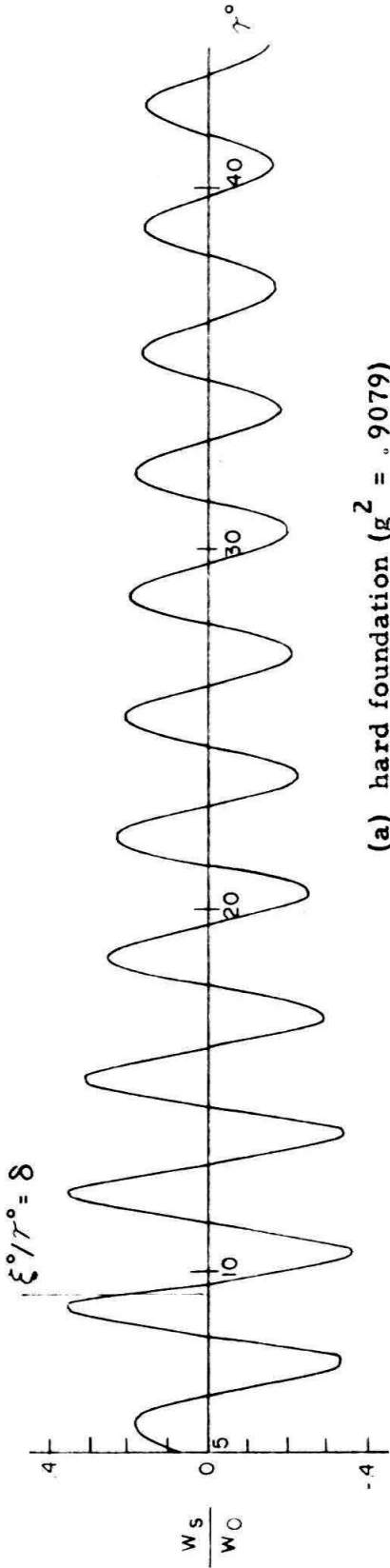
(a) hard foundation ($g^2 = .9079$)

$$\xi^\circ = 5$$



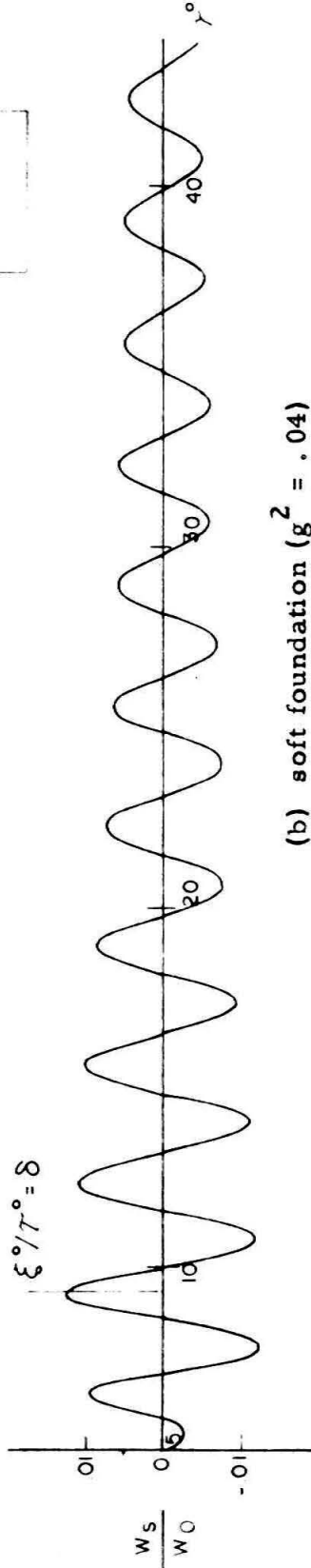
(b) soft foundation ($g^2 = .04$)

Figure 26. Total deflection time response: higher real arm.



(a) hard foundation ($g^2 = .9079$)

$\xi^0 = 5$



(b) soft foundation ($g^2 = .04$)

Figure 27. Shear deflection time response: higher real arm.

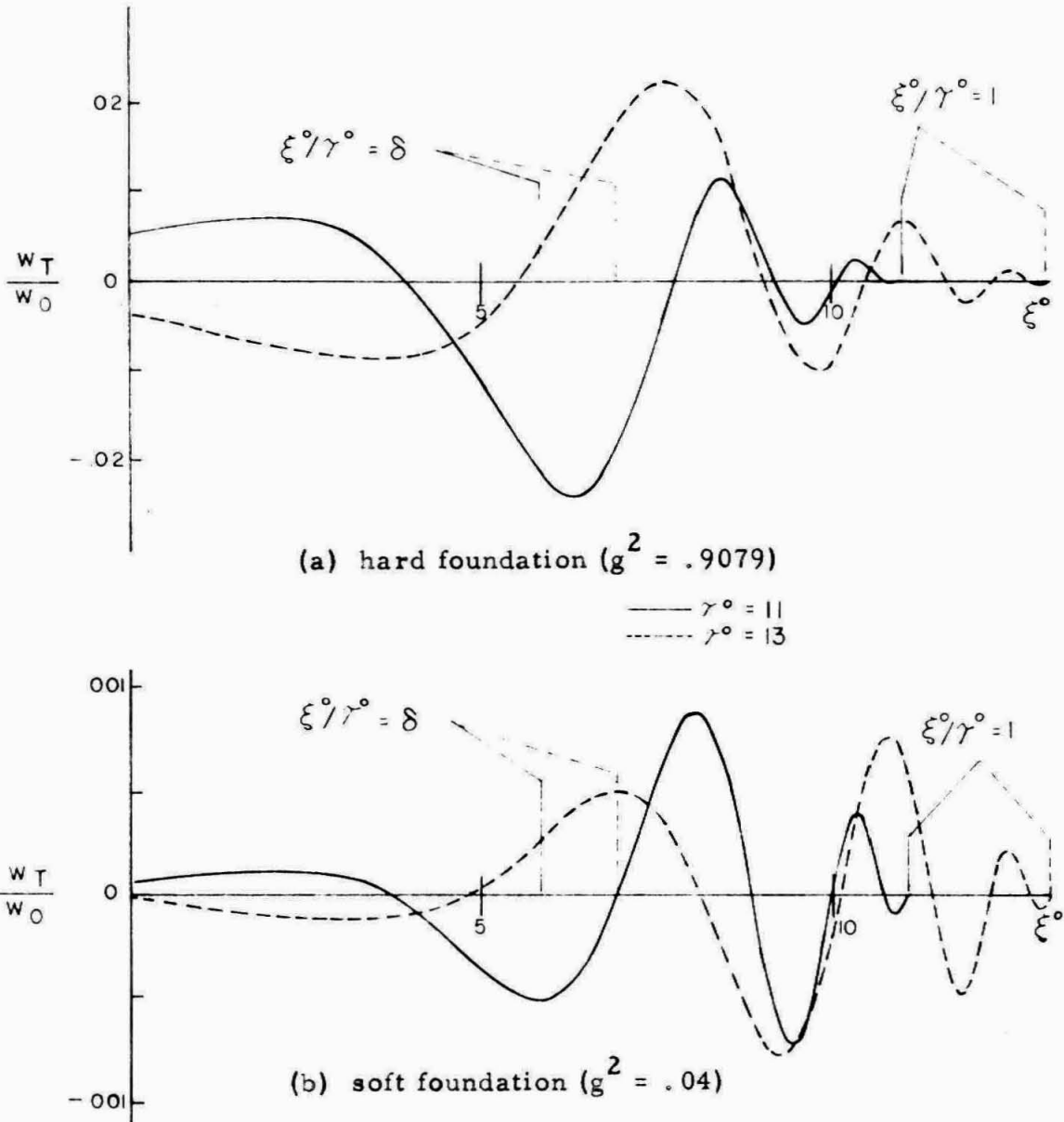
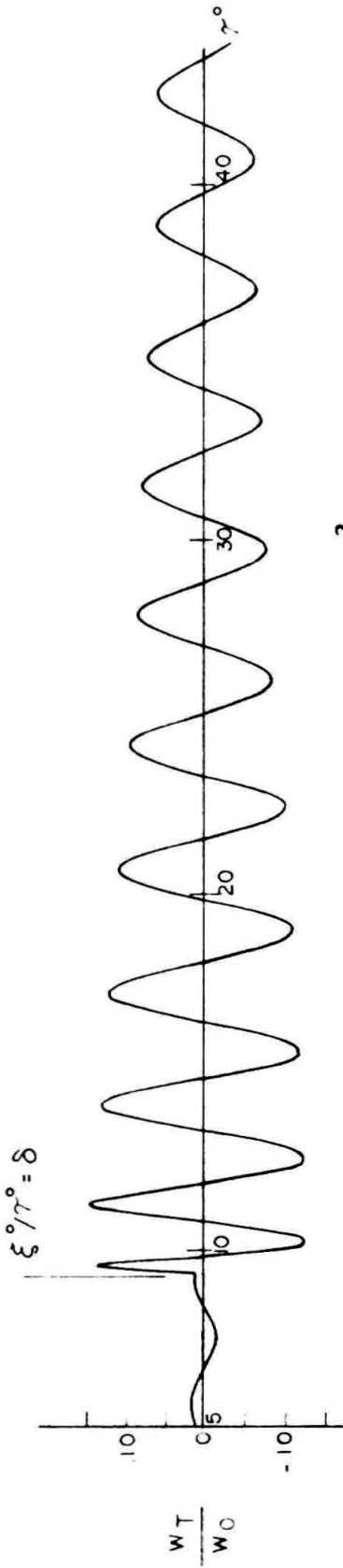
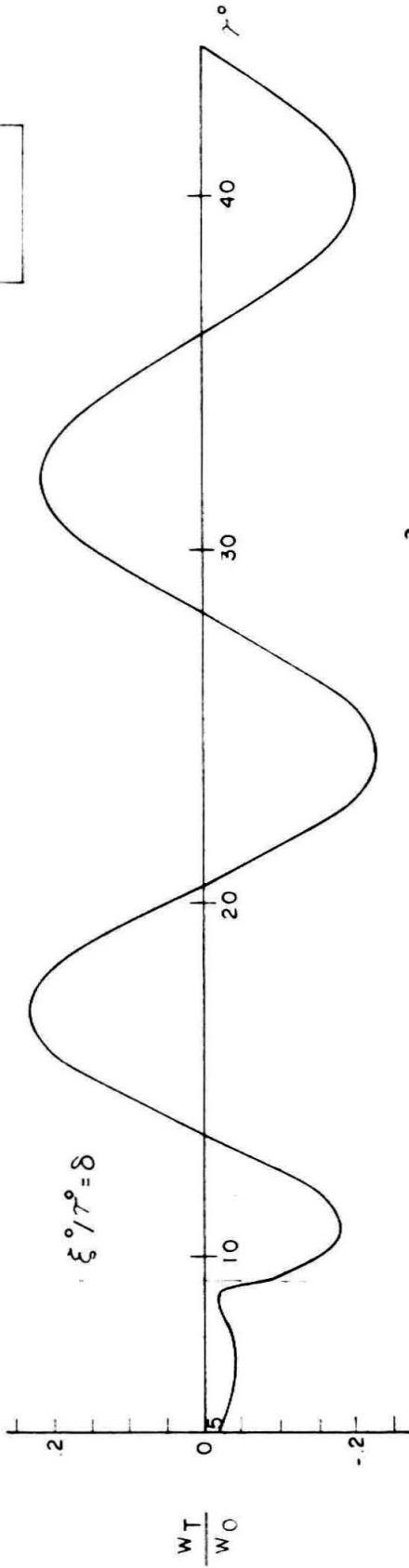


Figure 28. Total deflection station response: higher real arm.



(a) hard foundation ($g^2 = .9079$)

$\xi^0 = 5$



(b) soft foundation ($g^2 = .04$)

Figure 29. Total deflection time response: lower real arm, $|X| > |X_*|$.

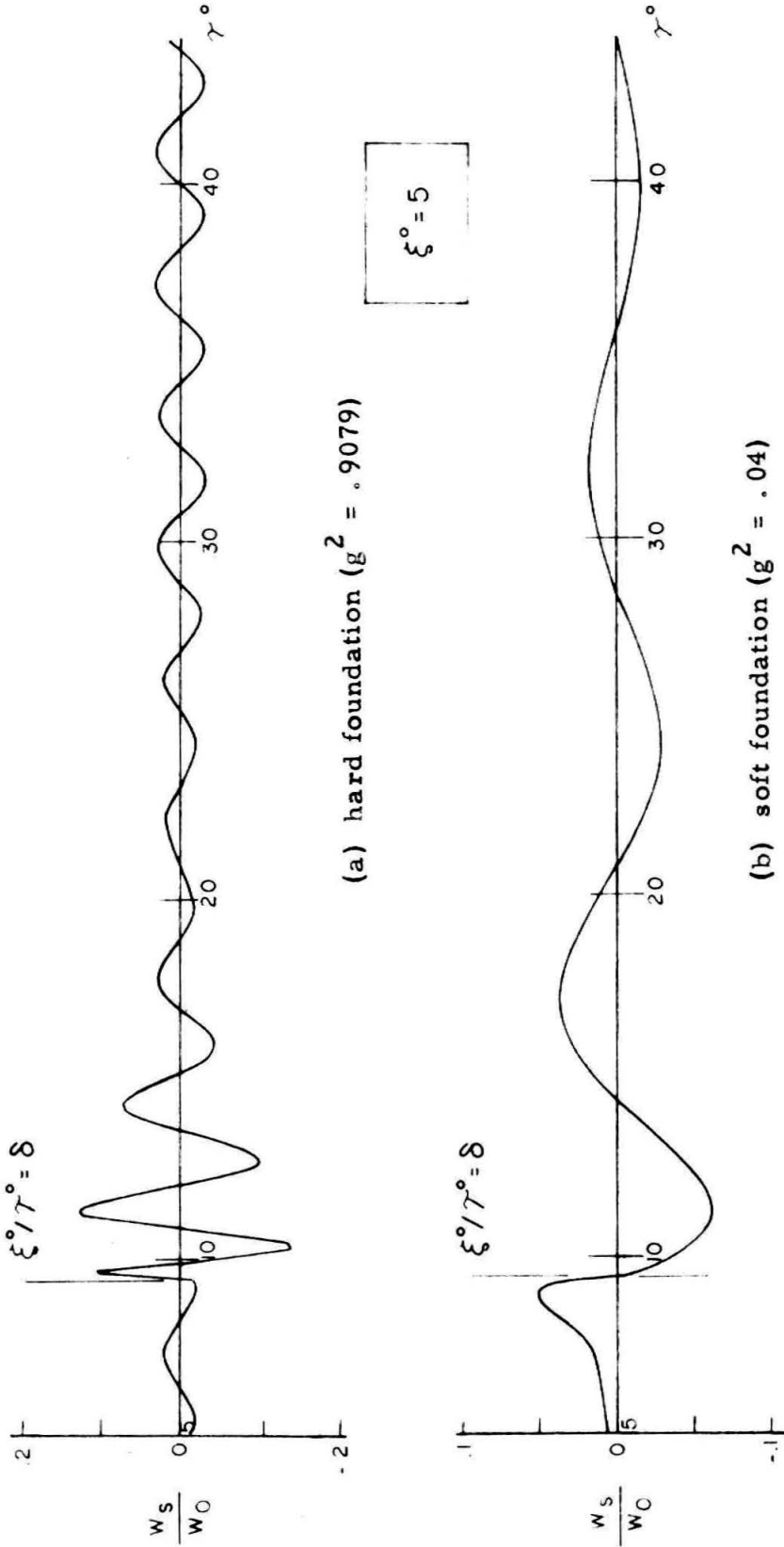


Figure 30. Shear deflection time response: lower real arm, $|X| > |X_*|$.

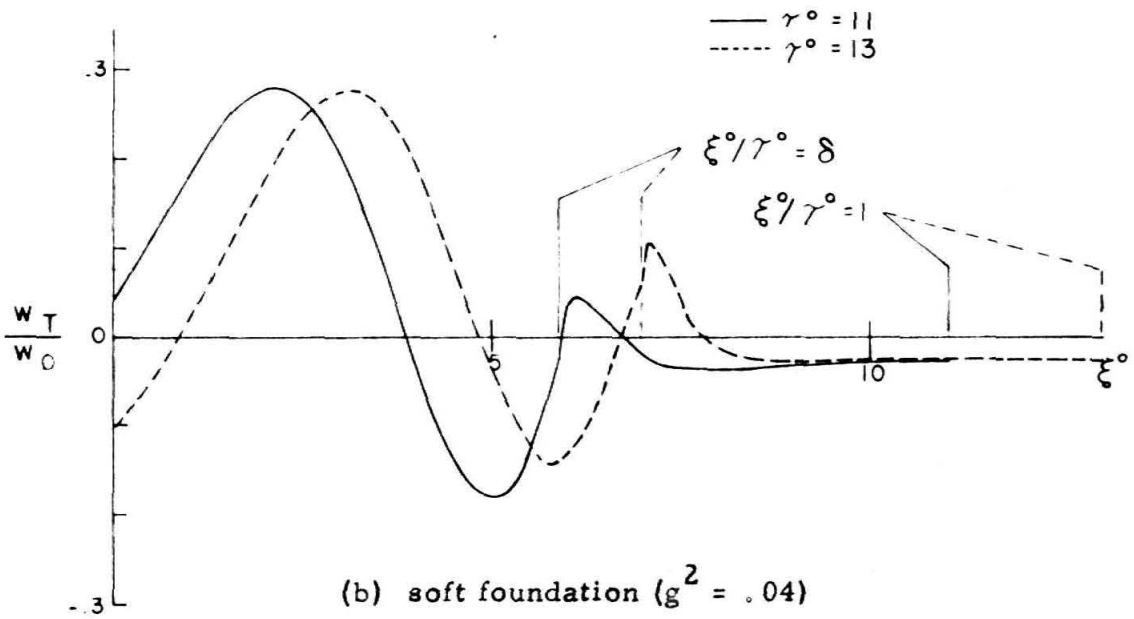
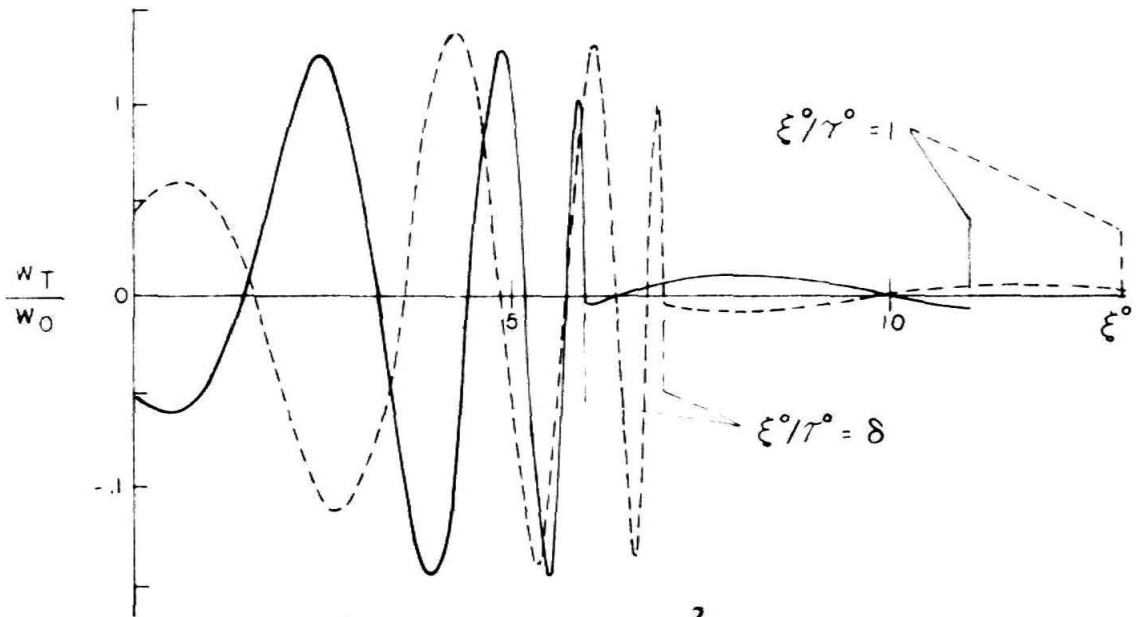


Figure 31. Total deflection station response: lower real arm, $|X| > |X_*|$.

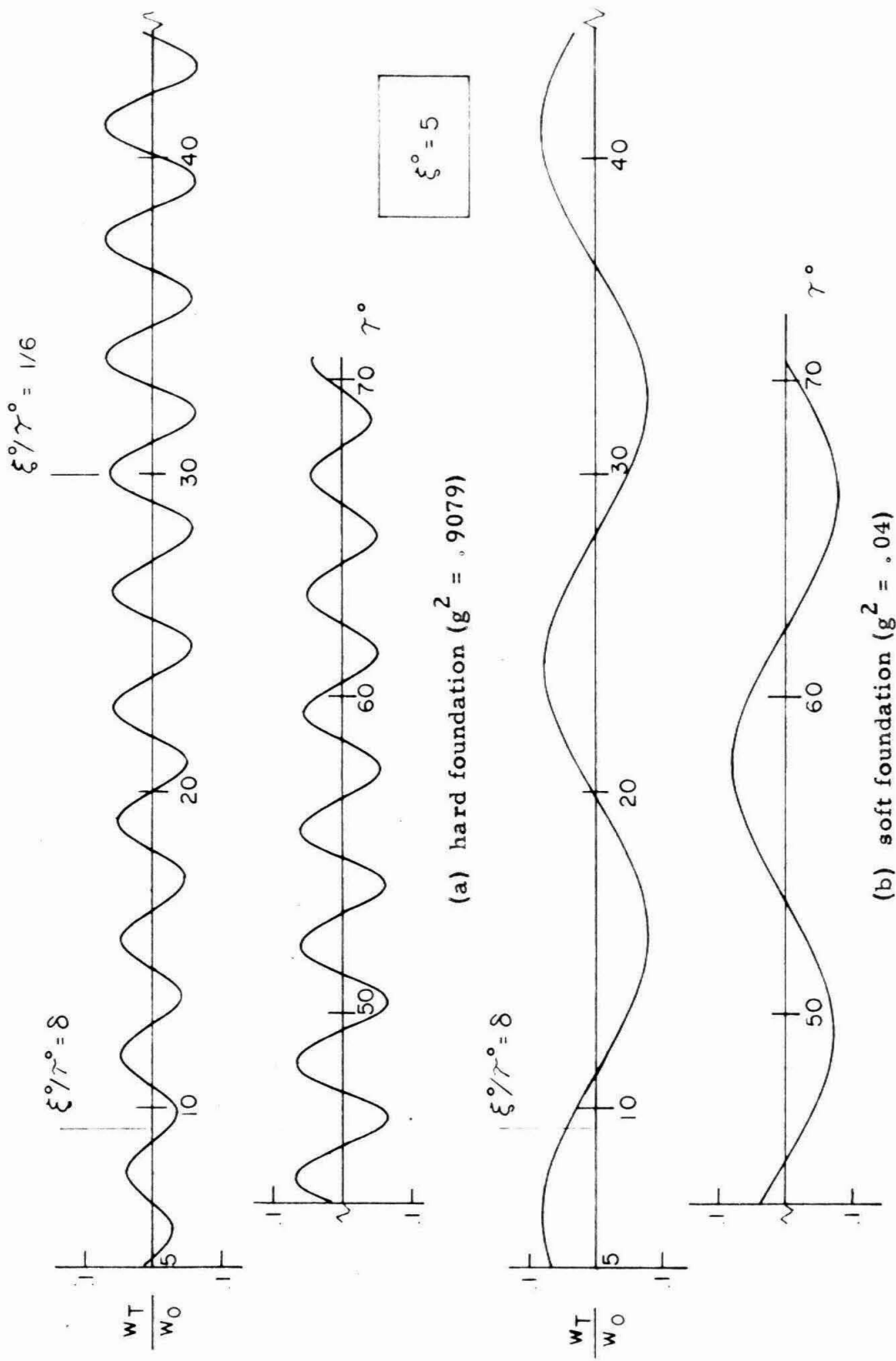


Figure 32. Total deflection time response: lower real arm, $|X| < |X^*|$.

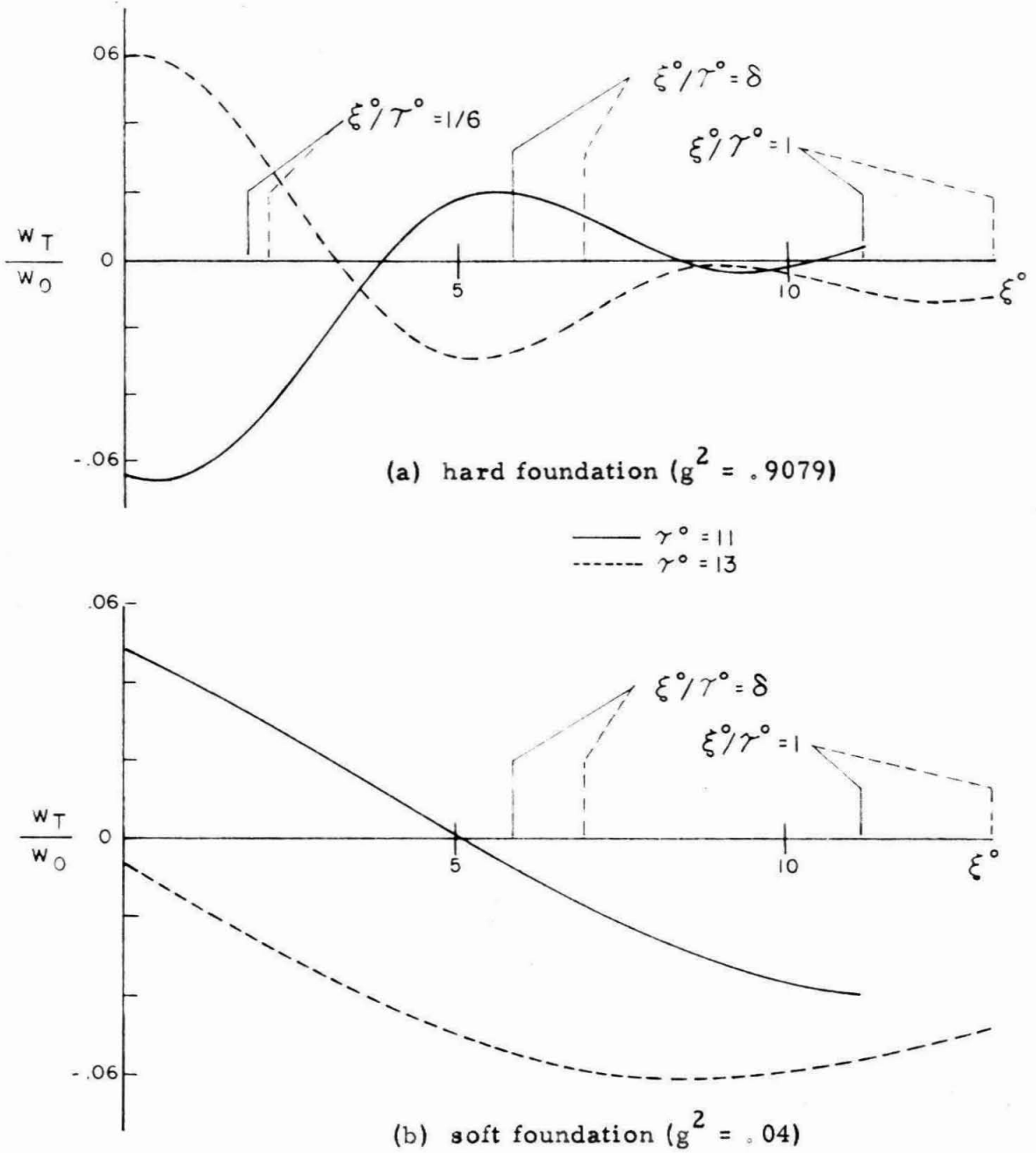
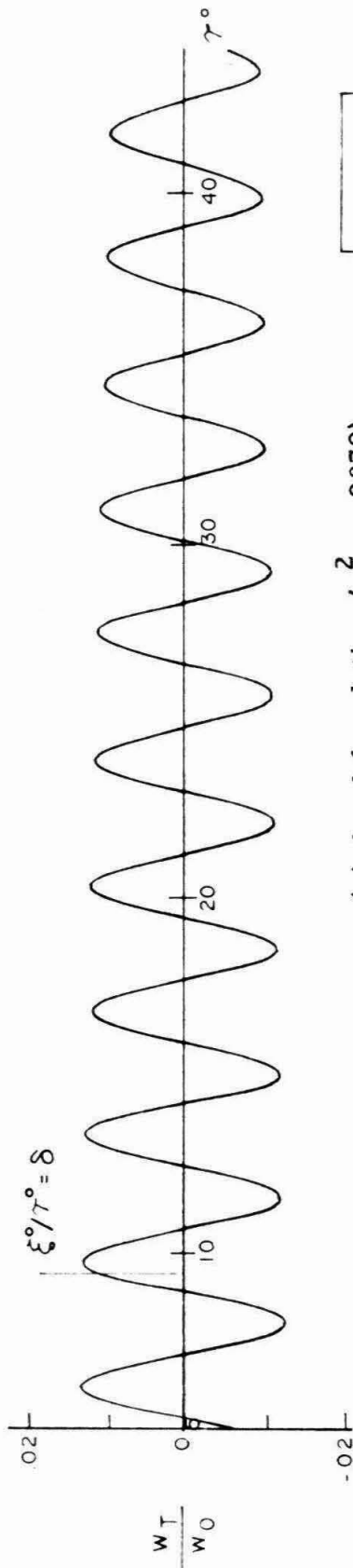
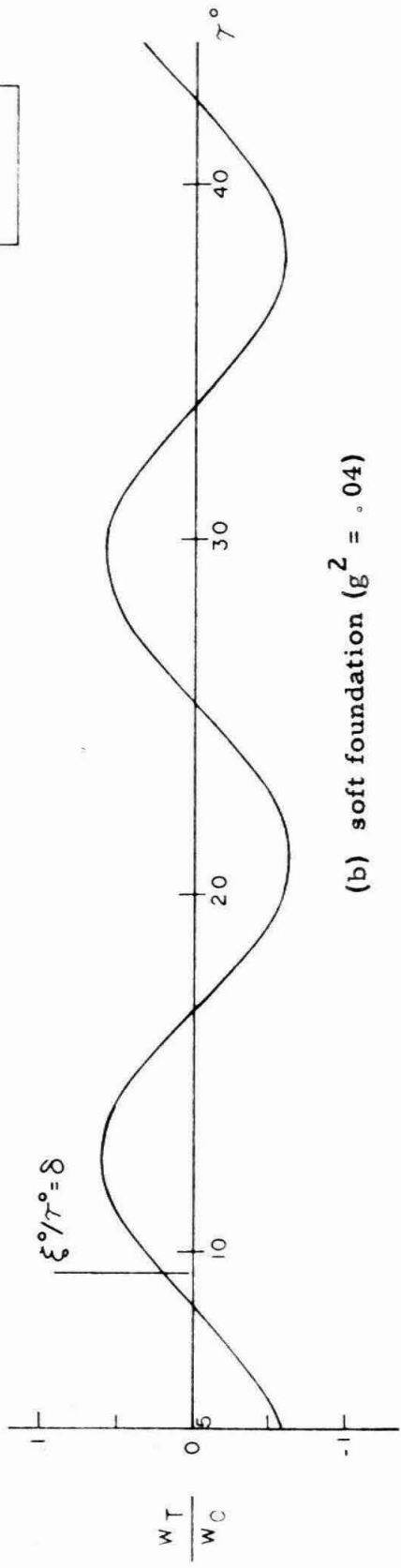


Figure 33. Total deflection station response: lower real arm $|X| < |X_*|$.



(a) hard foundation ($g^2 = .9079$)

$$\xi^0 = 5$$



(b) soft foundation ($g^2 = .04$)

Figure 34. Total deflection time response: imaginary arm.

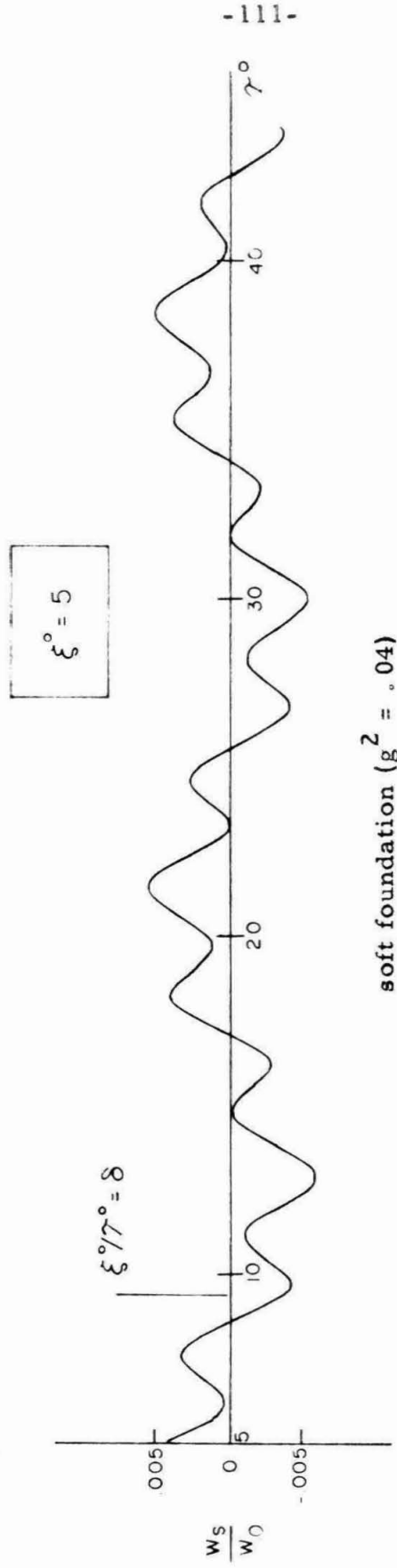
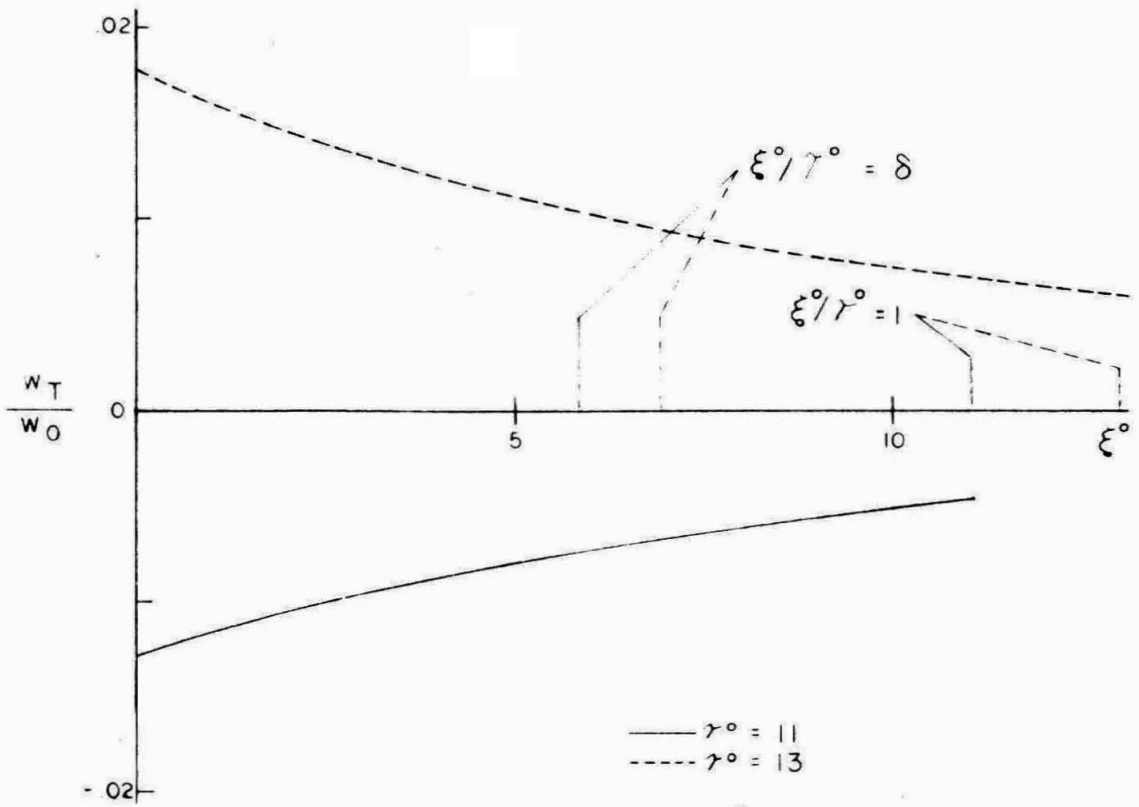
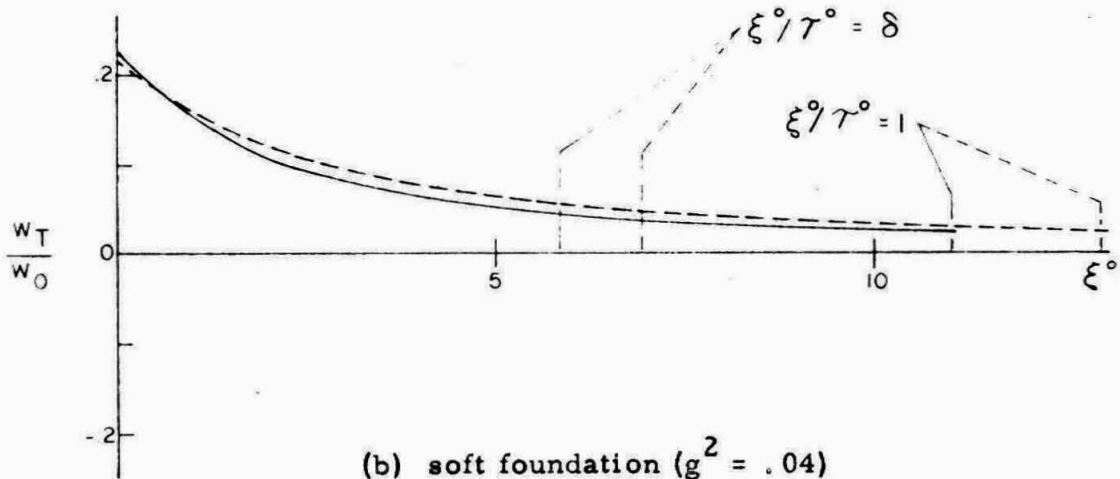


Figure 35. Shear deflection time response: imaginary arm.

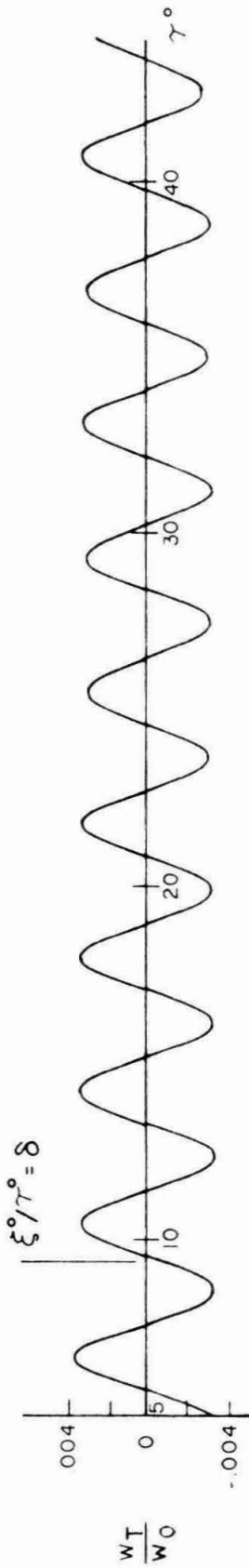


(a) hard foundation ($g^2 = .9079$)



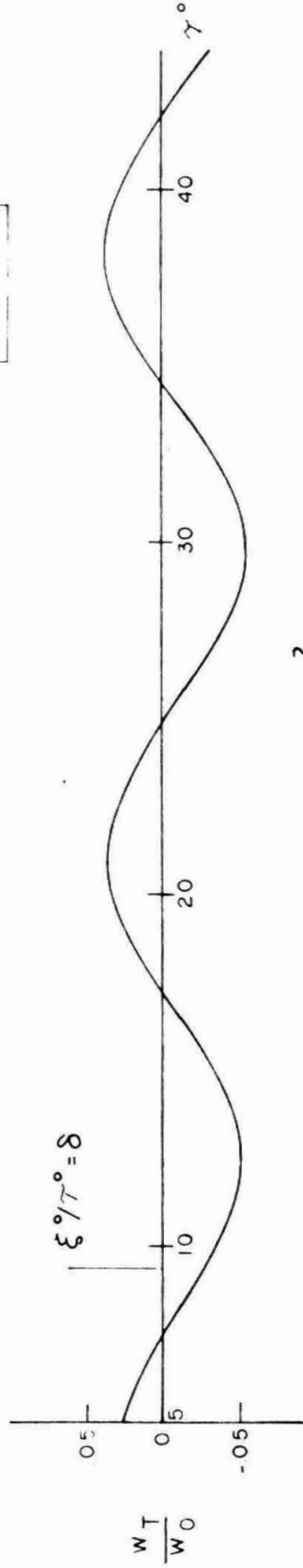
(b) soft foundation ($g^2 = .04$)

Figure 36. Total deflection station response: imaginary arm.



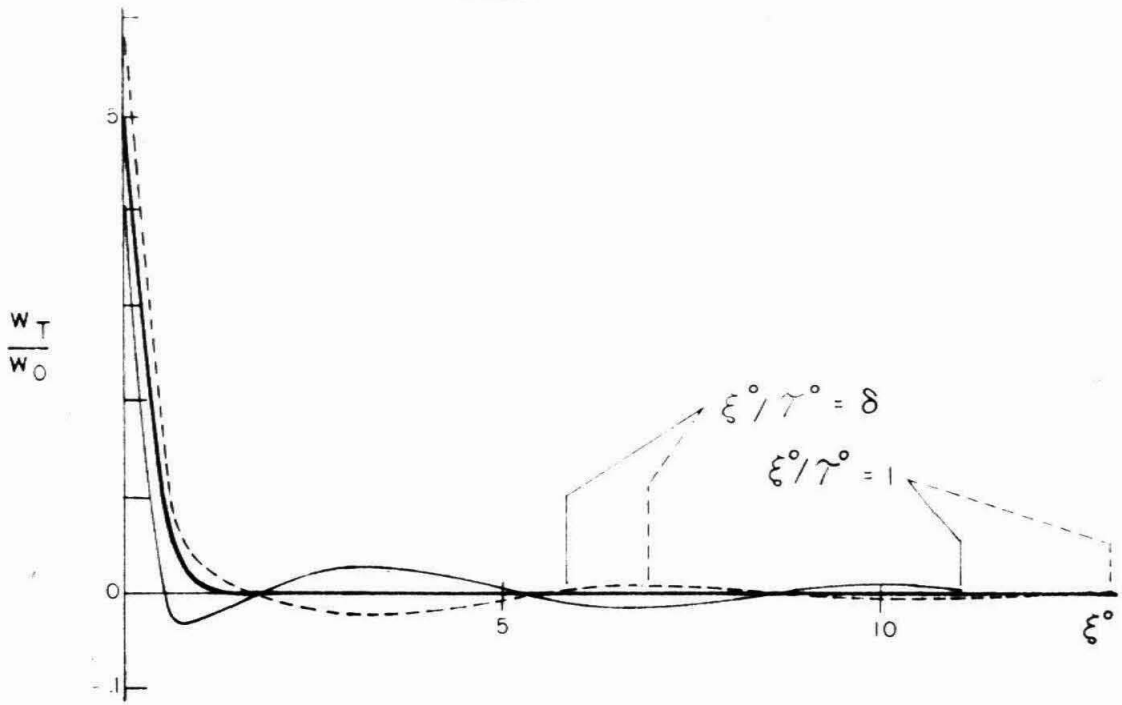
(a) hard foundation ($g^2 = .9079$)

$$\xi^0 = 5$$

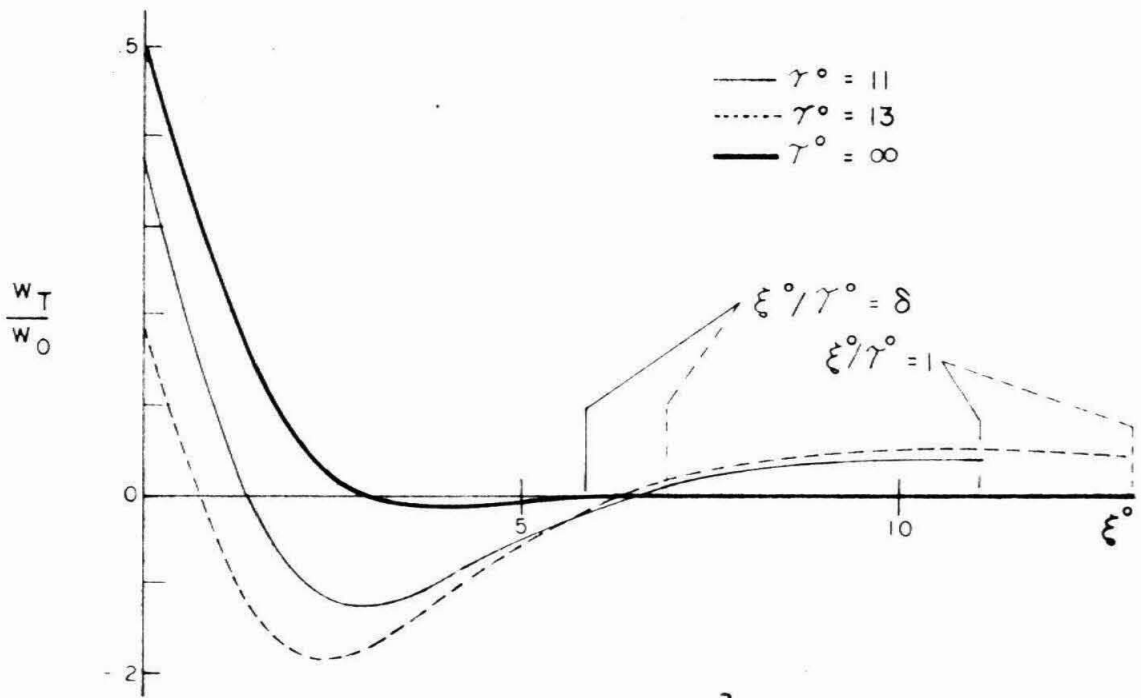


(b) soft foundation ($g^2 = .04$)

Figure 37. Total deflection time response: complex arm.



(a) hard foundation ($g^2 = .9079$)



(b) soft foundation ($g^2 = .04$)

Figure 38. Total deflection station response: complex arm.

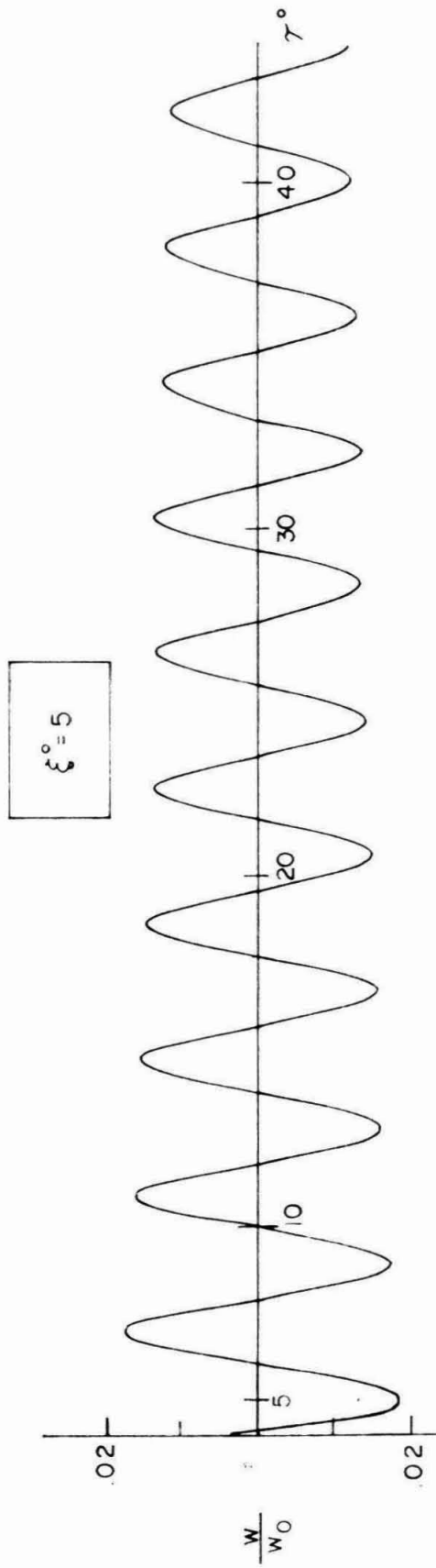


Figure 39. Total surface deflection time response computed from complex arm for exact plate with infinite foundation stiffness.

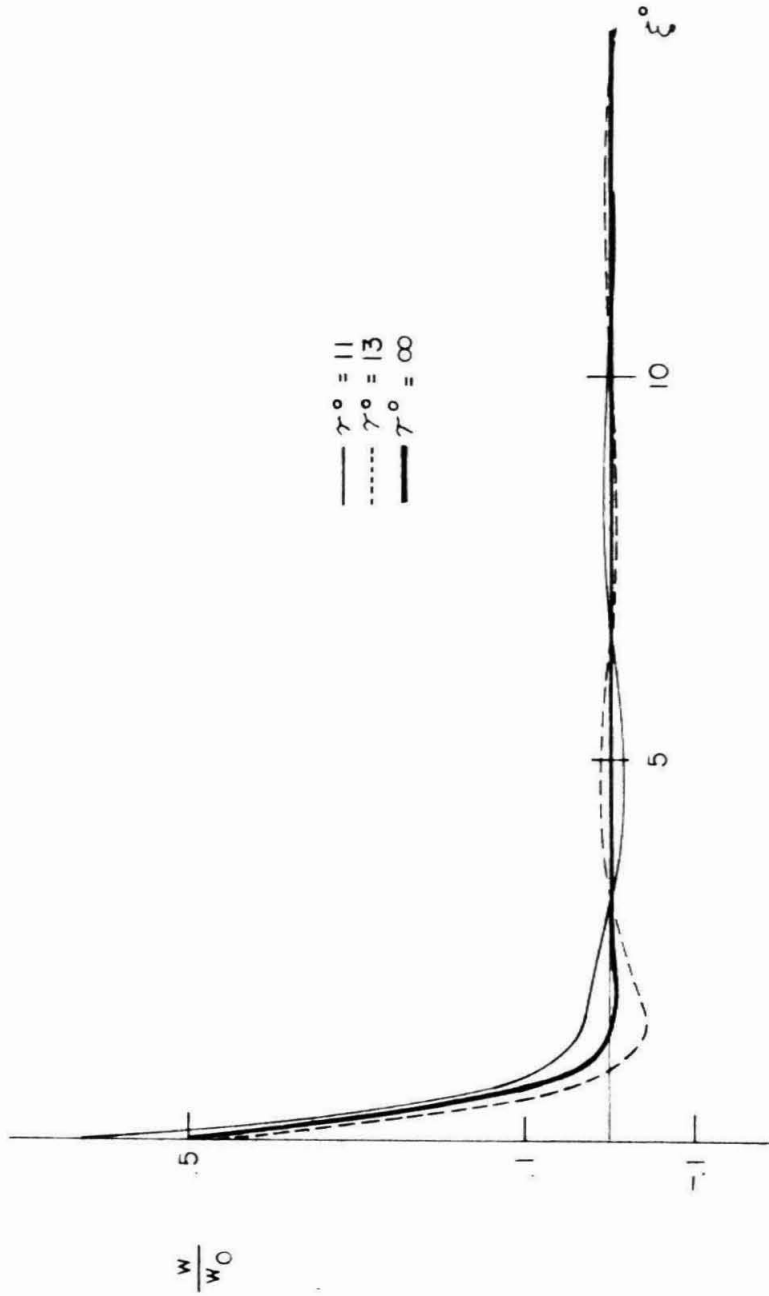
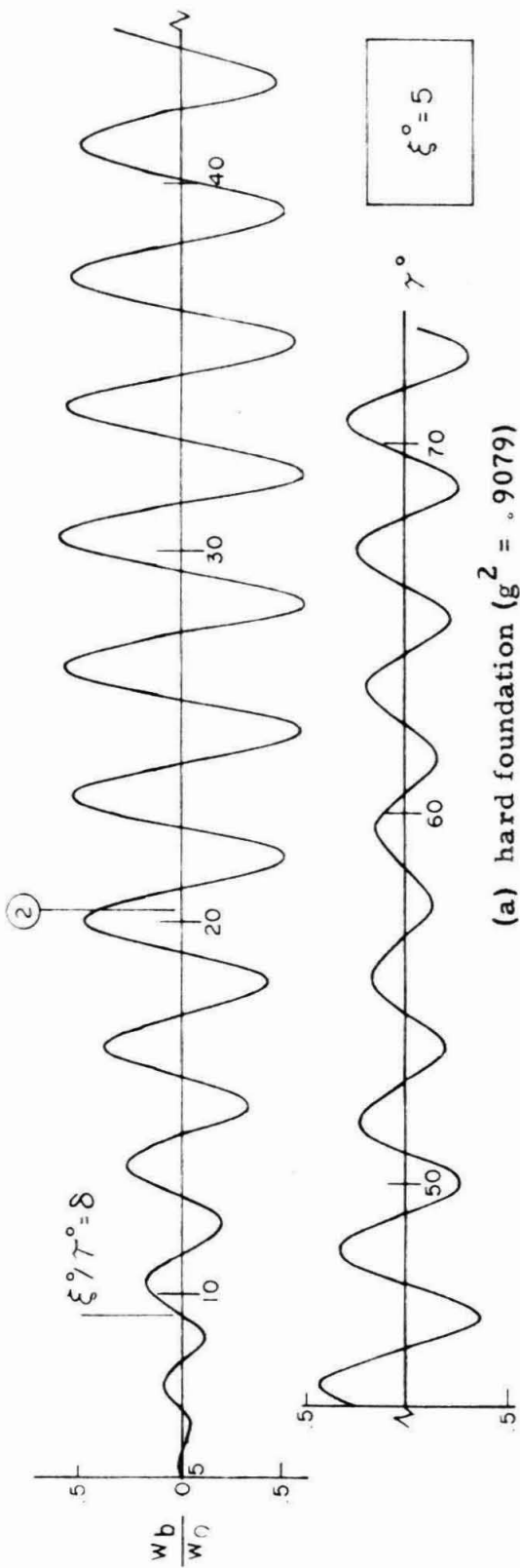
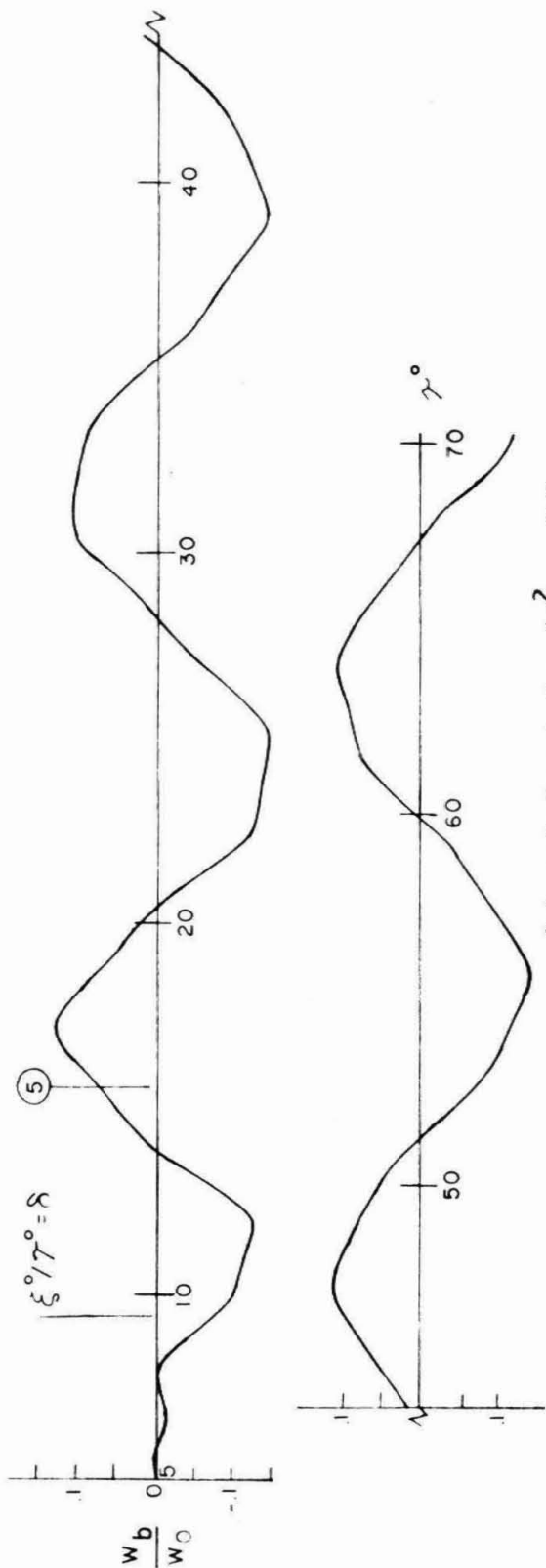


Figure 40. Total surface deflection station response computed from complex arm for exact plate with infinite foundation stiffness.



(a) hard foundation ($g^2 = .9079$)



(b) soft foundation ($g^2 = .04$)

Figure 41. Bending deflection time response.

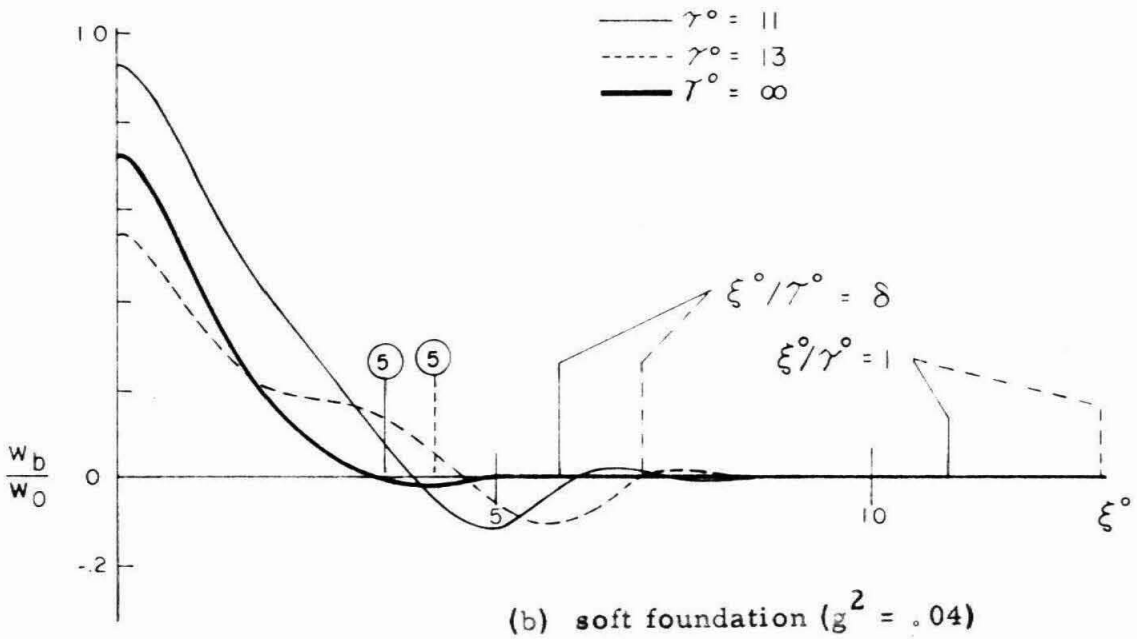
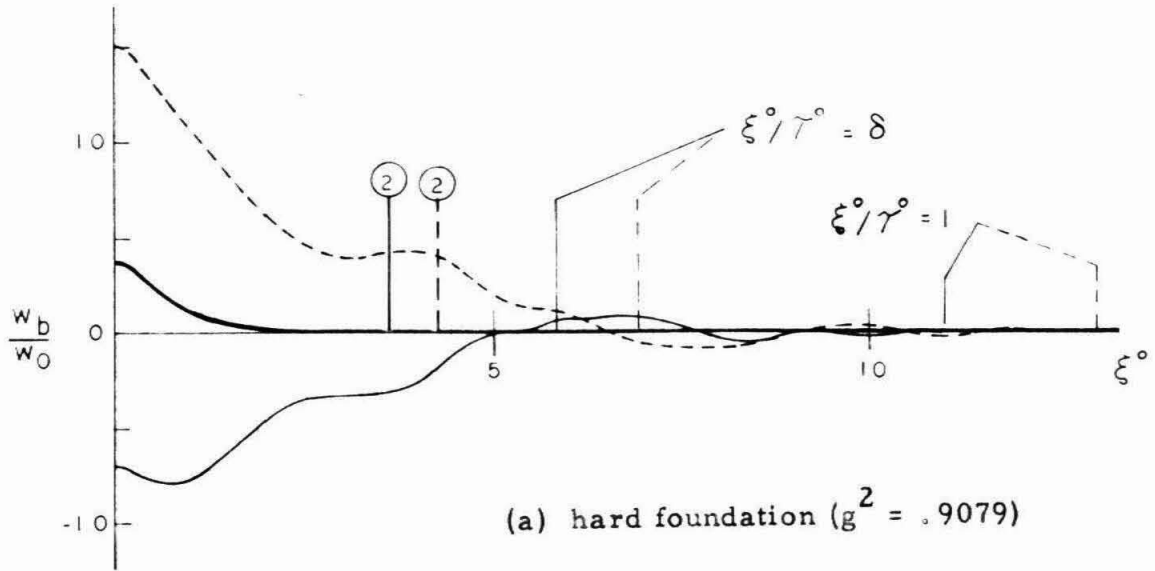


Figure 42. Bending deflection station response.

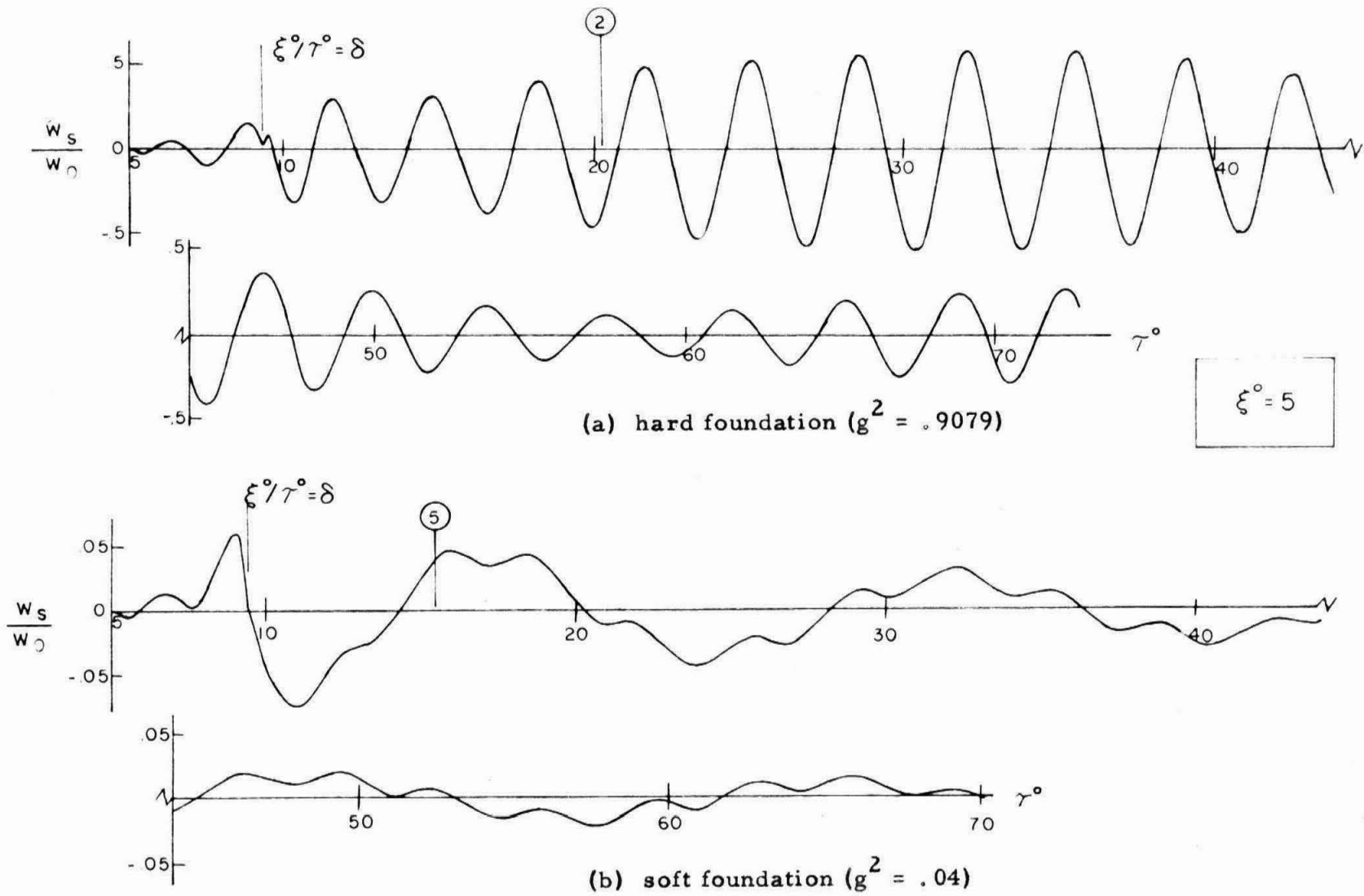


Figure 43. Shear deflection time response.

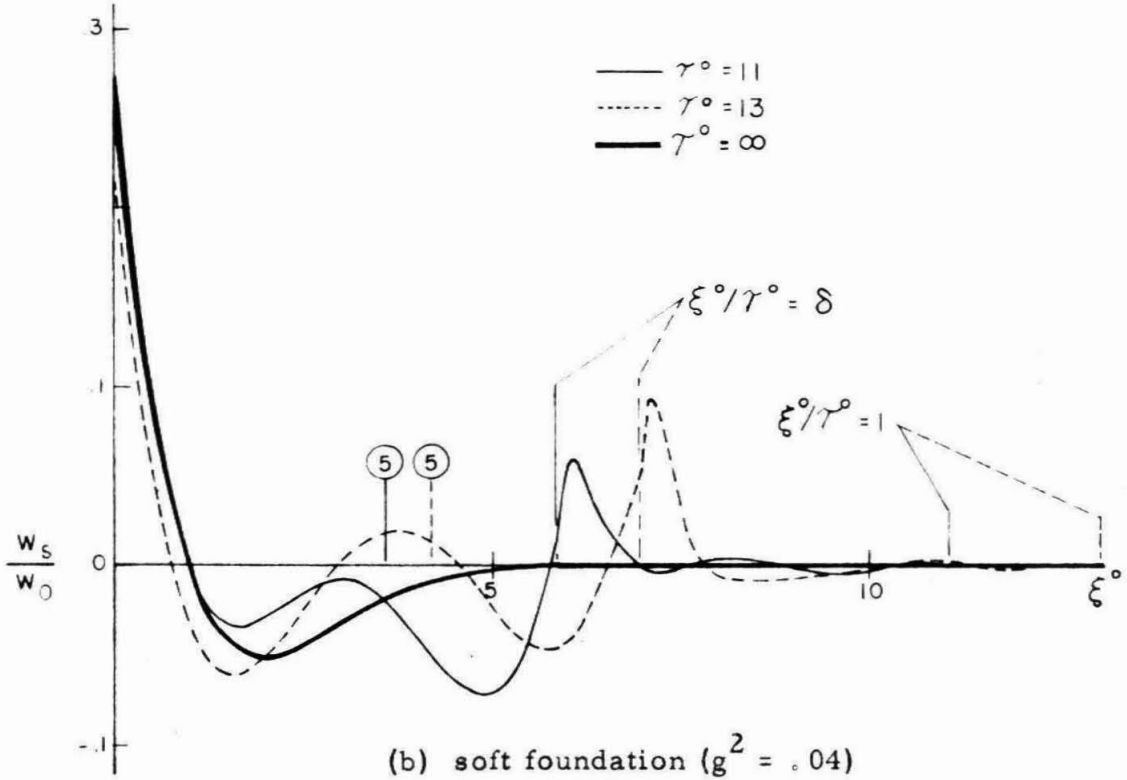
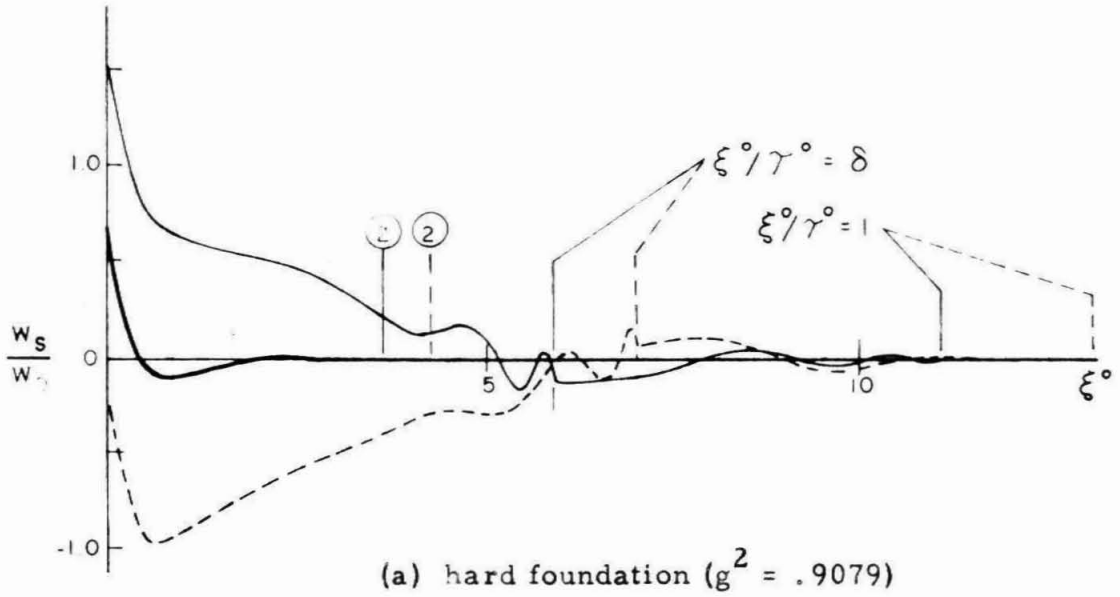


Figure 44. Shear deflection station response.

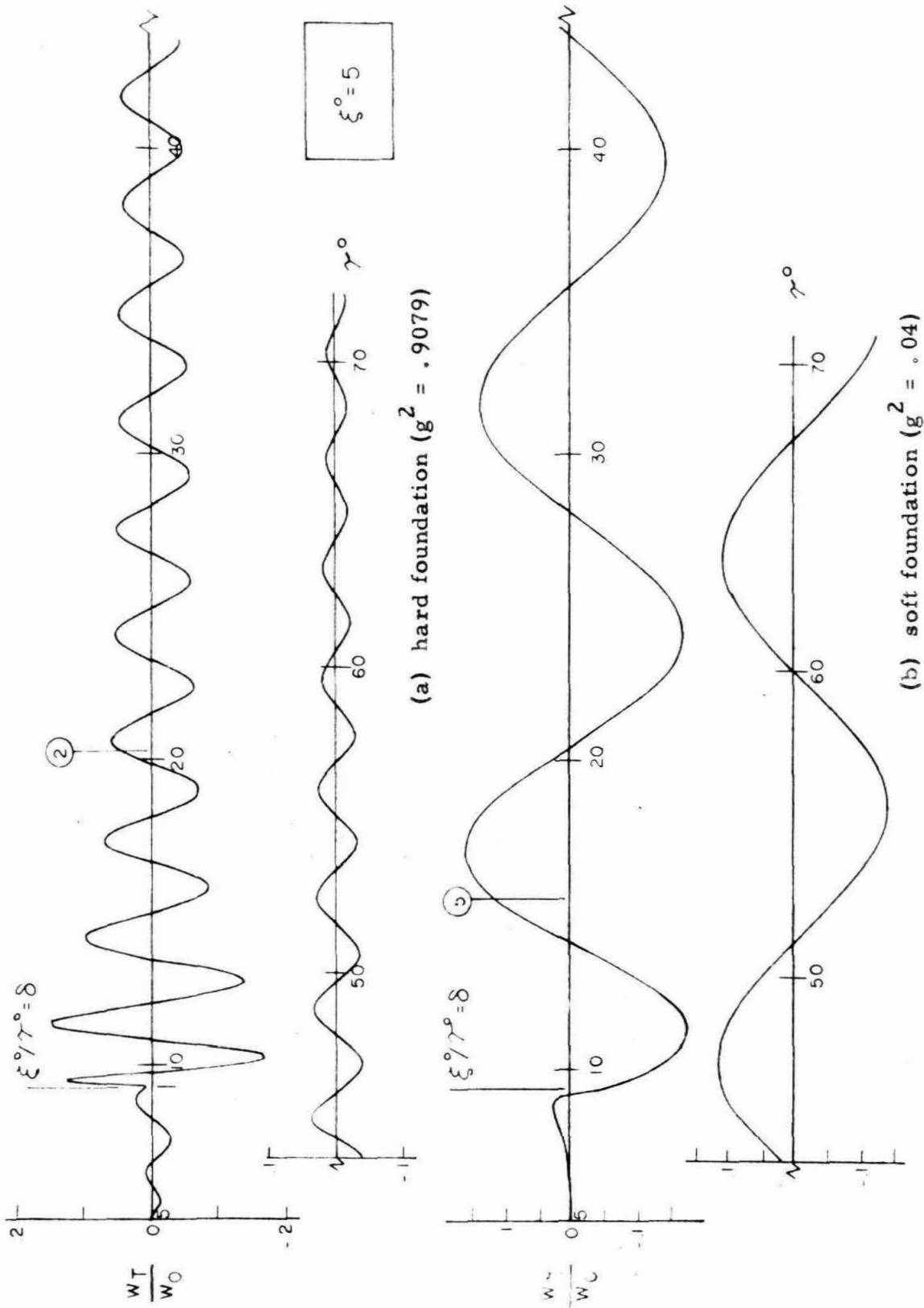


Figure 45. Total deflection time response.

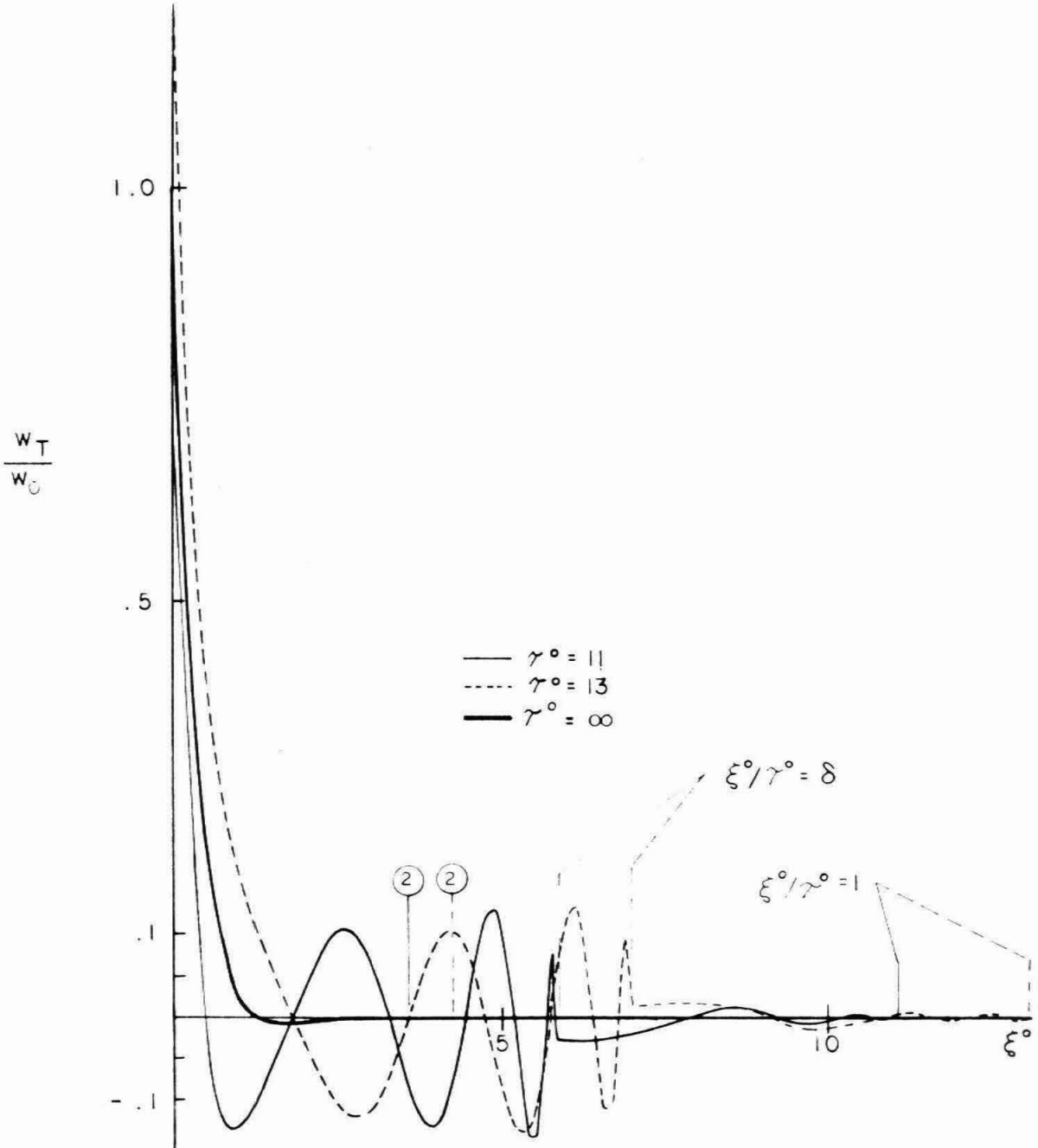


Figure 46a. Total deflection station response for hard foundation ($g^2 = .9079$).

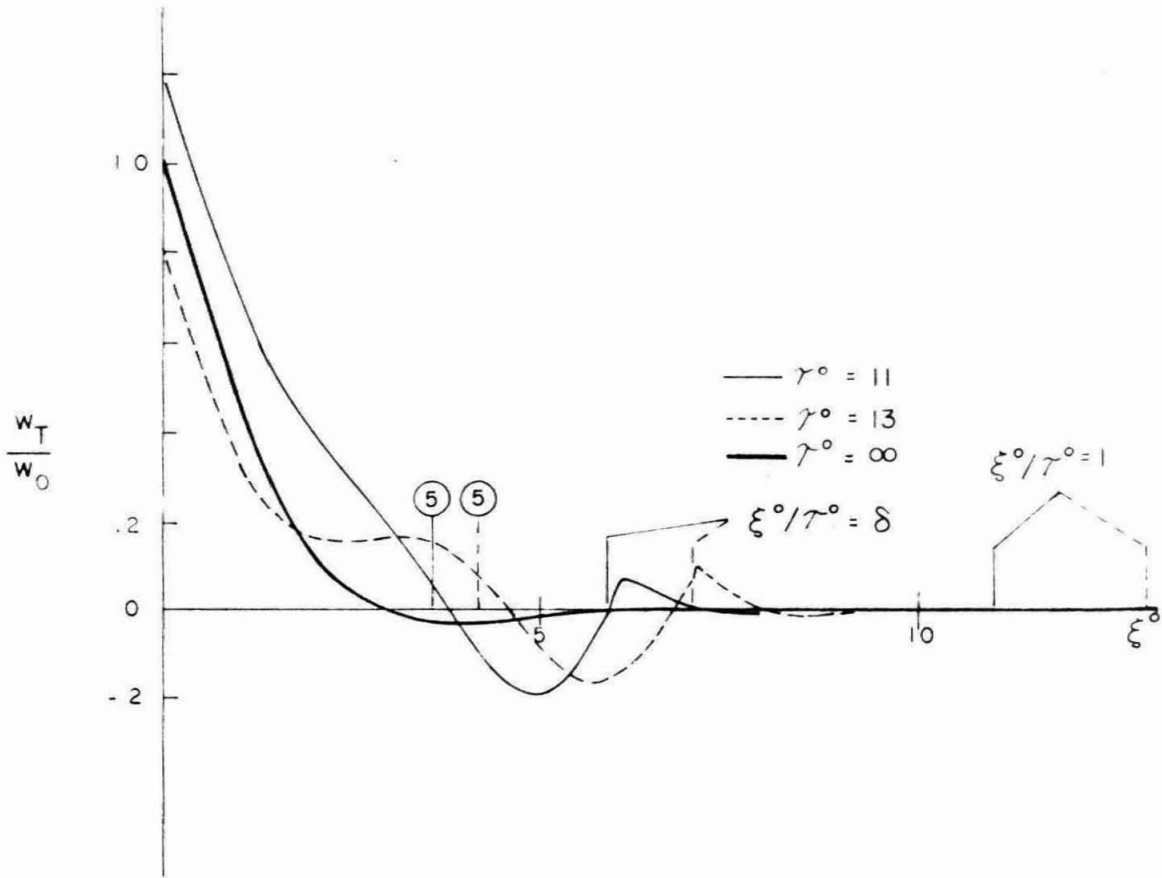


Figure 46b. Total deflection station response for soft foundation ($g^2 = .04$).

All deflections are normalized by the total static deflection, $w_0 = w_s + w_b$, at the source, $\xi^0 = 0$. For the two values of foundation hardness considered, this deflection is given by

$$\frac{\xi^2 F \ell_0}{\pi} h(I_{s_0} + I_{b_0})$$

From equations 52a and 52b

$$\left. \begin{aligned} g^2 = .9079, & \quad w_0 = .5169 \frac{f \ell}{E} \\ g^2 = .04, & \quad w_0 = 3.348 \frac{f \ell}{E} \end{aligned} \right\} \text{ for a plate}$$

The presentation and discussion proceeds first with the individual integral contributions to the total deflection, $w_T = w_s + w_b$, and in some cases w_s separately. Then the sum of these integrals is considered for w_s , w_b , and w_T .

Higher Real Arm (Integrals I_{b_1} and I_{s_1})

Figure 26a shows a time record response for the total deflection, w_T , computed from integrals I_{b_1} and I_{s_1} for $g^2 = .9079$. The dispersive nature of the response is reflected in the variation in the predominant period with time. Near the wave front the predominant period is small and increases with time until a definite limit is reached. By measuring the predominant period at its time of occurrence on this record, * the

* Near the wave front of this record (and others) the predominant period has been estimated by considering quarter waves (peak to zero) and calling the mid-point of such a quarter wave the time of the related full wave occurrence. For later times, when the frequency approaches its cutoff value and the predominant period is relatively constant, it has been measured over several wavelengths. Except in the neighborhood of wave fronts the points for all curves were computed at an interval $\Delta \gamma^0 = .5$, which in the case of figure 26a corresponds to approximately eight points per wave length. This accounts for some inaccuracy in measurements from these curves and results in point scattering.

behavior can be compared with that predicted by the stationary phase analysis shown in figure 24a.

Figure 26a shows that the total deflection, after reaching a fairly early occurring maximum, decays quite rapidly. It may also be noted that the entire curve is severely influenced by the long time predominant period corresponding to the cutoff frequency $\Omega = 1$ as figure 24a also shows. Miklowitz (36, 37) noted the same behavior in his study of waves in an elastic rod in which an approximate theory similar to the present governed. It is of interest to analyze this behavior further. Considering the results from integral I_{s_1} alone, figure 27a, it is seen that the shear deflection, w_s , does not decay as rapidly. Further, it can be deduced that w_b is approximately equal to $-w_s$ for long time. This result is obvious from the inspection of the bracketed term

$$\left[s^2 + p_2^2 / \zeta^2 \right] \tag{74}$$

of equation 50b, which distinguishes the integral solutions for w_b and w_s . For long times the wave number p_2 approaches zero and $s^2 = -1$. The elemental motion of the plate for this mode for long time appears to be independent of the normal forces and results in an internal energy transfer between the potential energy of distortion and the kinetic energy of rotation. This can be shown more easily by considering the comparison of the translational and rotational kinetic energy maxima in the vicinity of the cutoff frequency. For a plate element of length Δx and unit depth these energies are

$$\text{K.E.} \left| \begin{array}{l} \\ \text{rotational} \end{array} \right. = \frac{1}{2} \left(\frac{\rho h^3 \Delta x}{12} \right) \left[\frac{\partial^2 w_b}{\partial t \partial x} \right]^2$$

$$\text{K.E.} \Big|_{\text{translational}} = \frac{1}{2} (\rho h \Delta x) \left[\frac{\partial}{\partial t} (w_b + w_s) \right]^2$$

Assuming $w_s \simeq n w_b = A e^{i(\gamma x - \omega t)}$ for the long time response, the ratio of these energies is

$$R_E = \frac{\text{K.E.} \Big|_{\text{rotational}}}{\text{K.E.} \Big|_{\text{translational}}} = \frac{\Gamma_1^2}{(1+n)^2} \quad (75)$$

where $n = -\Omega^2 + \Gamma_1^2 / \delta^2$ and $\Gamma_1^2 = \gamma^2 h^2 / 12$ at the points (7), (9), and (13) of figures 23a, b through 25a, b. Near the cutoff frequency $\Omega = 1$, n approaches -1 and Γ_1 approaches zero. Noting that the derivative $d\Omega/d\Gamma_1 = 0$ for this mode at $\Omega = 1$, the l'Hospital limit of equation 75 gives this ratio to be infinity. This implies that for this upper mode the governing equations 25a and 25b are uncoupled for long time and all the energy is in the form of rotation and distortion. As time approaches infinity this energy approaches zero, and the deflections w_s and w_b approach zero as $1/\sqrt{\tau^0}$ in accordance with the stationary phase approximation.

Figure 26b shows the total deflection for the softer foundation $g^2 = .04$. As before the predominant period, time of occurrence analysis is shown, figure 24b. Again the total deflection decays rapidly near the cutoff frequency, and figure 27b indicates the same rotation-distortion coupling and its predominance. One important distinction is the relative amplitude of the deflections. For the softer foundation the normalized deflections for this mode are considerably less. This reflects a smaller plate distortional energy relative to other energy forms associated with

modes such as found in the total deflection, spring foundation coupling (translational energy).

Figures 28a and 28b show the plate deflection for two different times as a function of position for $g^2 = .9079$ and $g^2 = .04$, respectively. In a manner similar to that applied to the predominant-period, time-of-occurrence curves, the wave lengths have been measured and their stations noted. The results are shown in figures 25a and 25b. The response is characterized by infinitely short waves at the wave front and infinitely long waves at the loading station, $\xi^0 = 0$.

Lower Real Arm, $|X| > |X_*|$, (Integrals I_{b_5} and I_{s_5})

The total deflection as a function of time for $g^2 = .9079$ is shown in figure 29a and is computed from the integrals I_{b_5} and I_{s_5} . Reference to figure 24a shows that no stationary phase points exist for this mode of transmission for $\xi^0 < \tau^0 < \xi^0/\delta$, which describes the time range $x/c_p < t < x/c$.^{*} The record of figure 29a shows that in this time range the response is a low amplitude, long period wave. At the time of the shear speed arrival the integrals have a point of stationary phase. The abrupt change in slope in the deflection reflects a jump in shear force, conforming with the results from the wave front expansion. The remaining time response indicates that an infinitely short wave at $\tau^0 = \xi^0/\delta$ becomes progressively a long wave at long time corresponding to the cutoff frequency at $\Omega = \Omega_*$. This demonstrates the dispersive nature of this

^{*} For the softer foundation, figure 24b, a point of higher order stationary phase is seen to exist prior to the arrival of the shear wave front for this mode.

mode. In the time range where the integrals have points of stationary phase the predominant periods and wave lengths have been measured and are indicated in figures 24a and 25a. Similar results are indicated in figures 24b and 25b for the softer foundation response shown in figure 29b.

For long times the wave number and frequency of this mode approach X_* and Ω_* , respectively. The energy ratio given by equation 75 becomes

$$R_E = \frac{X_*^2}{1 + X_*^2 / \delta^2 - \Omega_*^2} \quad (76)$$

For $g^2 = .9079$

$$X_*^2 = .0694$$

$$\Omega_*^2 = .816$$

$$\therefore R_E = .162 \text{ and } w_s/w_b = -.570$$

For $g^2 = .04$

$$X_*^2 = .00560$$

$$\Omega_*^2 = .0398$$

$$\therefore R_E = .00572 \text{ and } w_s/w_b = -.02$$

(77)

The value of R_E shows the relative importance of the two governing equations for this mode at long time. For the softer foundation the greatest energy carried by the plate in the lowest mode is translational. Further, for the softer foundation the shear deflection is small and the relatively long waves at long time cause the shear force to be negligible, even though the loading force was shear in nature. The governing

equations for the plate on a soft foundation become uncoupled at long time for this mode, the primary energy transfer being between the kinetic energy of the bending deflection and the potential energy contained in the deflected foundation.

Comparison of figures 29a to 30a and 29b to 30b implicitly indicates the relative magnitudes of the bending deflection and shear deflection for the two foundation stiffnesses. These figures also show that just after the shear wave front these deflections, w_s and w_b , are of comparable magnitude. This indicates the significant coupling of the governing equations at the shear wave front and the shear nature of the forcing function.

Figures 31a and 31b for the two foundations show the total plate deflection as a function of position for two times. The jump in the shear stress at the wave front is indicated by the discontinuous slopes there. For the softer foundation the discontinuous slope is almost obscured by the steep slope of the deflection before the wave front. This is also true for the time record in figure 29b, indicating that shear stresses result from coupling with the bending deflection before the arrival of the shear wave. (The effect will be demonstrated more clearly in figure 44b where the shear deflection from all of the spectrum arms is shown.)

Lower Real Arm, $|X| < |X_*|$, (Integrals I_{b_3} and I_{s_3})

Figure 32a shows the total deflection time response for the foundation stiffness $g^2 = .9079$ computed from I_{b_3} and I_{s_3} . These integrals do not have points of stationary phase until $\tau^0 / \xi^0 = 6$, figure 24a. Then there is a second order stationary phase point which results in an Airy phase and accounts for the slight steady increase in the deflection amplitude

before this critical point. The Airy phase behavior would be more clearly defined for the far field, since for values of $\tau^0/\xi^0 < 6$ the integral is of the Fourier type governed by the Riemann-Lebesgue lemma for improper integrals and therefore decays as $1/\tau^0$. For $\tau^0/\xi^0 > 6$ the integral has two points of stationary phase, figure 24a, and therefore decays as $1/\sqrt{\tau^0}$. For the softer foundation the higher order stationary phase point occurs at such long time that this mode is not shown in scale in figure 24b, and its influence is not apparent in figure 32b.

The amplitude of the response from this arm at long time is comparable to that from the other lower real arm as can be seen by comparing figures 29a to 32a and 29b to 32b. Long time analysis for these two arms leads to a similar partition of energy between the governing equations at the frequency $\Omega = \Omega_*$. At the cutoff frequency $\Omega = g$, however, the rotational energy is zero, since the wave number X is zero there. This result is independent of the foundation stiffness. The relative magnitudes of the bending and shear deflections at this cutoff frequency are given by $w_s/w_b = -g^2$ from the expression 74. The prominent role of bending for the softer foundations is thereby demonstrated for long time at this frequency as well as at Ω_* .

Figures 33a and 33b reflect the long wave nature of this mode. Figure 33a in particular shows the aforementioned behavior at the higher order stationary phase point, namely that the amplitude response is largest for $\xi^0 < \tau^0/6$.

Imaginary Arm (Integrals I_{b_2} and I_{s_2})

The response computed for the imaginary arm is oscillatory in time and involves infinitely long waves that decay spacially. The integrals I_{b_2} and I_{s_2} do not have points of stationary phase. The results from their evaluation, therefore, cannot be compared with figures 24a, b or 25a, b.

Figures 34a and 34b show the time record of the total deflection for the two foundation stiffnesses considered. In each case the average period corresponds to the lower cutoff frequency $\Omega = g$. This follows from the fact that the contributions from regions outside the neighborhood of the cutoff frequencies have spacially decayed (wave number being imaginary), and the fact that the bending and shear deflections cancel at the higher cutoff frequency. This latter fact is clearly demonstrated in figure 35, where just the shear deflection is shown for the soft foundation. Here two sinusoidal waves are superimposed which have periods corresponding to the two cutoff frequencies, $\Omega = g$ and $\Omega = 1$. (Note that in figure 34b the latter higher frequency is not present.) The reason the shear deflection demonstrates this clearly is because its amplitude is small near the lower cutoff frequency and is therefore comparable in magnitude to the contribution near the higher cutoff frequency.

Figures 36a and 36b show the spacial decay and the absence of the oscillatory behavior indicative of real wave numbers greater than zero.

For long times these integrals, I_{b_2} and I_{s_2} , decay as $1/\tau^0$ according to the Riemann-Lebesgue lemma for improper Fourier integrals. By considering the amplitude of the response corresponding to the imaginary and complex arms, it is possible to estimate the error introduced by

approximating the net response, including all the arms, with only the stationary phase method applied to the positive traveling waves. For example, the maximum total deflection amplitude at $\gamma^0 = 40$ is .20 for the positive traveling wave corresponding to the lowest mode for the soft foundation, figure 29b. The corresponding contribution from the imaginary arm is approximately .06, figure 34b. By neglecting this contribution (considering only positive traveling groups) an error of approximately 30% could be introduced. On the basis of the amplitudes at $\gamma^0 = 40$ and the decay rates of integrals having points stationary phase ($1/\sqrt{\gamma^0}$) and integrals governed by the Riemann-Lebesgue lemma ($1/\gamma^0$) the relative importance will be 10% when $\gamma^0 \approx 360$. The result indicated here demonstrates a further shortcoming of the stationary phase method when applied to the type of transient problems considered in this study without regard to negative traveling waves.

Complex Arm (Integrals I_{b_4} and I_{s_4})

Integrals I_{b_4} and I_{s_4} do not have stationary phase points, and like the imaginary arm their contributions cannot be indicated in figures 24a, 24b, 25a and 25b. The time response of the total deflection is shown in figures 37a and 37b for the two foundation stiffnesses. The period of oscillation in both cases corresponds to the frequency Ω_* . This is again due to the spacial decay at frequencies outside the neighborhood of Ω_* , and can be seen more vividly in figures 38a and 38b. These figures show the plate deflection for fixed times. Here the long time limit of a half static deflection is demonstrated. This is evidenced by comparing the equivalent paths of integration that compose L_4 in figures 19 and 22. The

spacial variation indicated in figures 38a and 38b also reflect a moderately damped (spacially) oscillatory motion about the static solution with a wave length corresponding to the wave number X_* . The important feature here is the absence of a propagation speed and the appearance of nodal planes. (In figure 38b the first nodal plane is not as well defined as in figure 38a.)

The amplitude computed for this arm is considerably less than that from the lower real arms at Ω_* (for example, compare figures 37a and 37b with 29a and 29b) though it does not appear to be bounded by a steep exponential envelope as is evidenced in figures 38a and 38b. When the integral is written along its equivalent path in figure 22 the time dependent integral is governed by Watson's lemma and decays as $1/\tau^0$ for large time.

For comparison the integral for the exact theory, I_4 of equation 72, was computed* for this arm at the surface of the plate $\xi = 1$. As in the approximate theory case, the predominant period indicates the primary influence in the neighborhood of $\Omega_* \simeq .88$. The previously observed edgemode resonant frequency observed by Shaw (20) and computed by Gazis and Mindlin (19) ($\Omega \simeq .65$ for $\nu = .31$) is not evident here for long time. In the case of the exact theory this may be explained in terms of the coupling between the lowest symmetric mode and the complex arm. Recall that the edge mode frequency was determined by Gazis and Mindlin from the consideration of the relative magnitudes of the complex and real

* Here the complex wave numbers were computed at 200 evenly spaced values of frequency, and intermediate values were interpolated from the resulting table. A 50 point trapazoidal integration scheme was employed. The integral was made regular at its improper limit by a change of variables. Comparison with the results computed from a 200 point integration mesh indicated an error of less than 1% for the several values of τ^0 and ξ^0 tested. The initial wave arrival in the exact case occurs as a time corresponding to the dilatation speed c_d . The partial static deflection under the load and at the surface was computed to be $w_0 = .756 f_l / E$.

waves resulting through mode conversion of a steady real wave impinging upon a free edge. The results presented here, figures 39 and 40, do not contradict the existence of the edge mode for steady wave propagation but merely imply that the lowest symmetric mode in the transient case does not contribute significantly in the vicinity of the edge mode frequency for long time. The amplitude spectrum for the integral representing the real wave, equation 69, has a minimum near the edge mode frequency due to the smallness α' there.

Total Response (w_b , w_s and w_T)

The bending and shear deflection time records are shown in figures 41a and 43a for $g^2 = .9079$. Both w_b and w_s are seen to be zero at the arrival of the first wave and steadily increase into an oscillatory deflection without discontinuities in the slopes before the second wave arrival. The shear wave is marked by a discontinuous slope in the shear deflection w_s , reflecting a jump in shear load. The bending deflection, however, remains relatively unaffected in agreement with the wave front expansion there. For long time these deflections are out of phase, approximately of equal amplitude, and are roughly bound in a long period sinusoidal envelope, which decays as $1/\sqrt{\tau^0}$. The opposite phase and similarity in amplitude are characteristic of the long time frequencies, $\Omega = 1$, $\Omega = g$, and $\Omega = \Omega_*$, for this foundation stiffness. This effect has been discussed previously for the individual mode contributions. The behavior of the long period envelope is a result of the superposition of the various modal contributions near their long time frequencies. For example, the trigonometric identity

$$\sin \omega_1 t + \sin \omega_2 t = 2 \cos \left[\left(\frac{\omega_1 - \omega_2}{2} \right) t \right] \sin \left[\left(\frac{\omega_1 + \omega_2}{2} \right) t \right]$$

may be used to estimate the magnitude of this period. It represents the simple group with the amplitude and group velocity determined by the cosine term, and the phase wave and velocity by the sine term. The three possible combinations of frequencies that describe the envelope of the group and their associated predominant period are

$$\begin{aligned} 1-g &= .0472 \quad \rightarrow T_p \simeq 144 \\ g-\Omega_* &= .0498 \quad \rightarrow T_p \simeq 137 \\ 1-\Omega_* &= .0969 \quad \rightarrow T_p \simeq 70 \end{aligned}$$

The predominant period measured from figures 41a and 43a gives $T_p \simeq 120$, reflecting the combination of the limiting frequencies $g-\Omega_*$ and $1-g$.

The total deflection shown in figure 45a does not indicate the presence of an envelope, partly because the total deflection contribution from the upper cutoff frequency is negligible compared to the response at Ω_* and g . Recall the cancellation of w_s and w_b at the higher cutoff frequency. The period corresponding to the remaining combination between Ω_* and g is not evident because of the large transients at the shear wave arrival. Such a period measurement is not possible considering the limited time record.

The large deflection at the shear wave front, figure 45a, indicates that the bending and shear deflections are in phase and the governing equations are highly coupled in the sense that the rotational and translational energies are exchanged through the foundation. For increasing time the equations become relatively uncoupled, i.e., the rotational

energy is exchanged with shear and bending distortion energy at the higher cutoff frequency and the translational energy with the foundation and shear deflection energy at the lower long time frequencies. In this case the total response may be considered to be the superposition of two independent solutions at two different frequencies, each corresponding to a different type of motion. This behavior is more pronounced for the softer foundation, figures 41b and 43b, where the rotation-distortion energy is small at the higher frequency and the shear deflection is small at the lower long time frequencies. In this case almost all deflection is due to bending as may be seen by comparing the magnitudes in figures 41b and 43b for long time. The equation governing the rotation, equation 25a, becomes unimportant for long time as does the shear term in equation 25b. The only significant energy exchange is between the translational kinetic energy and the potential energy due to the foundation deflection and plate bending. Even the plate bending becomes insignificant for long enough time leaving only the classical one degree of freedom spring-mass mode of vibration with a slow amplitude decay of $O(1/\sqrt{\tau^D})$. For sufficiently soft foundations the elementary bending theory could give accurate long time information because of its applicability to situations where low frequencies and long waves prevail.

Though the influence of the higher cutoff frequency is evident in the bending and shear deflections this character is not observed in the total deflection, figures 41b, 43b, and 45b. Again this is due to the cancellation, $w_s = -w_b$ at the higher frequency.

The deflections along the plate for fixed times are shown in figures 42a, 42b, 44a, 44b, 46a, and 46b. The rather complicated responses

demonstrate the necessity of considering the individual contributions separately for the various modes, where the particular characteristics of these curves can be conveniently analyzed. Note should be made, however, of the shear deflections, figures 44a, and 44b, where the slope of these curves is proportional to the shear force. For the softer foundation the significant shear force preceding the shear wave arrival reflects the coupling between the bending and shear deflections as mentioned previously.

For the purposes of comparing the numerical results presented with those expected from the related exact problem, some qualifications must be made as to the regions of time and space where the approximate theory adequately describes the exact theory. Reference to figure 24a, for example, shows that in the time region preceding the time corresponding to point (2) the influence of the lowest mode and the complicated behavior of the other modes considered for the exact theory are not adequately duplicated in the approximate theory. For times beyond (2) the behavior of the approximate theory is qualitatively similar to the exact theory. Times corresponding to (2) are indicated in figures 41a, 43a, and 45a for reference. Using this criteria in figure 25a shows a significant discrepancy in the wave lengths of the two theories even to the left of (2), which is equivalent to the region of times greater than (2) in figure 24a. The behavior is, however, qualitatively correct and the point (2) is marked in figures 42a, 44a, and 46a for reference.

A similar criteria based on the point (2) would lead to the conclusion that the results are entirely in error for any region of dispersive response for the softer foundation. However, if the longitudinal response is small

compared to the bending response this statement is not necessarily true. The type of loading considered here (transverse line load) gives rise to a greater transverse deflection for the soft foundation, since the longitudinal displacements and stresses would be excited only through a Poisson's ratio effect. For long waves and low frequencies the influence of Poisson's ratio coupling can be neglected. The longitudinal motion for long waves is governed by the two mode segments (3) - (2) and (6) - (4), figure 23b. With the exception of these segments, the predominant-period, time-of-occurrence curves for the exact and approximate theory are seen to agree well for periods and wave lengths greater than (12) in figures 24b and 25b, respectively. Because of the extrema at (5) the validity of the approximate theory in describing the exact response for the upper two modes must be restricted accordingly, i. e., waves arriving before (5) must be discounted. The point (5) is indicated in figures 41b, 42b, 43b, 45b and 46b for reference.

CONCLUSIONS

The transient response of an elastic plate resting on an elastic foundation has been computed in section II and correlated with the frequency spectrum discussed in section I. The general conclusions that can be drawn from this response fall into two distinct areas:

1. The mechanism of the transient response

The influence of restraining elastic boundary affects a redistribution of the energy between the various modes of plate deformation. For a soft foundation the transverse excitation of a thin plate is characterized by the usual bending mechanism described by the elementary bending theory. The principle energy is in the form of translational motion and foundation and bending deformation. For the stiffer foundations the influence of rotational energy becomes significant, and the higher modes of deformation are prominent. This latter result leads to greater transverse shear as has been demonstrated in this study using the Timoshenko bending theory.

2. The methods of analysis

Two types of integrals that describe a transient solution are found which may be classified as "wave" and "nonwave". The "wave" integrals are of the stationary phase type and have an associated group velocity which is bounded. The "nonwave" integrals are governed by the Riemann-Lebesgue lemma and do not have a group velocity. These waves, however, serve mathematically to cancel contributions beyond the head of the wave. The "nonwave" response is associated with integrals which have points of stationary phase outside the limits of integration and appear to be waves

traveling toward the source of the forcing function. The "nonwaves" reflect the influence of the complex and imaginary arms in the related frequency spectrum.

Though the method of stationary phase appears to describe adequately the predominant periods and their related time of occurrence, the amplitudes predicted by this method of approximation suffer from rather severe limitations. Besides the deficiencies of this method in describing a particular integral (Appendix C), the usual predominance of this type of integral over the integrals governed by the Riemann-Lebesgue lemma, which describe the "nonwaves", occurs only in the very far field. For the intermediate field, not governed by either wave front expansions or the far field analysis, the only apparent means of evaluation is through direct numerical analysis. In this regard it has been possible to exploit the relatively simple forms of the approximate bending theories of Uflyand and Timoshenko for the intermediate field in terms of the frequency spectrum. Direct application of the methods presented here with similar numerical analysis can be accomplished with problems involving the exact theory of linear elasticity provided the frequency spectra are known.

REFERENCES

1. Harrison, M., "The Propagation of Elastic Waves in a Plate", The David W. Taylor Model Basin Report 872, Navy Department, Washington, D.C., (1954).
2. Kenney, J. T., Jr., "Steady-State Vibrations of Beam on Elastic Foundation for Moving Load", Journal of Applied Mechanics, 21, 359-364 (1954).
3. Mathews, P. M., "Vibrations of a Beam on Elastic Foundation", Zeitschrift fur Angewandte Mathematik and Mechanik, 38, 105-115 (1958).
4. Crandall, S.H., "The Timoshenko Beam on an Elastic Foundation", Third Midwestern Conference on Solid Mechanics, Ann Arbor, Michigan, pp. 146-169, (1957).
5. Das Gupta, S. C., "Propagation of Rayleigh Waves in a Layer Resting on a Yielding Medium", Bulletin of the Seismological Society, 45, 115-120 (1955).
6. Boley, B.A., "On a Dynamical Saint Venant Principle", Journal of Applied Mechanics, 27, 74-78 (1960).
7. Mindlin, R.D., "An Introduction to the Mathematical Theory of Elastic Plates", U.S. Army Signal Corps Engineering Laboratories Monograph, Fort Monmouth, N.J., (1955).
8. Timoshenko, S., Vibration Problems in Engineering, D. Van Nostrand Company, Inc., Third Edition, pp. 329-331 (1955).
9. Davies, R.M., "A Critical Study of the Hopkinson Pressure Bar", Philosophical Transactions of the Royal Society of London, 240 A, 375-457 (1948).
10. Love, A.E.H., A Treatise on the Mathematical Theory of Elasticity, Cambridge University Press, London, England, Fourth Edition, p.428 (1927).
11. Uflyand, Y.S., "The Propagation of Waves in the Transverse Vibration of Bars and Plates", Akad, Nauk SSSR Prikladnaya Matematika I Mekhanika (in Russian), 12, 287-300 (1948).
12. Mindlin, R.D., "Influence of Rotatory Inertia and Shear on Flexural Motions of Isotropic, Elastic Plates", Journal of Applied Mechanics, 18, 31-38 (1951).

13. Miklowitz, J., "Flexural Wave Solutions of Coupled Equations Representing the More Exact Theory of Bending", Journal of Applied Mechanics, 20, 511-514 (1953).
14. Miklowitz, J., "Flexural Waves in Beams According to the More Exact Theory of Bending", U.S. Naval Ordnance Test Station Report 2049, China Lake, California, (1953).
15. Miklowitz, J., "On the Use of Approximate Theories of an Elastic Rod in Problems of Longitudinal Impact", Proceedings of the Third U.S. National Congress on Applied Mechanics, Providence, Rhode Island, pp. 215-224, (1958).
16. Jones, R.P.N., "Transient Flexural Stresses in an Infinite Beam", Quarterly Journal of Mechanics and Applied Mathematics, 8, 373-384 (1955).
17. Adem, J., "On the Axially-Symmetric Steady Wave Propagation in Elastic Circular Rods", Quarterly of Applied Mathematics, 12, 261-275 (1954).
18. Mindlin, R.D., and Onoe, M., "Mathematical Theory of Vibration of Elastic Plates", Eleventh Annual Symposium on Frequency Control, U.S. Army Signal Corps Engineering Laboratories, Fort Monmouth, N.J., pp. 17-40, (1957).
19. Gazis, D.C., and Mindlin, R.D., "Extensional Vibrations and Waves in a Circular Disk and a Semi-Infinite Plate", Journal of Applied Mechanics, 27, 541-547 (1960).
20. Shaw, E.A.G., "On the Resonant Vibrations of Thick Barium Titanate Disks", Journal of the Acoustical Society of America, 28, 38-50 (1956).
21. Mindlin, R.D., and Medick, M.A., "Extensional Vibrations of Elastic Plates", Journal of Applied Mechanics, 26, 561-569 (1959).
22. Miklowitz, J., "Flexural Stress Waves in an Infinite Elastic Plate Due to Suddenly Applied Concentrated Transverse Load", Journal of Applied Mechanics, 27, 681-689 (1960).
23. Mindlin, R.D., and McNiven, H.D., "Axially Symmetric Waves in Elastic Rods", Journal of Applied Mechanics, 27, 145-151 (1960).
24. Whittaker, E. T., and Watson, G.N., A Course of Modern Analysis, Cambridge University Press, London England, Fourth Edition, (1927).
25. Bateman, H., (Erdelyi, A., Magnus, W., Oberhettinger, F., and Tricomi, F.G.), Higher Transcendental Functions, Volume 2, Bateman Manuscript Project, McGraw-Hill Book Company, Inc., New York, p. 82, (1953).

26. Ewing, W.M., Jardetzky, W.S., and Press, F., Elastic Waves in Layered Media, McGraw-Hill Book Company, Inc., New York, p. 44, (1957).
27. Miklowitz, J., "Transient Compressional Waves in an Infinite Elastic Plate or Elastic Layer Overlying a Rigid Half-Space", To be presented at the American Society of Mechanical Engineers Annual Meeting (Nov. 27-Dec. 1, 1961), New York City, (in press, Journal of Applied Mechanics).
28. Skalak, R., "Longitudinal Impact of a Semi-Infinite Circular Bar", Journal of Applied Mechanics, 24, 59-64 (1957).
29. Folk, R., Fox, G., Shook, C.A., and Curtis, C.W., "Elastic Strain Produced by Sudden Application of Pressure to One End of a Cylindrical Bar, I. Theory", Journal of the Acoustical Society of America, 30, 552-558 (1958).
30. Jones, O.E., "Theoretical and Experimental Studies on the Propagation of Longitudinal Elastic Strain Pulses in Wide Rectangular Bars", Ph.D. Thesis, California Institute of Technology, Pasadena, California, (1961).
31. Boley, B.A., and Chao, C.C., "Some Solutions of the Timoshenko Beam Equations", Journal of Applied Mechanics, 22, 579-586 (1955).
32. Boley, B.A., "On the Use of Sine Transforms in Timoshenko Beam Impact Problems", Journal of Applied Mechanics, 24, 152-153, (1957).
33. Jeffries, Sir Harold, and Swirles, Bertha, Methods of Mathematical Physics, Cambridge University Press, London, England, Third Edition, (1956).
34. Havelock, T.H., The Propagation of Disturbances in Dispersive Media, Cambridge University Press, London, England, pp. 79-81, (1914).
35. Milne, W.E., Numerical Calculus, Princeton University Press, N.J., pp. 285-290, (1949).
36. Miklowitz, J., "Traveling Compressional Waves in an Elastic Rod According to the More Exact One-Dimensional Theory", The Second Congress of Applied Mechanics, Ann Arbor, Michigan, pp. 179-186, (1954).
37. Miklowitz, J., "The Propagation of Compressional Waves in a Dispersive Elastic Rod, Part I - Results from the Theory", Journal of Applied Mechanics, 24, 231-239 (1957).

38. Sherwood, J. W. C., "Propagation in an Infinite Elastic Plate", Journal of the Acoustical Society of America, 30, 979-984 (1959).
39. McLachlan, N. W., Complex Variable Theory and Transform Calculus, Cambridge University Press, London, England, Second Edition, p. 77, (1953).
40. Pekeris, C. L., "Theory of Propagation of Explosive Sound in Shallow Water", Geological Society of America Memoir 27, pp. 60-63, (1948).

APPENDIX A

The Geometric Behavior of Complex Frequency Spectra

Assume a functional relation of two complex variables Ω and Γ of the form

$$F(\Gamma, \Omega) = 0 \tag{A-1}$$

where F is analytic in each variable such that the derivatives $d^n F/d\Gamma^n$ and $d^n F/d\Omega^n$ may be formed for all Γ and Ω . Then Ω is implicitly an analytic function of Γ , since $d^n \Omega/d\Gamma^n$ is defined at every point. A conformal mapping, therefore, exists between the Ω - and Γ -planes.

Consider the functional relationship (A-1) to be a frequency equation which is even in Ω . Assume further that branches are known which map parts of the real Γ -axis onto the real Ω -axis. Because of the conformal mapping between these planes each such branch must map the entire real Γ -axis onto the entire Ω -axis unless $d\Omega/d\Gamma$ is zero at some point, say Γ_* , on the real Γ -axis. At such a critical point the mapping is no longer conformal and the first nonzero derivative $d^N \Omega/d\Gamma^N \Big|_{\Gamma = \Gamma_*}$ must be determined. Expanding in the neighborhood of Γ_* , Ω is given by

$$\Omega - \Omega_* = \frac{(\Gamma - \Gamma_*)^N}{N!} \left(\frac{d^N \Omega}{d\Gamma^N} \right)_{\Gamma = \Gamma_*} \tag{A-2}$$

or

$$\Gamma - \Gamma_* = A^{1/N} (\Omega - \Omega_*)^{1/N} \tag{A-3}$$

where

$$A = \frac{N!}{\left(\frac{d^N \Omega}{d\Gamma^N} \right)_{\Gamma = \Gamma_*}}$$

Consider a branch and its mapping in the Γ - and Ω -planes which has one critical point, Γ_* , as depicted in figure A-1. The real positive Ω -axis is shown mapped onto the positive real Γ -axis and a complex curve which emanates from the real axis at an angle ϕ given by*

$$\phi = \frac{\pi}{N}$$

Since the function $F(\Gamma, \Omega)$ was assumed even in Ω , the negative real Ω -axis must also map onto the same path as did the real positive Ω -axis. This is possible only if the mapping at (3) is not conformal, i.e.,

$$\left. \frac{d\Gamma}{d\Omega} \right|_{(3)} = 0 \tag{A-4}$$

since

$$\left. \frac{d\Gamma}{d\Omega} \right|_{\Omega=+0} = \left. \frac{d\Gamma}{d\Omega} \right|_{\Omega=-0}$$

Several conclusions can be drawn regarding the spectra indicated by imposing real Ω on the frequency equation $F(\Gamma^2, \Omega^2) = 0$. Consider, for example, a three-dimensional plot of real Ω against complex Γ , i.e., $\Gamma = X + iY$, as in figure 12. Real arms are assumed to exist. A complex arm emanates only from a branch where $\frac{d\Omega}{dZ} = 0$, ($\frac{d\Omega}{dX} = \frac{d\Omega}{dY} = 0$). In the neighborhood of this critical point the complex arm lies in the plane $\Omega = \Omega_*$, where Ω is real, making an angle ϕ , $0 < \phi \leq \frac{\pi}{2}$, with the X-plane. The derivative $d^N \Omega / d\Gamma^N$ at the critical point is the same in the plane of the complex arm as $d^N \Omega / dX^N$ in the real arm due to the analytic behavior of this quantity. Furthermore, if the complex arm intersects

* This result has been established by Sherwood (38) using a slightly different approach.

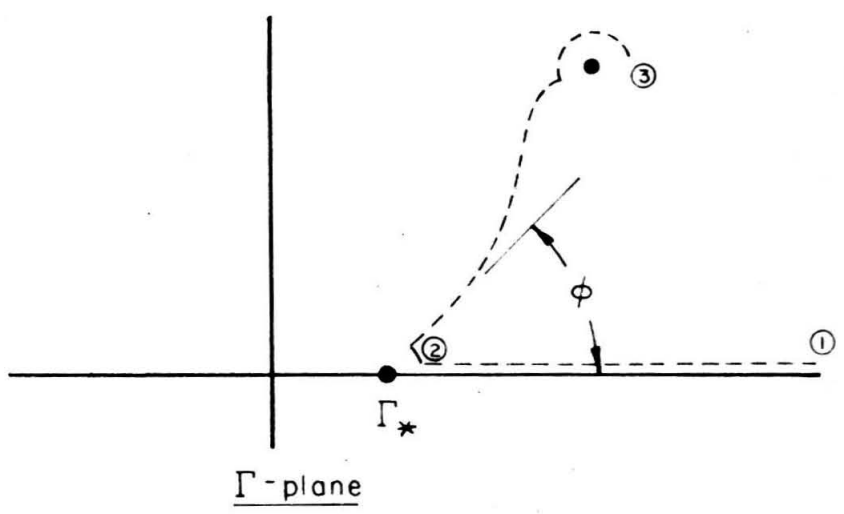
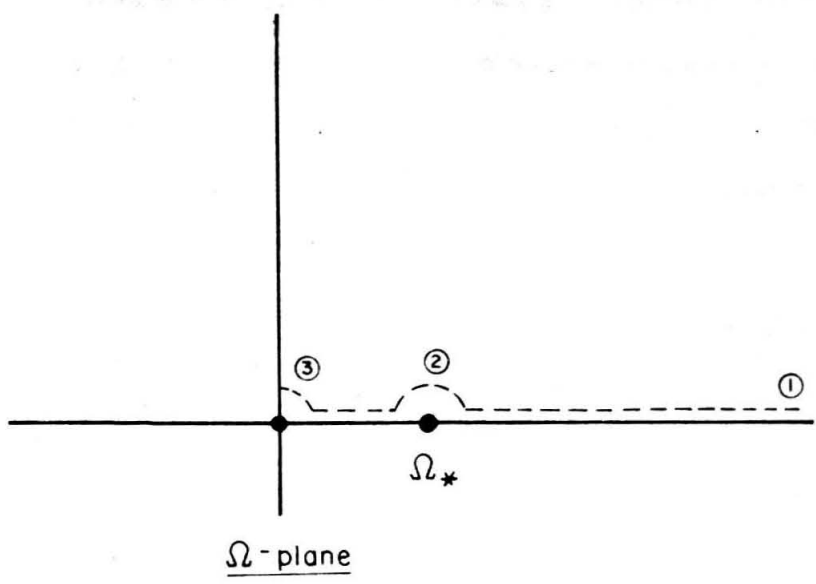


Figure A-1. Mapping of frequency and wave number planes.

the $\Omega = 0$ plane, it intersects normally according to equation A-4.

Similar arguments hold for complex arms emanating from imaginary arms as shown for the more exact bending theory in figure 12. Imaginary arms connected to real arms is a special case of the complex arms where $\Gamma_* = 0$ and $N = 2$.

APPENDIX B

Branch Point Analysis and Contour Integration of Equation 51b

Evaluation of the integral

$$I_s = \frac{1}{2} \int_{Br_1} \left[\frac{(s^2 + p_2^2 / \delta^2)}{p_2(p_2^2 - p_1^2)} e^{ip_2 \xi'} + \frac{(s^2 + p_1^2 / \delta^2)}{p_1(p_1^2 - p_2^2)} e^{ip_1 \xi'} \right] e^{s\tau'} \frac{ds}{s} \quad (B-1)$$

for $\text{Im } p_j > 0$ on Br_1 is accomplished by completing Br_1 in a closed path to the left.

Possible branch points in the s -plane correspond to the zeros of p_1, p_2 , and Z where

$$\left. \begin{aligned} p_j^2 &= -\frac{1}{2} \left[s^2(1 + \delta^2) + g^2 \right] + (-1)^j Z \\ Z^2 &= \frac{1}{4} \left[s^2(1 + \delta^2) + g^2 \right]^2 - \delta^2(g^2 + s^2)(1 + s^2) \end{aligned} \right\} \quad (B-2)$$

In the former case there are zeros of p_j only for p_2 , which are seen to be at $\pm i$ and $\pm ig$. The zeros of Z are located at $\pm S_j$ where

$$S_j^2 = \frac{1}{1 - \delta^2} \left[(-1)^j \left(2 \frac{\delta^2}{1 - \delta^2} - g^2 \right) + \frac{2\delta^2}{1 - \delta^2} \sqrt{1 - g^2(1 - \delta^2)} \right] \quad (B-3)$$

Comparison of equation B-3 with equation 33 shows that

$$\Omega_{j*}^2 = (-1)^{j+1} S_j^2$$

The regions shown in figure 14 describe the nature of the branch points given by equation B-3. Since interest is no longer restricted to real frequencies (imaginary s) as required to describe the frequency spectrum,

all roots given by equation B-3 must be considered. The four regions give the following values for S_j^2 :

Region I	S_j^2 complex
Region II	$S_1^2 < 0 < S_2^2$
Region III	$0 < S_j^2$
Region IV	$S_2^2 < 0 < S_1^2$

Study will be confined to region III as before and with values of g^2 less than $1 + \zeta^2$. These branch points are sketched in figure 19 for $g^2 < 1$.

The integration of B-1 is carried out along the path shown in figure 19. (Later the results will be extended to include the range $1 \leq g^2 < 1 + \zeta^2$.) This path is suggested by the stationary phase integrals resulting from a similar contour used by Miklowitz (15). In the present work the individual integrals comprising the final solution are related directly to specific branches of the frequency spectrum. Before completing Br_1 to the left, the wave character of the governing equations can be studied in detail by completing Br_1 to the right.

Completion of Br_1 to the Right

The path of integration Br_1 was necessarily chosen to the right of all singularities. Integration around the closed path composed of Br_1 and a large arc to the right of Br_1 (C_1 in figure 19) must be zero according to the Cauchy integral theorem. As the radius of this arc becomes very large the integrand of integral B-1 can be expanded for large s , and gives for equation B-1

$$I_s \simeq -\frac{i}{2} \int_{C_1} \left[-\frac{1}{\zeta(1-\zeta^2)^2} e^{s(\gamma' - \zeta \xi')} + \frac{s^2}{\zeta^2} e^{s(\gamma' - \xi')} \right] \frac{ds}{s^4} \quad (B-4)$$

Since both terms in the integrand are of order $1/s^k$, $k > 0$, (24), the integration along C_1 contributes nothing provided the coefficient of s in the exponential is negative. This means that the value of I_s is zero for $\gamma' < \delta \xi'$. Only the first term contributes for times in the range $\delta \xi' < \gamma' < \xi'$. Both terms contribute for $\gamma' > \xi'$.

In terms of dimensional parameters (since $\delta = c/c_p$) these time ranges correspond to

$$t < \frac{x}{c_p}$$

$$\frac{x}{c_p} < t < \frac{x}{c}$$

$$\frac{x}{c} < t$$

indicating the arrival of two different wave fronts. Integrations are carried out for the time ranges after first wave arrivals over a contour obtained by completing the Bromwich contour to the left.

Completion of Br_1 to the Left

When the coefficient of s in the exponentials become positive it can be shown that integration along the small arcs C_2 and C_3 vanish (39). In this case

$$\int_{Br_1} = \int_{Br_2}$$

since no singularities are enclosed by the path of integration. It remains only to write down the integrals along each of the paths using analytic continuation of the selected branches of p_j on Br_1 . The branch points of Z can be dealt with by writing it as

$$Z = \frac{1-\delta^2}{2} \left[(s^2+S_1^2)(s^2-S_2^2) \right]^{1/2} = \frac{1-\delta^2}{2} \sqrt{\rho_1\rho_2\rho_3\rho_4} e^{i \frac{(\phi_1+\phi_2+\phi_3+\phi_4)}{2}} \quad (\text{B-5})$$

where the ρ_i and ϕ_i are, respectively, the moduli and arguments of the complex vectors emanating from the four branch points of Z , figure 19. This type of representation has been used by Miklowitz (36) for a similar function. Since on Br_1 the variation of the argument, ϕ , of s must be restricted to $-\pi/2 < \phi < \pi/2$, the ϕ_i also have the same restriction, i.e., $-\pi/2 < \phi_i < \pi/2$.

The contour integration is carried out by continuing analytically the integrand functions in integral B-1 from Br_1 to and on Br_2 . The complex vectors defined in equation B-5 aid in this process.

Imposing $|s| \gg 1$ at the beginning of path L_1 , figure 19, the arguments of the p_j and Z (consistent with $\text{Im } p_j > 0$ on Br_1) are 0 and $-\pi$, respectively. Using equation B-5 it follows that on paths L_1 , L_2 and L_3 the argument of Z remains $-\pi$, since on these paths the $\sum \phi_i$ remains fixed and Z does not go through any of its zeros in going from L_1 to L_3 . About the branch point $-iS_1$ just the argument ϕ_3 changes from $-\pi/2$ to $\pi/2$; hence the argument of Z changes to $-\pi/2$, the value it also has on path L_5 . On path L_1 it follows that

$$p_j = \frac{1}{2} \left[\eta^2(1+\delta^2) - \frac{g^2}{2} - (-1)^j Z_1 \right]^{1/2}$$

where

$$Z_1 = |Z| = \frac{1-\delta^2}{2} \left| (\eta^2-S_1^2)(\eta^2+S_2^2) \right|^{1/2}$$

$$s^2 = \eta e^{-i(\pi/2)}$$

Expanding the p_j in the neighborhood of $s = -i$ and retaining only the leading terms gives

$$p_j^2 = -\frac{1}{2} \left[g^2 - (1 + \delta^2) \right] + (-1)^j \left| g^2 - (1 + \delta^2) \right| \left\{ 1 - \frac{i \rho_0 \delta^2 (1 - g^2) e^{i \phi_0}}{\left[g^2 - (1 + \delta^2) \right]^2} \right\}$$

where $s = -i + \rho_0 e^{i \phi_0}$ as shown in figure B-1. Since $g^2 < 1$ has been assumed, it is seen that $s = -i$ is a zero of p_2 only as pointed out earlier (and consequently not a branch point of p_1). The term p_2 can then be written as

$$p_2 = \left[\frac{\delta^2 (1 - g^2)}{1 + \delta^2 - g^2} \right]^{1/2} \sqrt{\rho_0} e^{\frac{i}{2} (\phi_0 + \frac{\pi}{2})}$$

where the branch of the square root has been chosen in agreement with p_2 real and greater than zero on L_1 , i.e., when $\phi_0 = -\pi/2$. The p_2 is seen to behave in the usual manner in the neighborhood of a square root branch point, and its argument increases by $\pi/2$ as ϕ_0 goes from $-\pi/2$ to $\pi/2$. This analytic continuation to path L_2 gives p_1 and Z unchanged and p_2 as

$$p_2 = e^{i \frac{\pi}{2}} \left[-\frac{1}{2} \eta^2 (1 + \delta^2) + \frac{1}{2} g^2 + Z_1 \right]^{1/2}$$

Along L_2 the arguments of p_j and Z remain unchanged. At $-ig$ the p_j can be expanded in a manner similar to that applied at $-i$. This point is also found to be a zero of p_2 , and analytic continuation to path L_3 gives p_1 and Z unchanged again and

$$p_2 = - \left[\frac{1}{2} \eta^2 (1 + \delta^2) - \frac{g^2}{2} - Z_1 \right]^{1/2}$$

The point $-iS_1$ is a branch point of both p_j as well as Z and analytic continuation to path L_4 gives

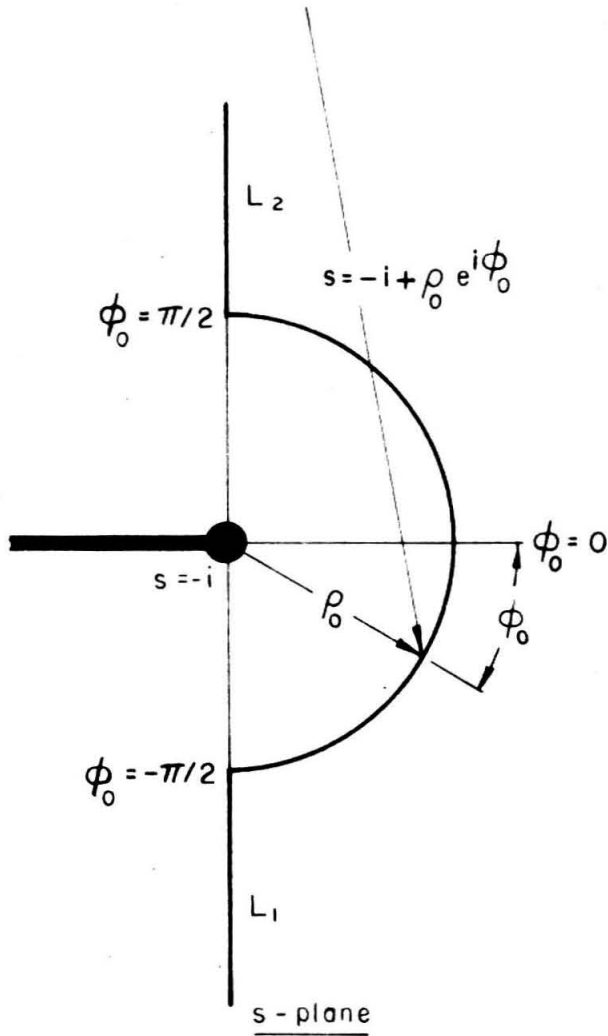


Figure B-1. Detail of complex s -plane in neighborhood of branch point $s = -i$.

$$p_j = (-1)^{j+1} \left[\frac{1}{2} \eta^2 (1 + \delta^2) - \frac{g^2}{2} - (-1)^j i Z_1 \right]^{1/2}$$

where p_1 has been carried along unchanged from path L_1 to the branch point $-iS_1$. Note that for $\eta^2 > g^2/1 + \delta^2$ the $\text{Im } p_j > 0$. Continuing analytically to values of $\eta^2 \leq g^2/1 + \delta^2$, $\text{Im } p_j$ must remain greater than zero, and the p_j may be written in the equivalent form

$$p_j = i \left[\frac{g^2}{2} - \frac{1}{2} \eta^2 (1 + \delta^2) + (-1)^j i Z_1 \right]^{1/2}$$

Continuing from path L_4 to L_5 results only in a change of form, since s is real on path L_5

$$p_j = i \left[\frac{g^2}{2} + \frac{1}{2} \eta^2 (1 + \delta^2) + (-1)^j i Z \right]^{1/2}$$

where

$$Z_2 = \frac{1 - \delta^2}{2} \left| (\eta^2 + S_1^2)(\eta^2 - S_2^2) \right|^{1/2}$$

$$s = \eta$$

As a check on the procedure, the values of p_j and Z can be continued analytically from L_5 around S_2 and along the real axis to Br_1 . It is readily seen that on the real axis, for $|s| > S_2$, p_j is positive imaginary as required.

Further simplification of the integration can be made by noting that analytic continuation onto the upper half s -plane will give the p_j to be the negative complex conjugate of the p_j on the corresponding path in the lower half s -plane. The integrands of B-1 must behave similarly. Since the directions of integration along these equivalent paths are opposite in sense, the contribution from such an integral pair is twice the real part from either one of the paths.

Expansions in the neighborhood of the branch points shows that the contribution to the integral from the small arcs vanish in the limit. A half residue results from the small arcs at the origin.

After some algebra the integral B-1 is given by the integrals presented on page 59 in the text.

APPENDIX C

A Criterion for Estimating the Range of Validity of the
Stationary Phase Approximation

Consider an integral of the form

$$I = \int_{a_1}^{a_2} f(\eta) e^{i\tau' \chi(\eta)} d\eta \quad (C-1)$$

where τ' is a large positive real parameter, $\chi(\eta)$ a real continuous function of the real variable η , and $f(\eta)$ a real or complex continuous function. It is assumed that $\chi'(\eta_0) = 0^*$ in $a_1 \leq \eta_0 \leq a_2$; i. e., integral C-1 has one or more points of stationary phase (critical points) in the range of integration.

It is well known that an integral of this type can be approximated for sufficiently large values of the parameter τ' by using the method of stationary phase (33). Pekeris (40) has estimated the range of τ' over which this approximation is valid by including the next term which is of order $(1/\tau')$, the leading term being of order $(1/\sqrt{\tau'})$. In his work Pekeris extended the integral limits to infinity, and only the higher derivatives in $\chi(\eta)$ were considered. In the present study the integrals under consideration have finite limits close to the stationary phase point and may not be conveniently extended to infinity. Further, the function $f(\eta)$ is not assumed to be slowly varying. The following study attempts to include these sources of error in the estimate of τ' .

There exists an upper and a lower limit of integration around the

* The dots ()' will denote differentiation with respect to η .

critical point, η_c , beyond which further contribution to the integral C-1 may be disregarded as being less than some acceptable error \mathcal{E} . If this bound is within the limits of the integral, does not contain other stationary phase points, and specifies a range over which the higher order terms of the Taylor's series expansions of $f(\eta)$ and $\chi(\eta)$ satisfy the conditions

$$\left. \begin{aligned} \frac{|f^{(n)}(\eta_0)| |\eta_c - \eta_0|^n}{n! |f(\eta_0)|} &\sim O(\mathcal{E}) & n = 1, 2, \dots \\ \frac{|\chi^{(n)}(\eta_0)| |\eta_c - \eta_0|^n}{n!} &\sim O(\mathcal{E}) & n = 3, 4, \dots \end{aligned} \right\} \quad (C-2)$$

then the error introduced by approximating the integral C-1 by the methods of stationary phase will be of order \mathcal{E} and hence acceptable. The following establishes the value of η_c .

Assume there is one point of stationary phase, η_0 , in $a_1 \leq \eta \leq a_2$ and that $\chi''(\eta_0) > 0$. Expanding $\chi(\eta)$ and $f(\eta)$ in a Taylor's series about η_0 and retaining only the terms $f(\eta_0)$, $\chi(\eta_0)$, and $\chi''(\eta_0)$ gives, upon rewriting integral C-1

$$I/A = \int_0^{\eta_1} e^{i\eta^2} d\eta + \int_0^{\eta_2} e^{i\eta^2} d\eta \quad (C-3)$$

where

$$A = \frac{f(\eta_0)}{\sqrt{\frac{\tau_1}{2} |\chi''(\eta_0)|}} e^{i\tau_1 \chi(\eta_0)}$$

$$\eta_1 = (\eta_0 - a_1) \sqrt{\frac{\tau_1}{2} |\chi''(\eta_0)|}$$

$$\eta_2 = (a_2 - \eta_0) \sqrt{\frac{\gamma'}{2} |\chi''(\eta_0)|}$$

The integrals in equation C-3 are Fresnel's integrals and may be approximated by an asymptotic expansion (33)

$$\int_0^{H_c} e^{i\eta^2} d\eta \sim e^{i\pi/4} \frac{\sqrt{\pi}}{2} - \frac{e^{i(H_c^2 + \pi/2)}}{2H_c} + \dots$$

where $1 \ll H_c \leq \eta_1 \leq \eta_2$ is assumed. The following inequality in the limit for large H_c prevails

$$\left| \frac{2}{\sqrt{\pi}} e^{-i\pi/4} \int_0^{H_c} e^{i\eta^2} d\eta - 1 \right| \leq \frac{1}{\sqrt{\pi} H_c} \quad (C-4)$$

The term on the right of equation C-4 is an estimate of the upper bound in the error caused by using the ordinary stationary phase approximation on integrals like those in equation C-3, where the integral limit is finite. A similar expression to equation C-4 can be derived for $\chi''(\eta_0) < 0$ and is given by

$$\left| \frac{2}{\sqrt{\pi}} e^{i\pi/4} \int_0^{H_c} e^{-i\eta^2} d\eta - 1 \right| \leq \frac{1}{\sqrt{\pi} H_c} \quad (C-5)$$

Assume that it is desired to maintain an upper bound in the error less than \mathcal{E} such that

$$H_c = \frac{1}{\sqrt{\pi} \mathcal{E}}$$

This dictates an integral limit H_c beyond which further integration is considered negligible. In terms of the integral C-1 this limit is given by

$$\eta_c = \eta_0 \pm \frac{1}{\sqrt{\gamma'} \epsilon} \sqrt{\frac{2}{\pi |\chi''(\eta_0)|}} \quad (C-6)$$

where η_c must satisfy $a_1 < \eta_c < a_2$. This last condition imposes a lower limit on γ' which is described by the inequalities

$$\left. \begin{aligned} \gamma' &\geq \frac{2}{\pi \epsilon^2} \frac{1}{|\chi''(\eta_0)| (a_2 - \eta_0)^2} \\ \gamma' &\geq \frac{2}{\pi \epsilon^2} \frac{1}{|\chi''(\eta_0)| (\eta_0 - a_1)^2} \end{aligned} \right\} \quad (C-7)$$

Writing the order terms $O(\epsilon) = \epsilon$ in equation C-2, this pair of equations also dictates a lower limit on γ' :

$$\left. \begin{aligned} \gamma' &\geq \frac{2}{\pi \epsilon^2 |\chi''(\eta_0)|} \left| \frac{f^{(n)}(\eta_0)}{\epsilon^{n!} f(\eta_0)} \right|^{2/n}, \quad n = 1, 2, \dots \\ \gamma' &\geq \frac{2}{\pi \epsilon^2 |\chi''(\eta_0)|} \left| \frac{\chi^{(n)}(\eta_0)}{\epsilon^{n!}} \right|^{2/n}, \quad n = 3, 4, \dots \end{aligned} \right\} \quad (C-8)$$

For a value of γ' that satisfies both equations C-7 and C-8, the approximation of integral C-1 by using the method of stationary phase will produce an estimated error of order ϵ . The accuracy of this estimate may possibly reflect a rather severe handicap on the method of stationary phase, when in reality the error could be considerably less. The rough error estimate made in equation C-2 is in general probably too harsh, since the maximum error in $f(\eta)$ and $\chi(\eta)$ due to the neglect of the higher order terms of their expansion occurs in the region of highest oscillation of the integrand of integral C-1.

Numerical Example

Examples are carried out for the two integrals I_{s_1} and I_{s_5} of equation 52b. These integrals are of the stationary phase type and are improper at their lower limit. The function $f(\eta)$ defined in this appendix can be crudely approximated by letting the coefficient of the exponential be some function of the form

$$f(\eta) = \frac{f_0}{\sqrt{\eta^{-a_1}}}$$

The integrals under consideration are therefore of the form

$$I = f_0 \int_{a_1}^{\infty} \frac{1}{\sqrt{\eta^{-a_1}}} e^{i\gamma'[\eta^{-P_{ij}(\eta)}\xi'/\gamma']} d\eta$$

where the $\chi(\eta)$ defined in this appendix is

$$\chi(\eta) = \eta^{-P_{ij}(\eta)}\xi'/\gamma'$$

and

$$[P_{ij}(\eta)]^2 = \frac{1}{2} \left[\eta^{2(1+\delta^2)-g^2} \right] - (-1)^j \left\{ \left[\frac{\eta^{2(1+\delta^2)-g^2}}{2} \right]^2 - \delta^2(g^2 - \eta^2)(1-\eta^2) \right\}^{\frac{1}{2}}$$

$a_1 = 1$ for I_{s_1}

$$a_1 = s_1 = \left[\frac{1}{1-\delta^2} \left(g^{2-2} \frac{\delta^2}{1-\delta^2} + \frac{2\delta^2}{1-\delta^2} \sqrt{1-g^2(1-\delta^2)} \right) \right]^{1/2}$$

for I_{s_5}

Numerical evaluation of the pertinent information has been carried out for $\delta^2 = .28375$ and $g^2 = .9079$. The results are indicated in Table

C-1 and establish the value of γ' (and thereby define the far field) at which the order of the error, \mathcal{E} , is 0.1. Only the derivatives $\chi'''(\eta_0)$ and $f'(\eta_0)$ have been considered. The values of γ'/ξ' studied are

$$\gamma'/\xi' = 1.3317, \quad \frac{tc_p}{x} = 2.5$$
$$\gamma'/\xi' = .62590, \quad \frac{tc_p}{x} = 1.18$$

The former case corresponds to a point of stationary phase for both integrals and represents a time at which significant dispersion is present. In the latter case only integral I_{s_1} has a stationary phase point, this time being before the arrival of the second wave.

In each case considered the improper nature of the integrands at their lower limit has necessitated severe requirements on γ' . Recall that for a plate

$$\gamma' = \sqrt{12} \frac{ct}{h} = \sqrt{12} \delta \frac{c_p t}{h} = 1.84 \frac{c_p t}{h}$$
$$\xi' = \sqrt{12} \frac{x}{h} = 3.464 \frac{x}{h}$$

For $\gamma' = 10^4$ and $\gamma'/\xi' = 1.3317$, for example,

$$t = 5.40 \times 10^3 \text{ h}/c_p$$

and

$$x = 2.15 \times 10^3 \text{ h}$$

Table C-1

	I_{s_5}	I_{s_1}	
γ' / ξ'	1.3317	1.3317	.62590
η_0	1.2313	1.0632	2.11983
$P_{ij}(\eta_0)$.97160	.12488	.94695
a_1	.90307	1.000	1.000
a_2	∞	∞	∞
$ \chi^{\cdot\cdot}(\eta_0) $.774	4.00	.160
$ \chi^{\cdot\cdot\cdot}(\eta_0) $	4.17	75.5	.270
$ f^{\cdot}(\eta_0)/f(\eta_0) $	1.52	7.9	.446
The minimum γ' for $\xi = .1$			
from first of equation C-7	0	0	0
from second of equation C-7	7.6×10^2	4.0×10^3	3.2×10^2
from first of equation C-8	1.9×10^4	1.0×10^5	8.1×10^3
from second of equation C-8	3.0×10^2	4.0×10^2	2.3×10^2
greatest minimum of γ'	1.9×10^4	1.0×10^5	8.1×10^3